Supplementary Material

1 Feldman Cousins intervals for the likelihood fit

The one-dimensional confidence intervals for the observables from the likelihood fit, determined using the Feldman-Cousins technique [1] are given in Figs. 1–20 below. Nuisance parameters have been treated with the plug-in method [2]. The confidence interval from the profile-likelihood technique is also shown. In general there is a good agreement between the Feldman-Cousins and profile-likelihood intervals, except in the least occupied q^2 bin (see Figs. 3 and 13).

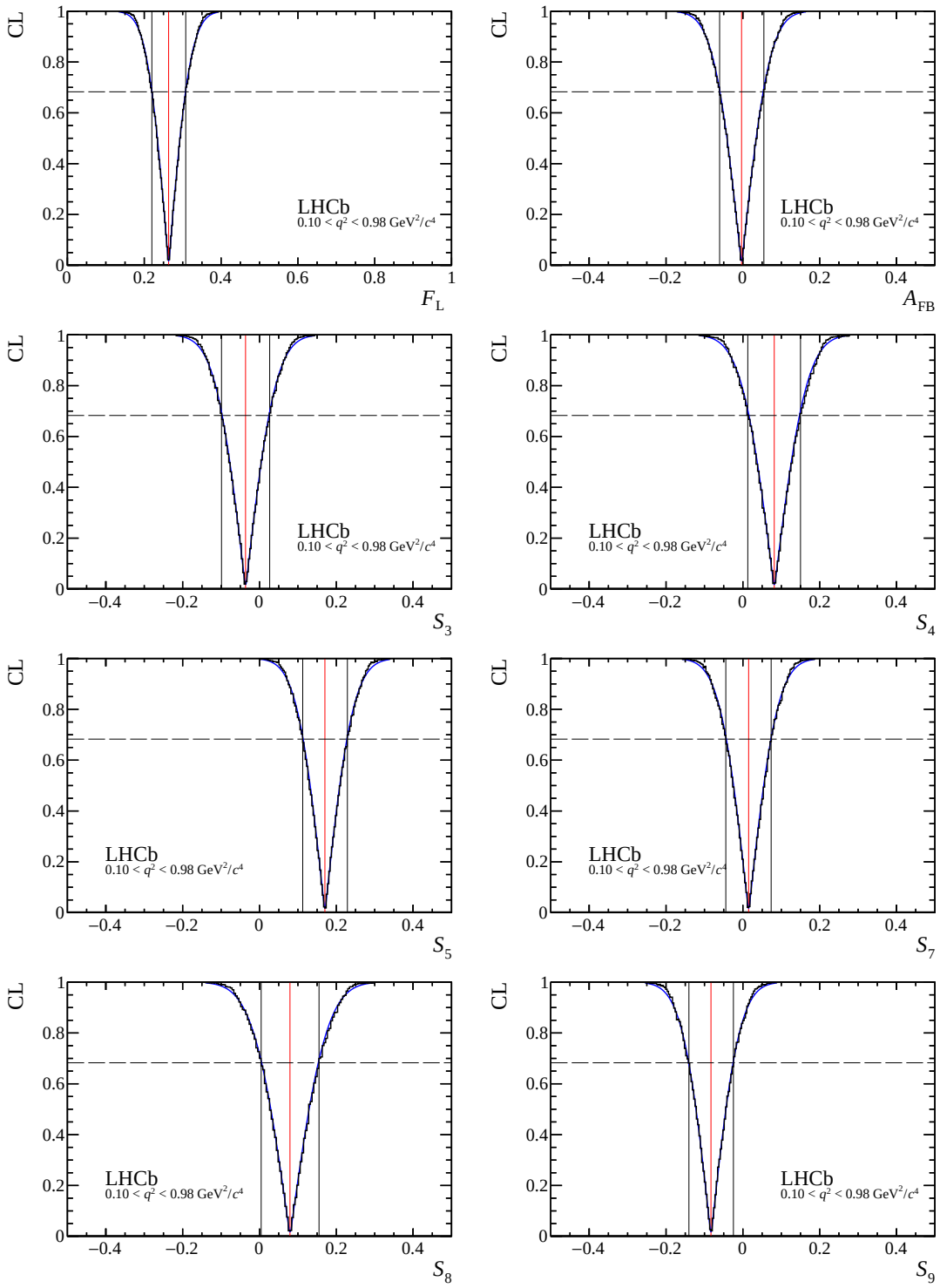

Figure 1: Confidence level (CL) obtained from a Feldman-Cousins scan using the likelihood ratio as an ordering principle (black). Nuisance parameters (including the other signal parameters) are treated with the plug-in method. The CL from a profile likelihood scan of the parameter is shown as the continuous (blue) curve. The 68% confidence interval from the Feldman-Cousins scan is indicated by the vertical lines.

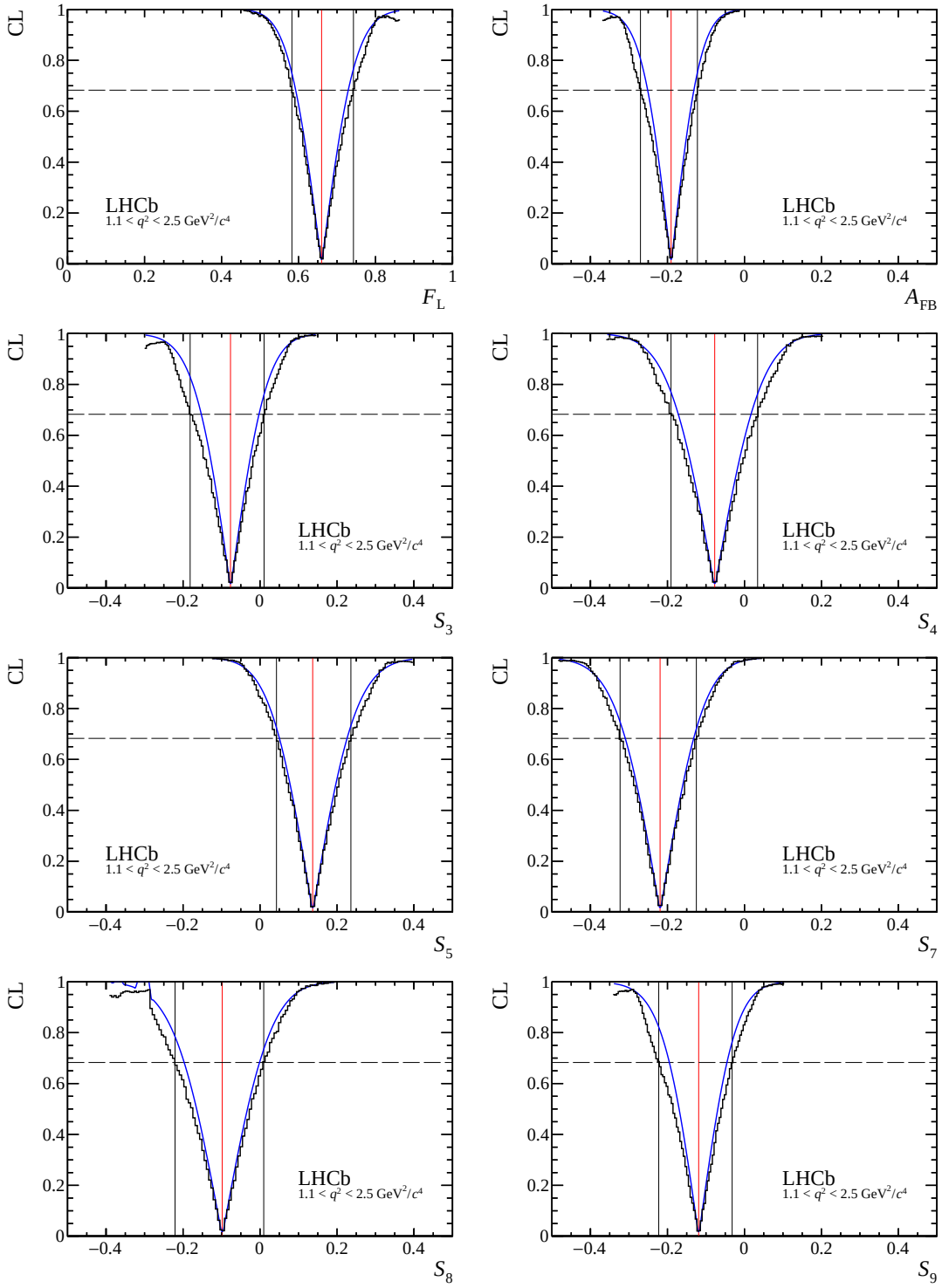

Figure 2: Confidence level (CL) obtained from a Feldman-Cousins scan using the likelihood ratio as an ordering principle (black). Nuisance parameters (including the other signal parameters) are treated with the plug-in method. The CL from a profile likelihood scan of the parameter is shown as the continuous (blue) curve. The 68% confidence interval from the Feldman-Cousins scan is indicated by the vertical lines.

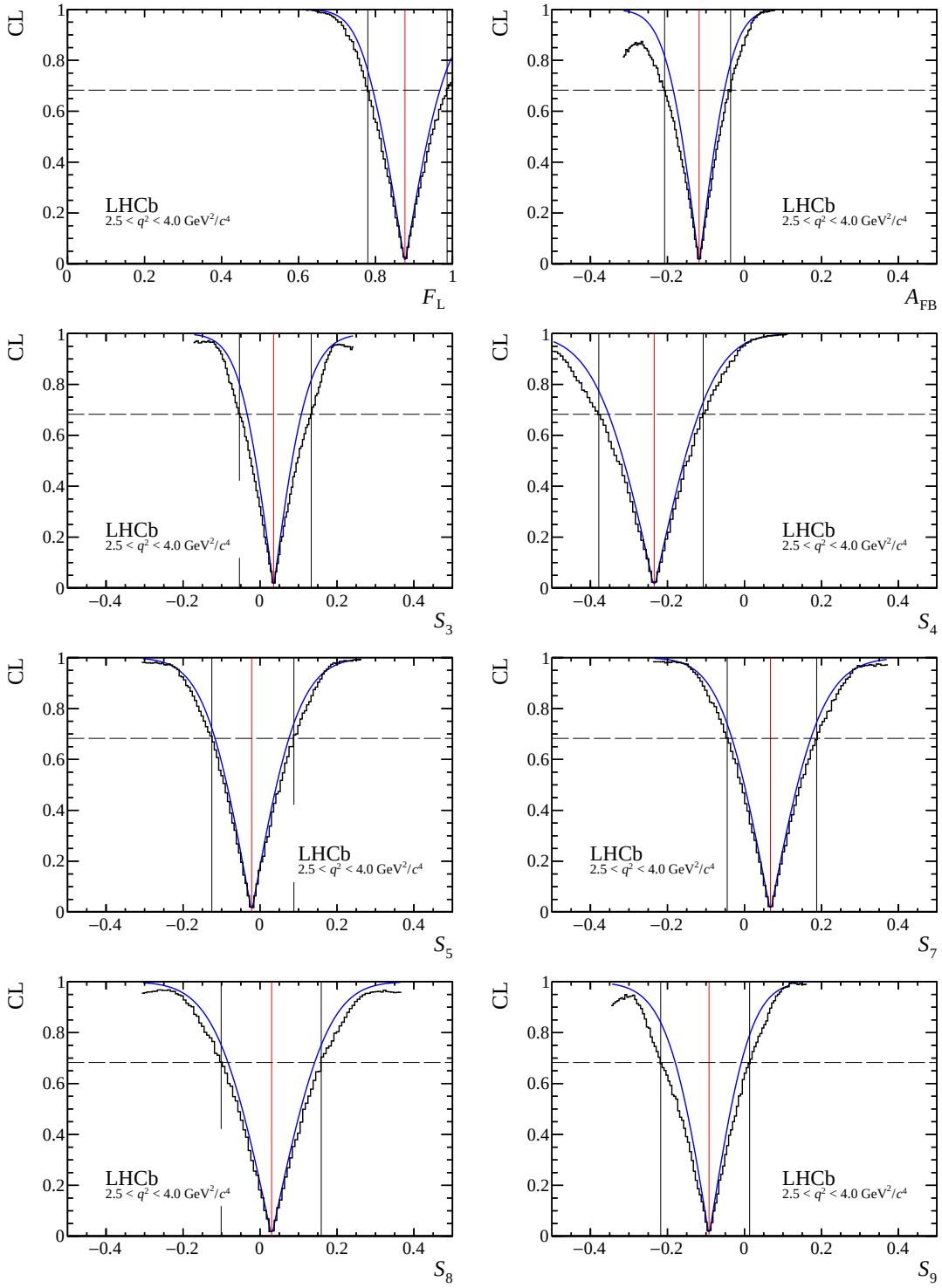

Figure 3: Confidence level (CL) obtained from a Feldman-Cousins scan using the likelihood ratio as an ordering principle (black). Nuisance parameters (including the other signal parameters) are treated with the plug-in method. The CL from a profile likelihood scan of the parameter is shown as the continuous (blue) curve. The 68% confidence interval from the Feldman-Cousins scan is indicated by the vertical lines.

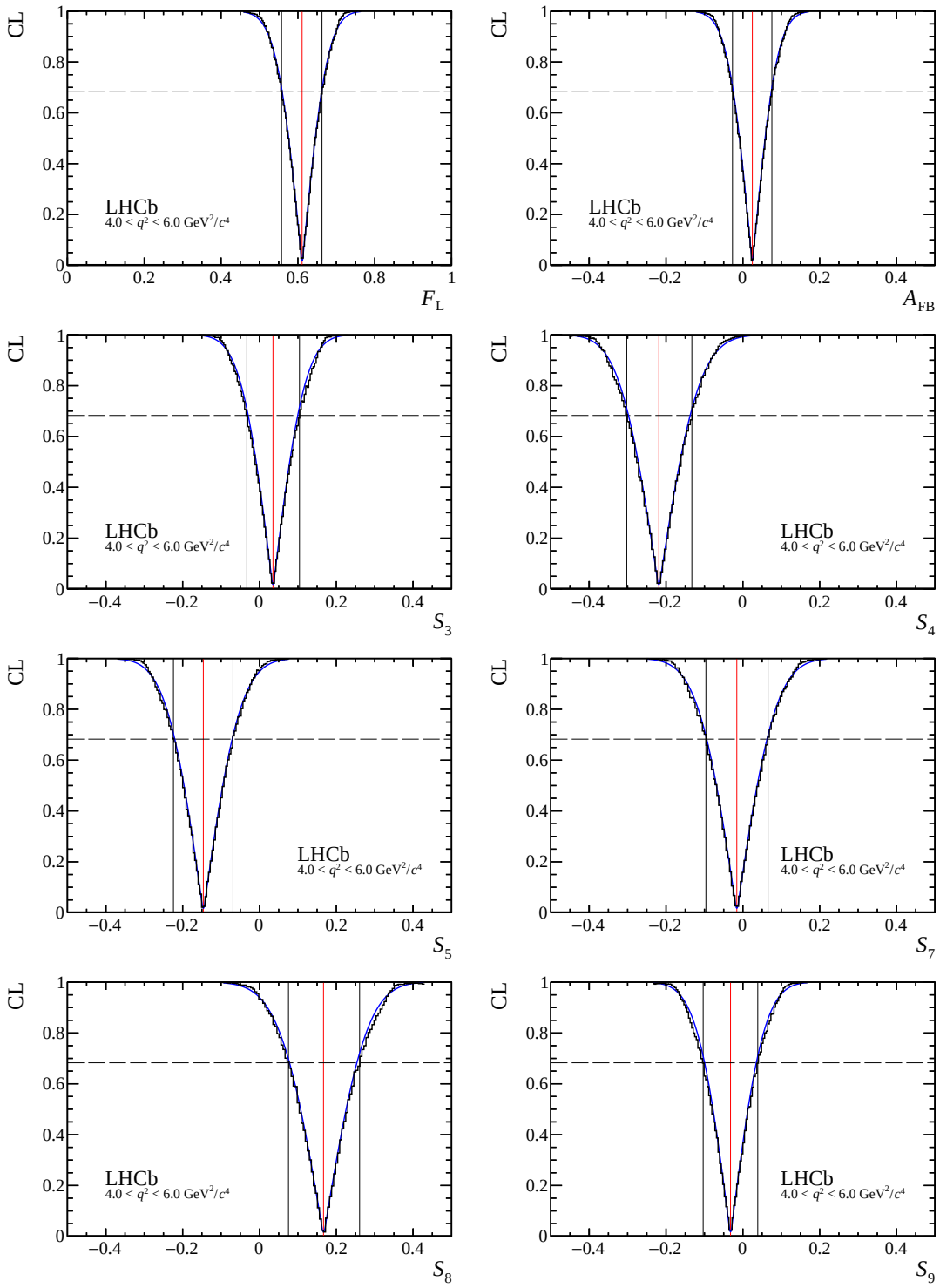

Figure 4: Confidence level (CL) obtained from a Feldman-Cousins scan using the likelihood ratio as an ordering principle (black). Nuisance parameters (including the other signal parameters) are treated with the plug-in method. The CL from a profile likelihood scan of the parameter is shown as the continuous (blue) curve. The 68% confidence interval from the Feldman-Cousins scan is indicated by the vertical lines.

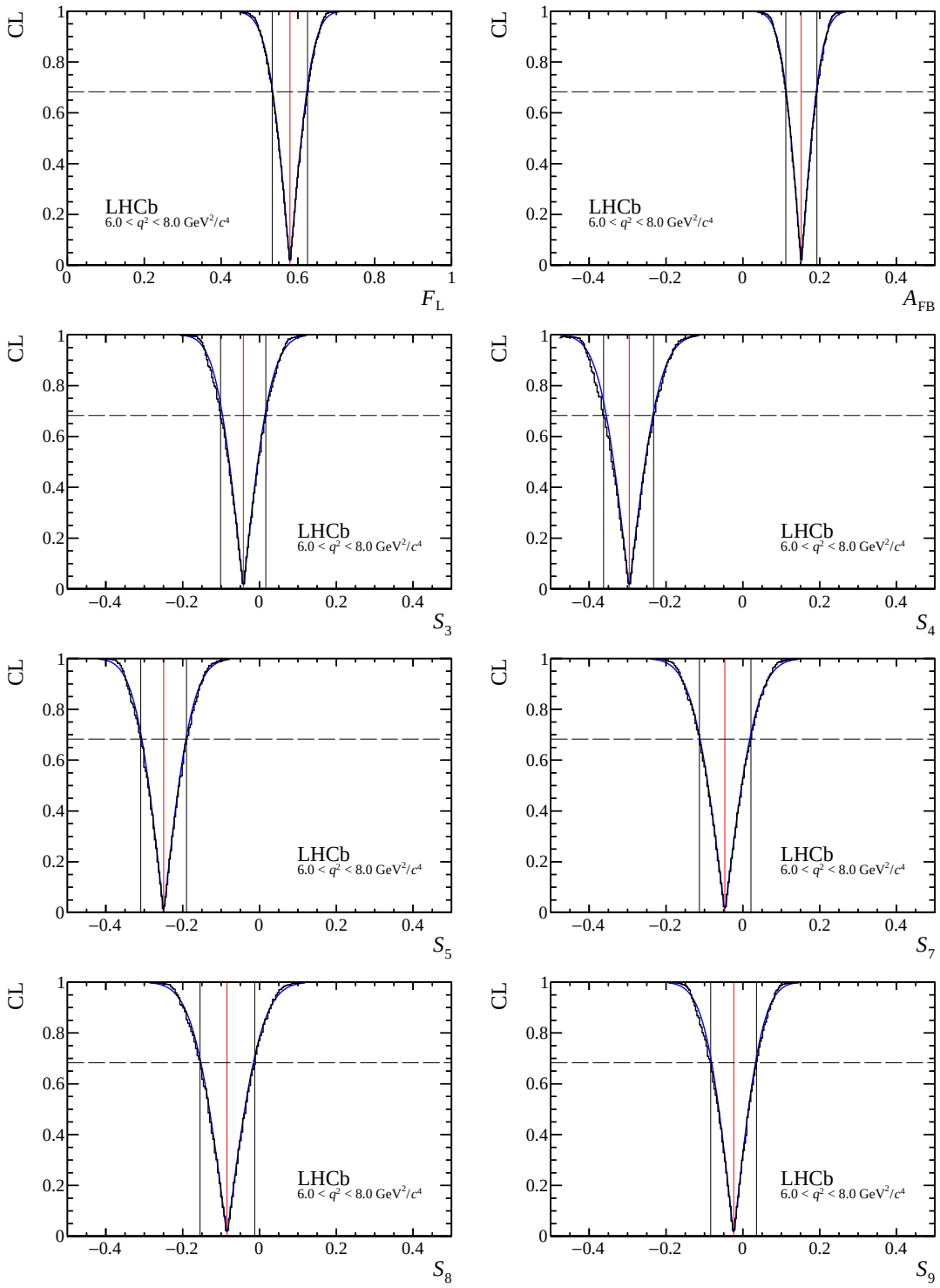

Figure 5: Confidence level (CL) obtained from a Feldman-Cousins scan using the likelihood ratio as an ordering principle (black). Nuisance parameters (including the other signal parameters) are treated with the plug-in method. The CL from a profile likelihood scan of the parameter is shown as the continuous (blue) curve. The 68% confidence interval from the Feldman-Cousins scan is indicated by the vertical lines.

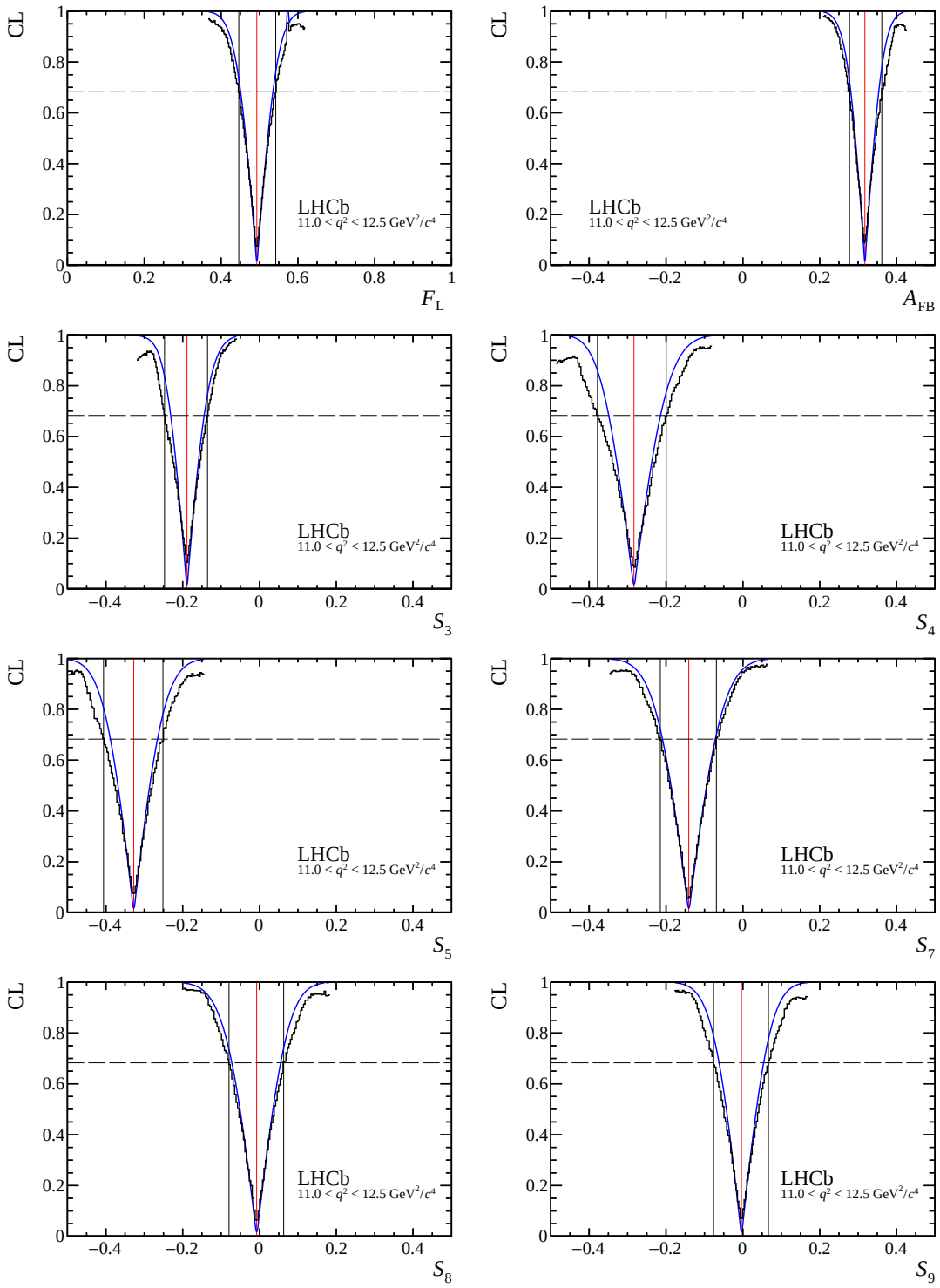

Figure 6: Confidence level (CL) obtained from a Feldman-Cousins scan using the likelihood ratio as an ordering principle (black). Nuisance parameters (including the other signal parameters) are treated with the plug-in method. The CL from a profile likelihood scan of the parameter is shown as the continuous (blue) curve. The 68% confidence interval from the Feldman-Cousins scan is indicated by the vertical lines.

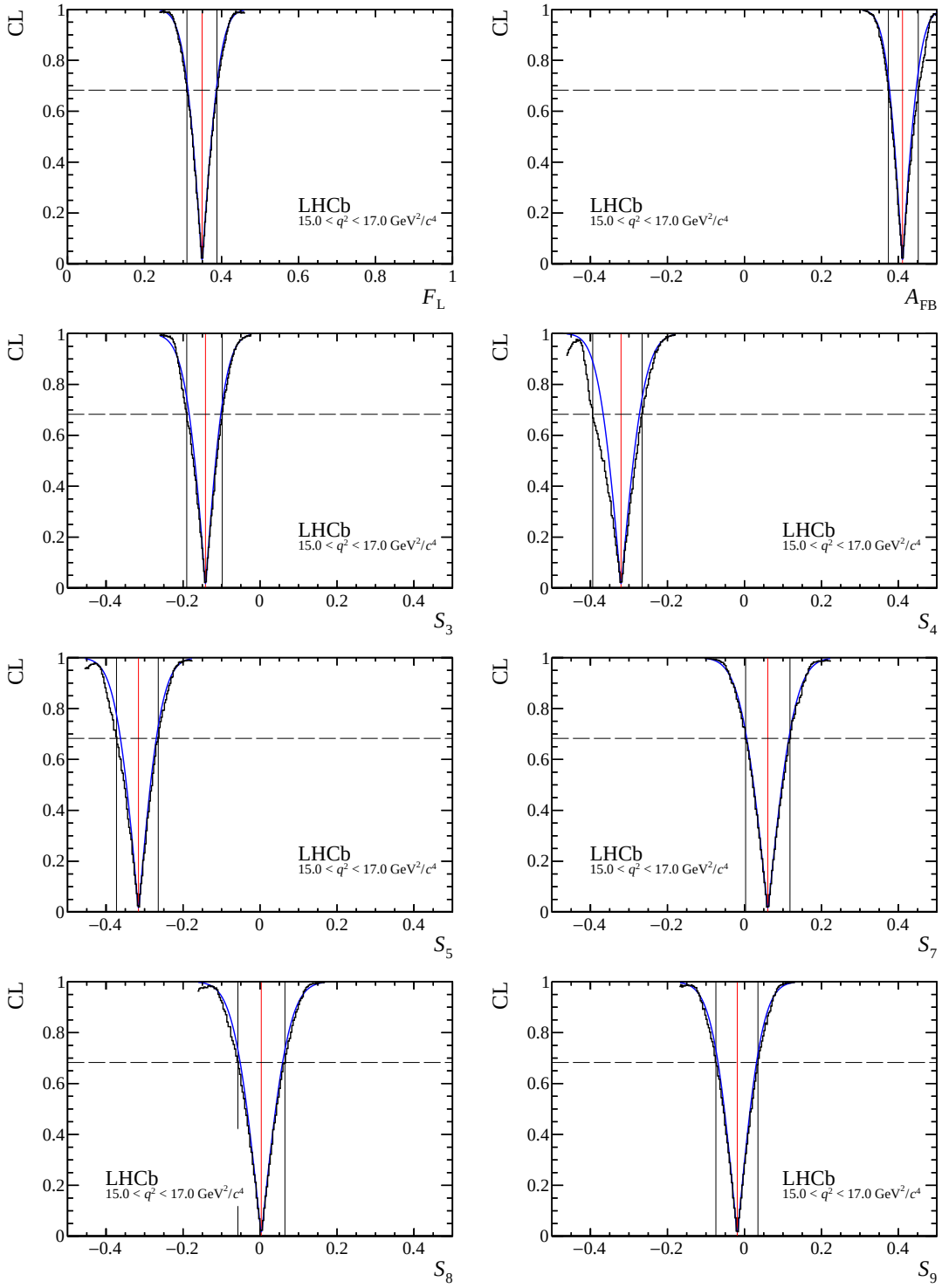

Figure 7: Confidence level (CL) obtained from a Feldman-Cousins scan using the likelihood ratio as an ordering principle (black). Nuisance parameters (including the other signal parameters) are treated with the plug-in method. The CL from a profile likelihood scan of the parameter is shown as the continuous (blue) curve. The 68% confidence interval from the Feldman-Cousins scan is indicated by the vertical lines.

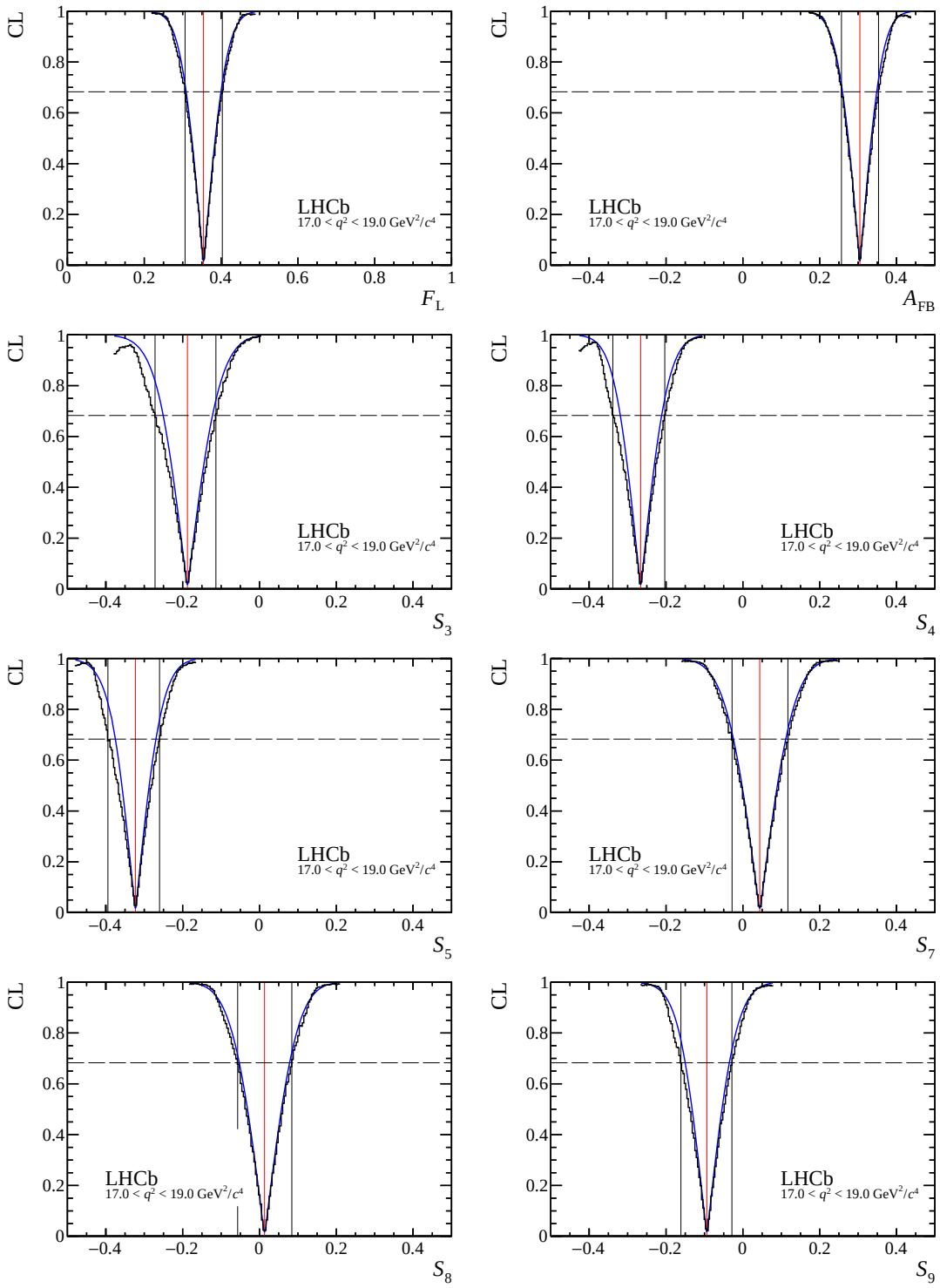

Figure 8: Confidence level (CL) obtained from a Feldman-Cousins scan using the likelihood ratio as an ordering principle (black). Nuisance parameters (including the other signal parameters) are treated with the plug-in method. The CL from a profile likelihood scan of the parameter is shown as the continuous (blue) curve. The 68% confidence interval from the Feldman-Cousins scan is indicated by the vertical lines.

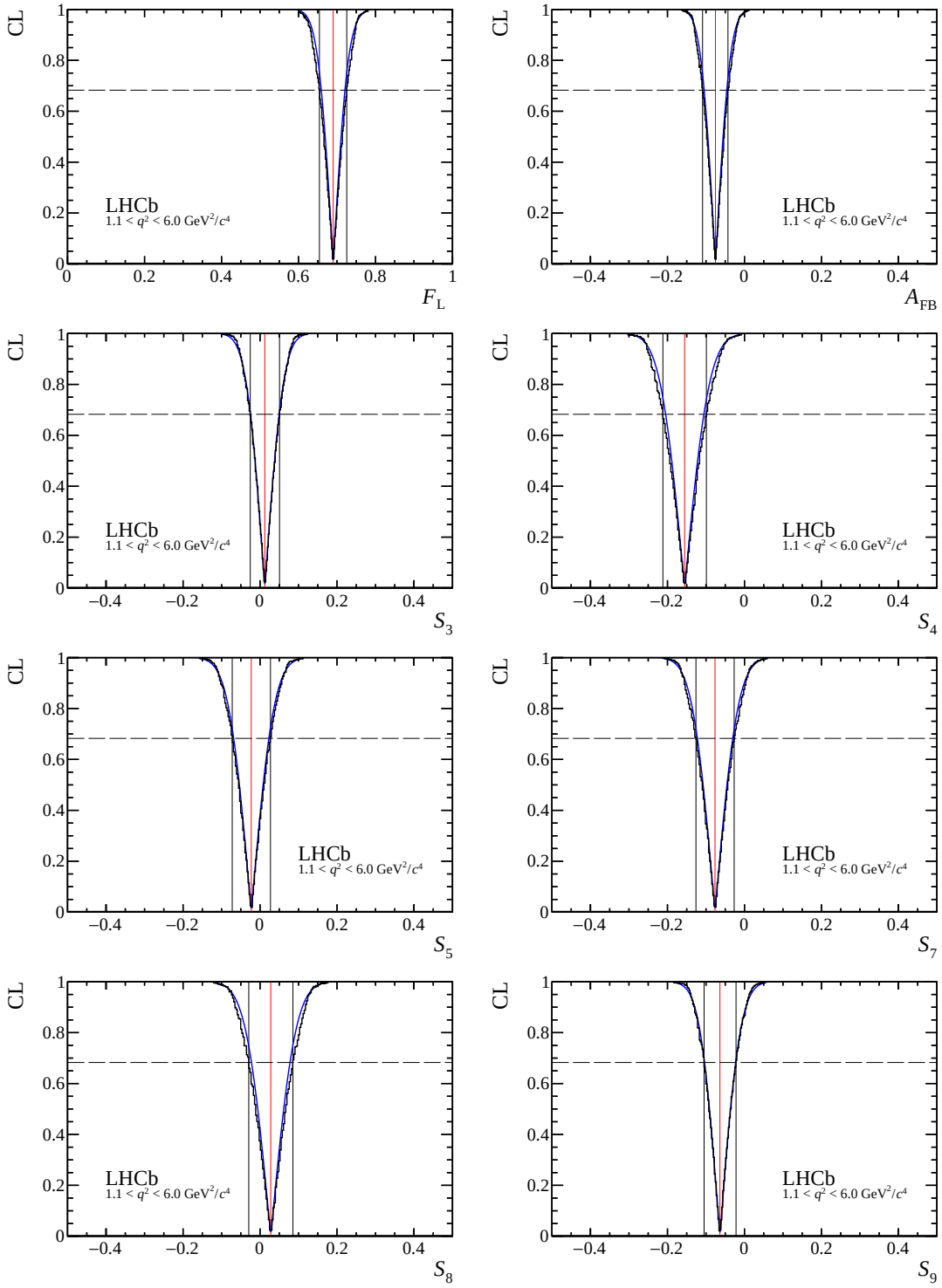

Figure 9: Confidence level (CL) obtained from a Feldman-Cousins scan using the likelihood ratio as an ordering principle (black). Nuisance parameters (including the other signal parameters) are treated with the plug-in method. The CL from a profile likelihood scan of the parameter is shown as the continuous (blue) curve. The 68% confidence interval from the Feldman-Cousins scan is indicated by the vertical lines.

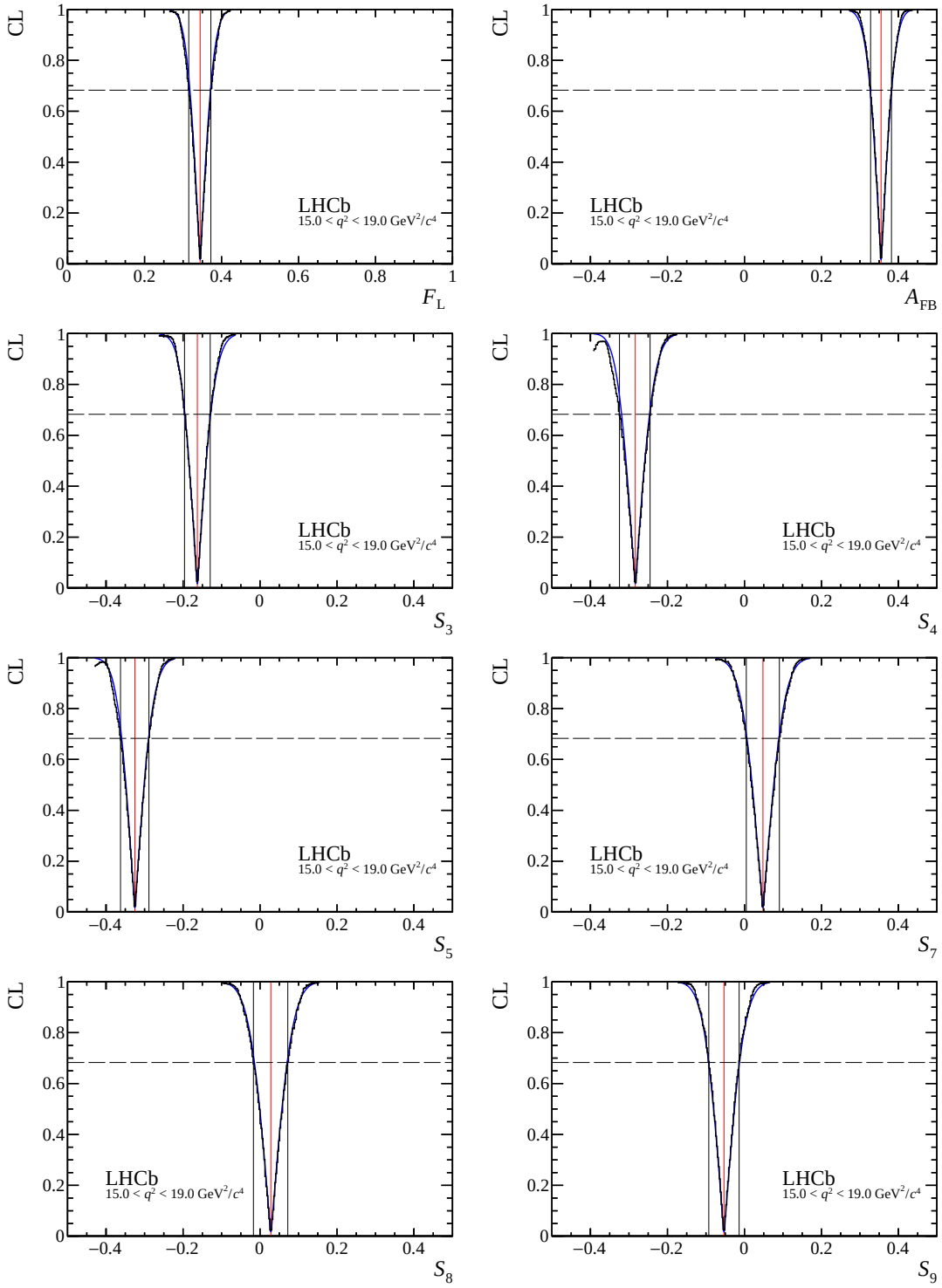

Figure 10: Confidence level (CL) obtained from a Feldman-Cousins scan using the likelihood ratio as an ordering principle (black). Nuisance parameters (including the other signal parameters) are treated with the plug-in method. The CL from a profile likelihood scan of the parameter is shown as the continuous (blue) curve. The 68% confidence interval from the Feldman-Cousins scan is indicated by the vertical lines.

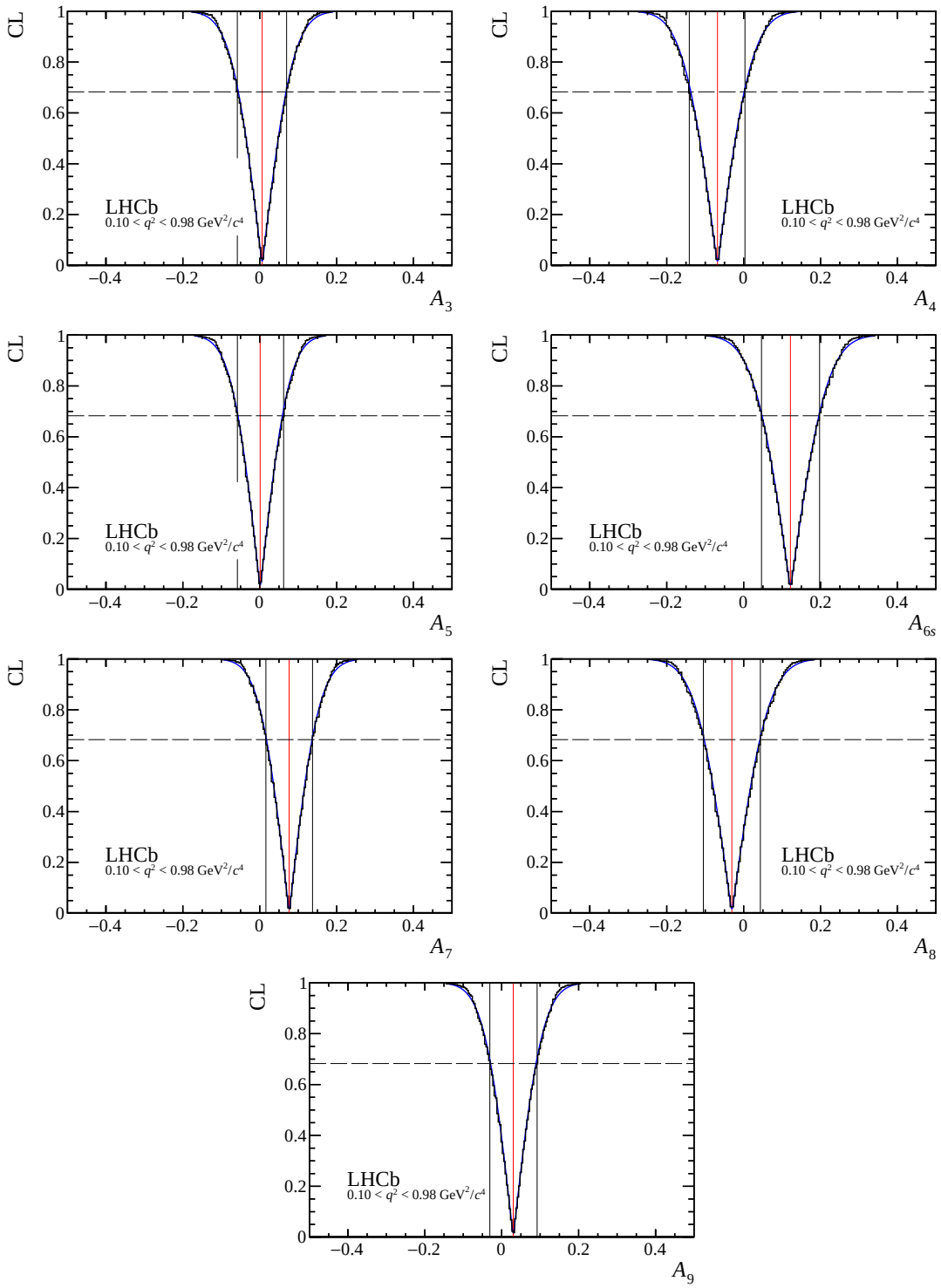

Figure 11: Confidence level (CL) obtained from a Feldman-Cousins scan using the likelihood ratio as an ordering principle (black). Nuisance parameters (including the other signal parameters) are treated with the plug-in method. The CL from a profile likelihood scan of the parameter is shown as the continuous (blue) curve. The 68% confidence interval from the Feldman-Cousins scan is indicated by the vertical lines.

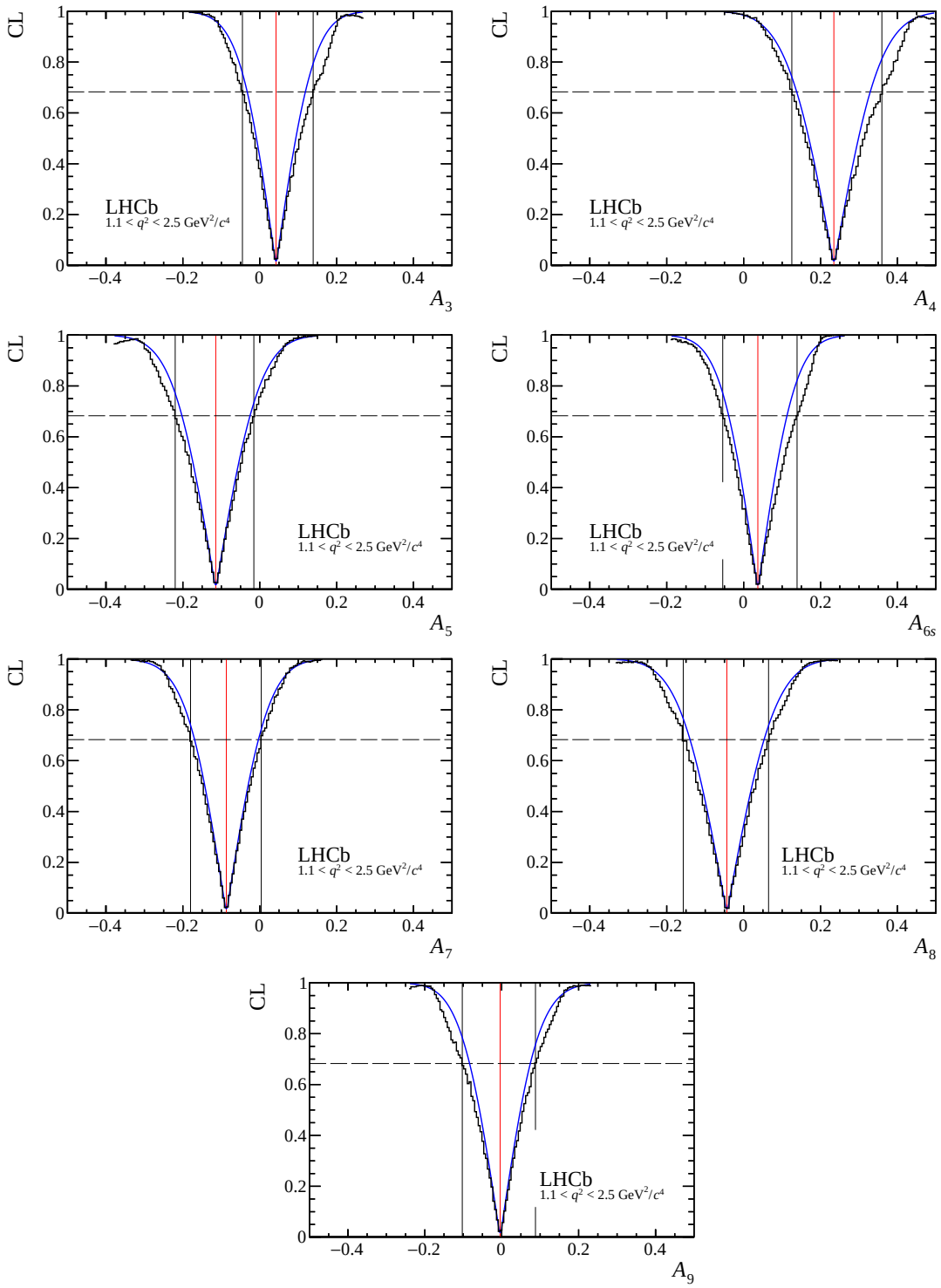

Figure 12: Confidence level (CL) obtained from a Feldman-Cousins scan using the likelihood ratio as an ordering principle (black). Nuisance parameters (including the other signal parameters) are treated with the plug-in method. The CL from a profile likelihood scan of the parameter is shown as the continuous (blue) curve. The 68% confidence interval from the Feldman-Cousins scan is indicated by the vertical lines.

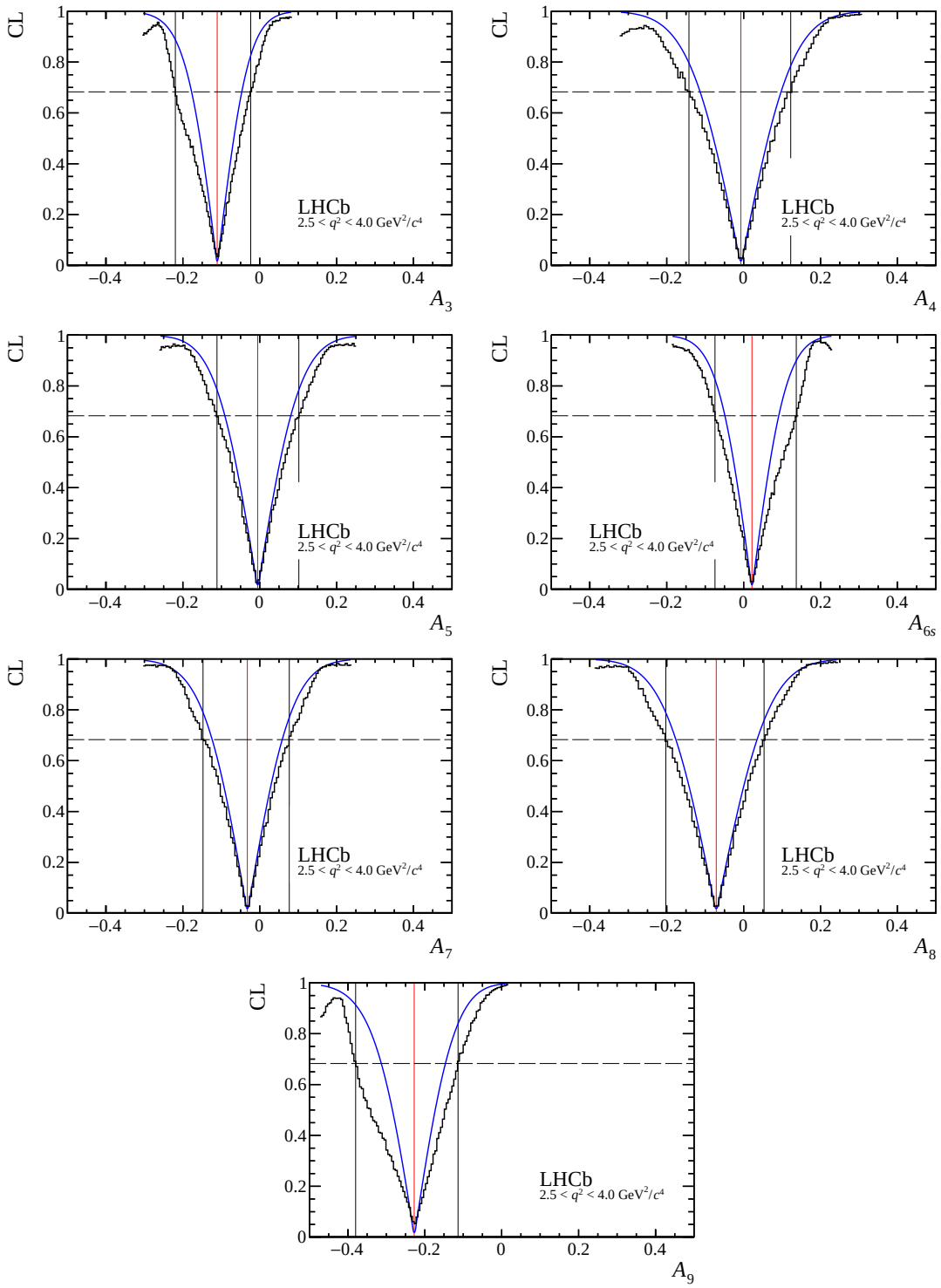

Figure 13: Confidence level (CL) obtained from a Feldman-Cousins scan using the likelihood ratio as an ordering principle (black). Nuisance parameters (including the other signal parameters) are treated with the plug-in method. The CL from a profile likelihood scan of the parameter is shown as the continuous (blue) curve. The 68% confidence interval from the Feldman-Cousins scan is indicated by the vertical lines.

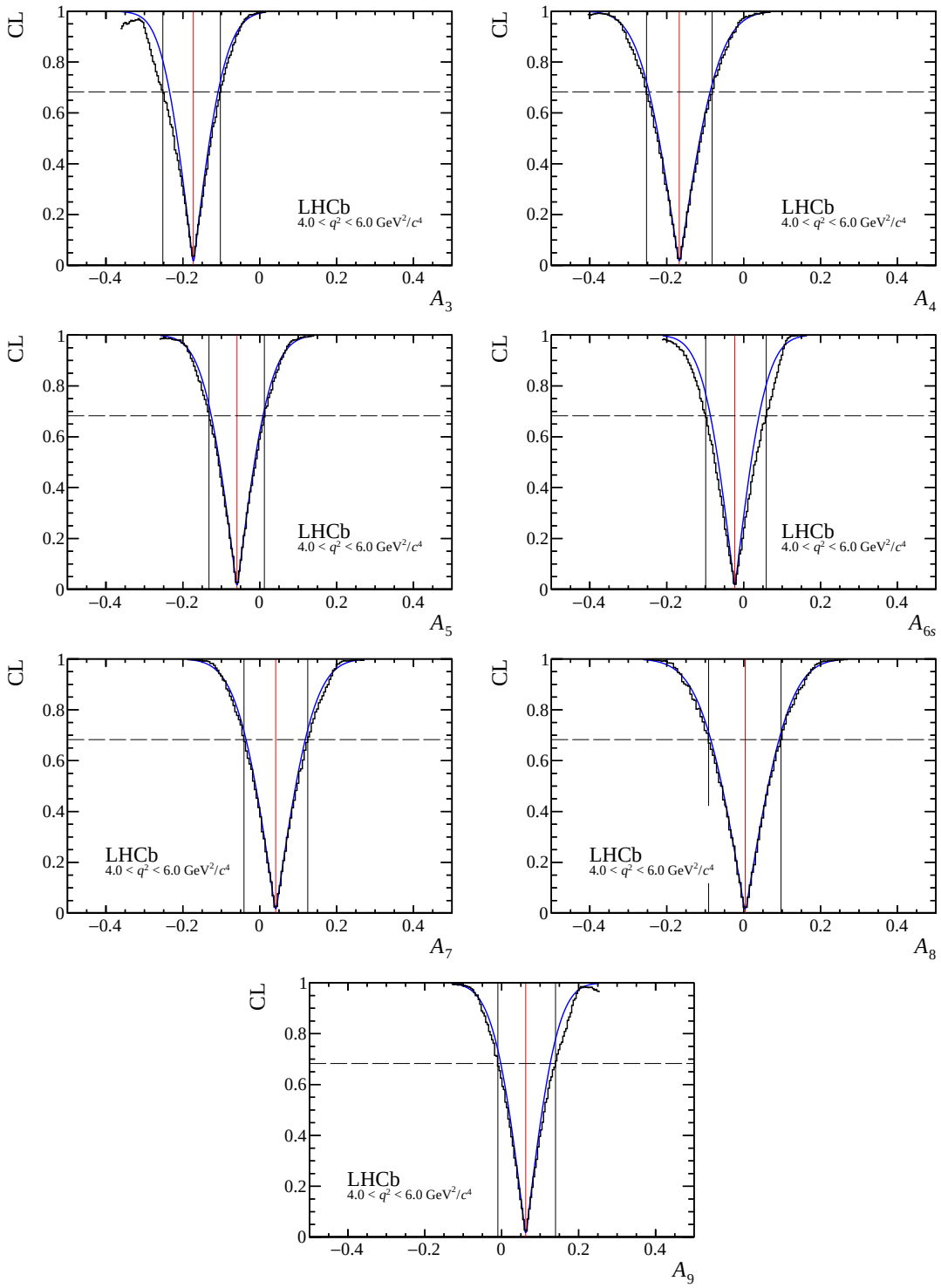

Figure 14: Confidence level (CL) obtained from a Feldman-Cousins scan using the likelihood ratio as an ordering principle (black). Nuisance parameters (including the other signal parameters) are treated with the plug-in method. The CL from a profile likelihood scan of the parameter is shown as the continuous (blue) curve. The 68% confidence interval from the Feldman-Cousins scan is indicated by the vertical lines.

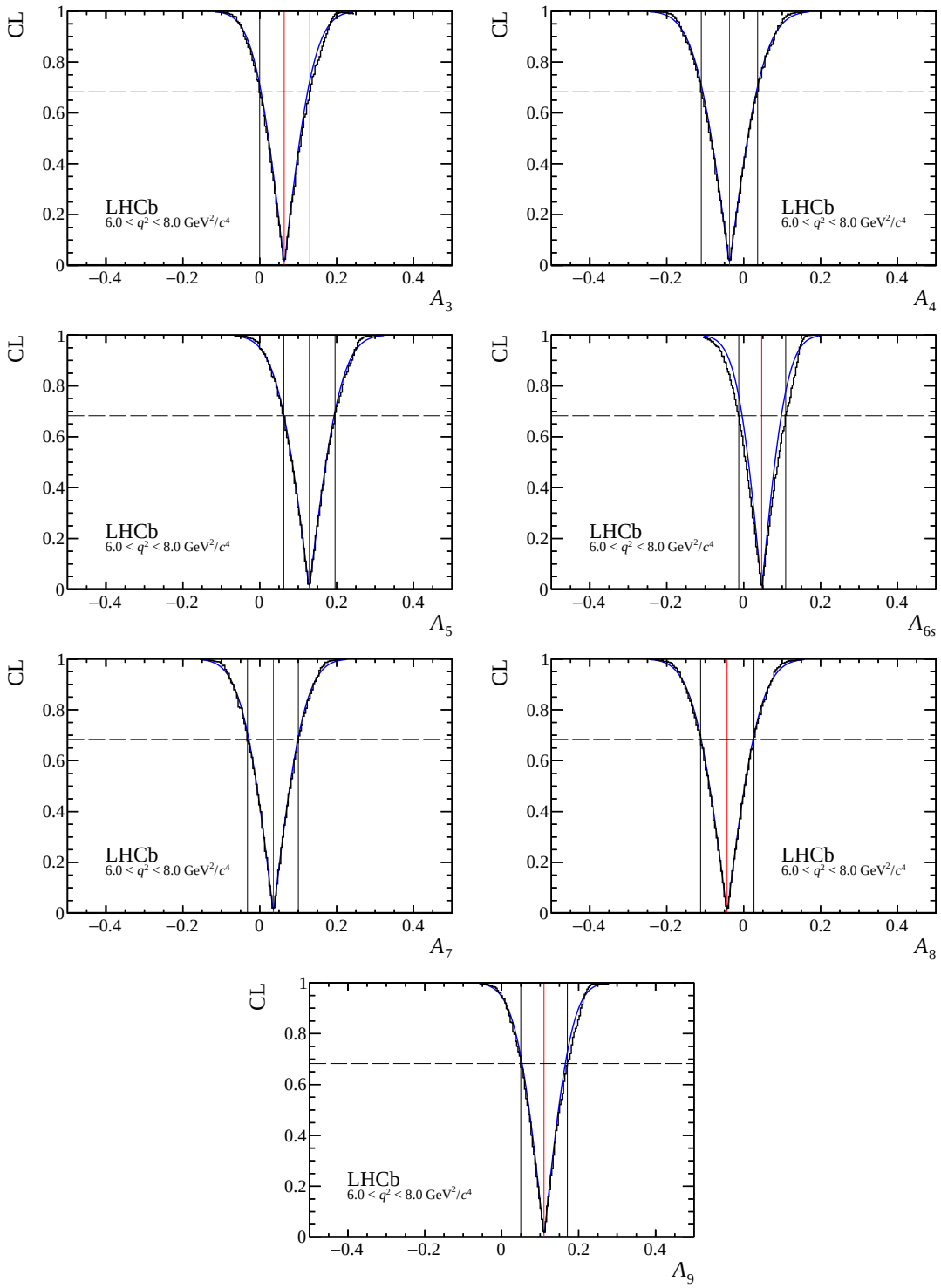

Figure 15: Confidence level (CL) obtained from a Feldman-Cousins scan using the likelihood ratio as an ordering principle (black). Nuisance parameters (including the other signal parameters) are treated with the plug-in method. The CL from a profile likelihood scan of the parameter is shown as the continuous (blue) curve. The 68% confidence interval from the Feldman-Cousins scan is indicated by the vertical lines.

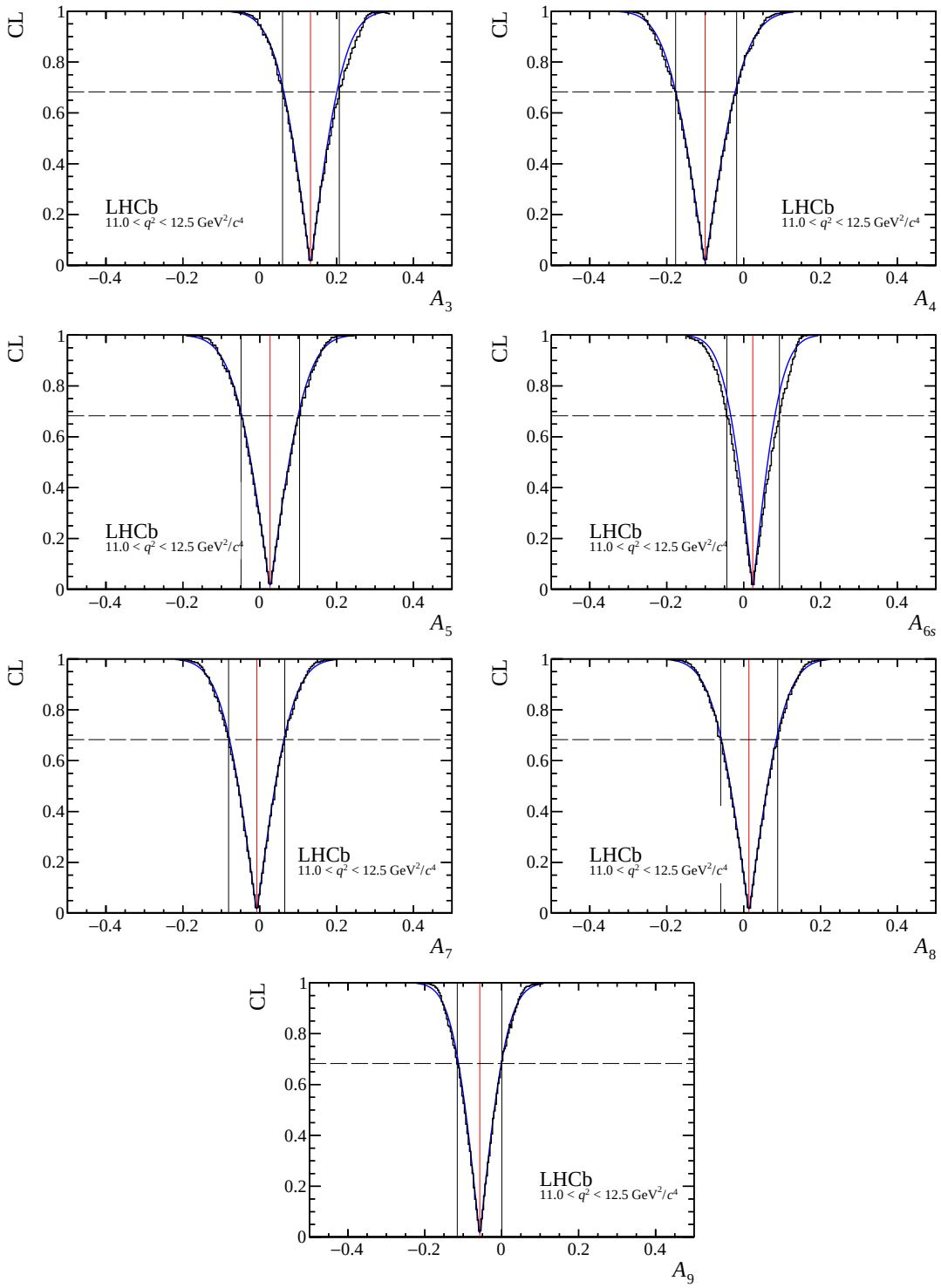

Figure 16: Confidence level (CL) obtained from a Feldman-Cousins scan using the likelihood ratio as an ordering principle (black). Nuisance parameters (including the other signal parameters) are treated with the plug-in method. The CL from a profile likelihood scan of the parameter is shown as the continuous (blue) curve. The 68% confidence interval from the Feldman-Cousins scan is indicated by the vertical lines.

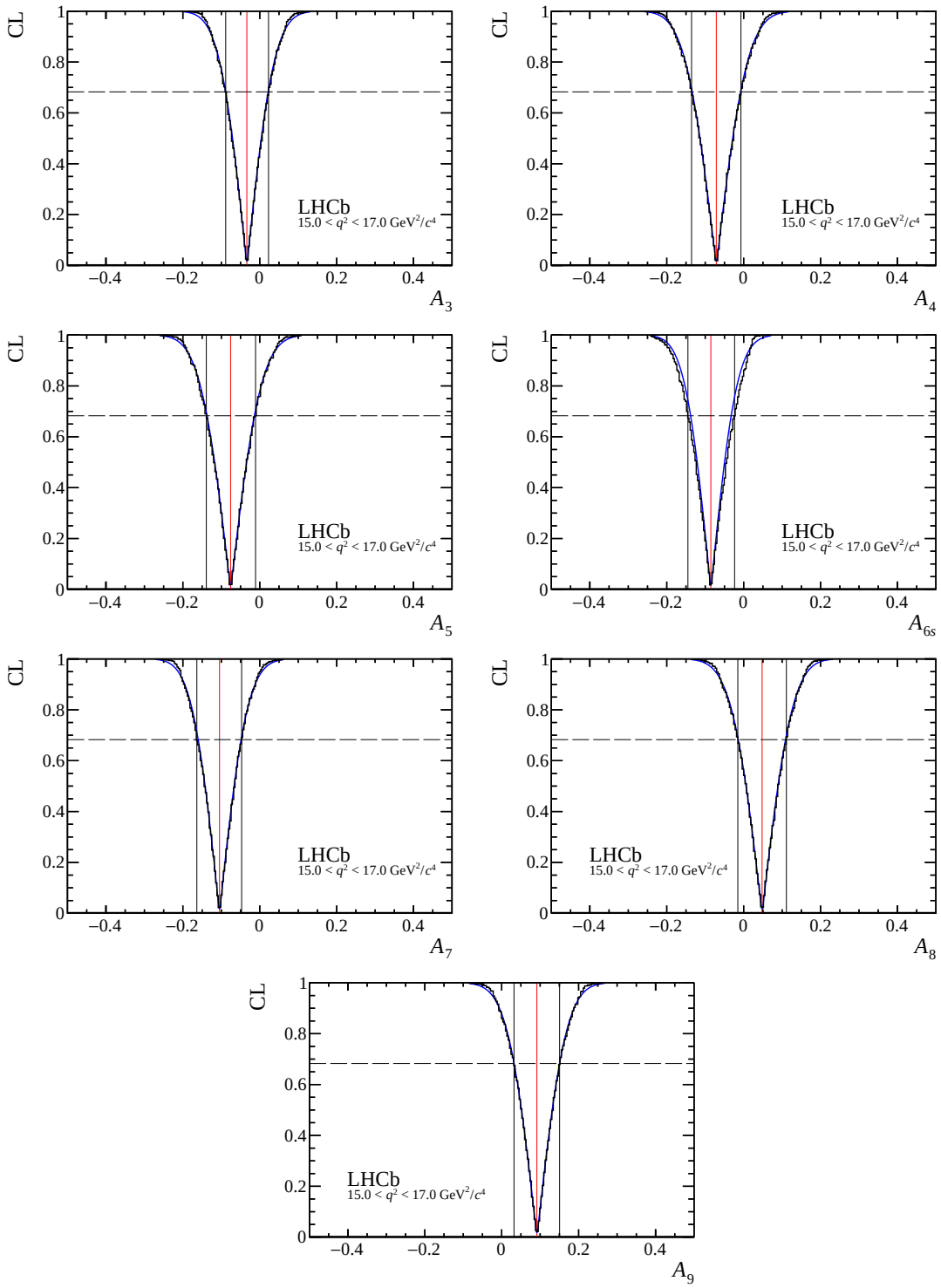

Figure 17: Confidence level (CL) obtained from a Feldman-Cousins scan using the likelihood ratio as an ordering principle (black). Nuisance parameters (including the other signal parameters) are treated with the plug-in method. The CL from a profile likelihood scan of the parameter is shown as the continuous (blue) curve. The 68% confidence interval from the Feldman-Cousins scan is indicated by the vertical lines.

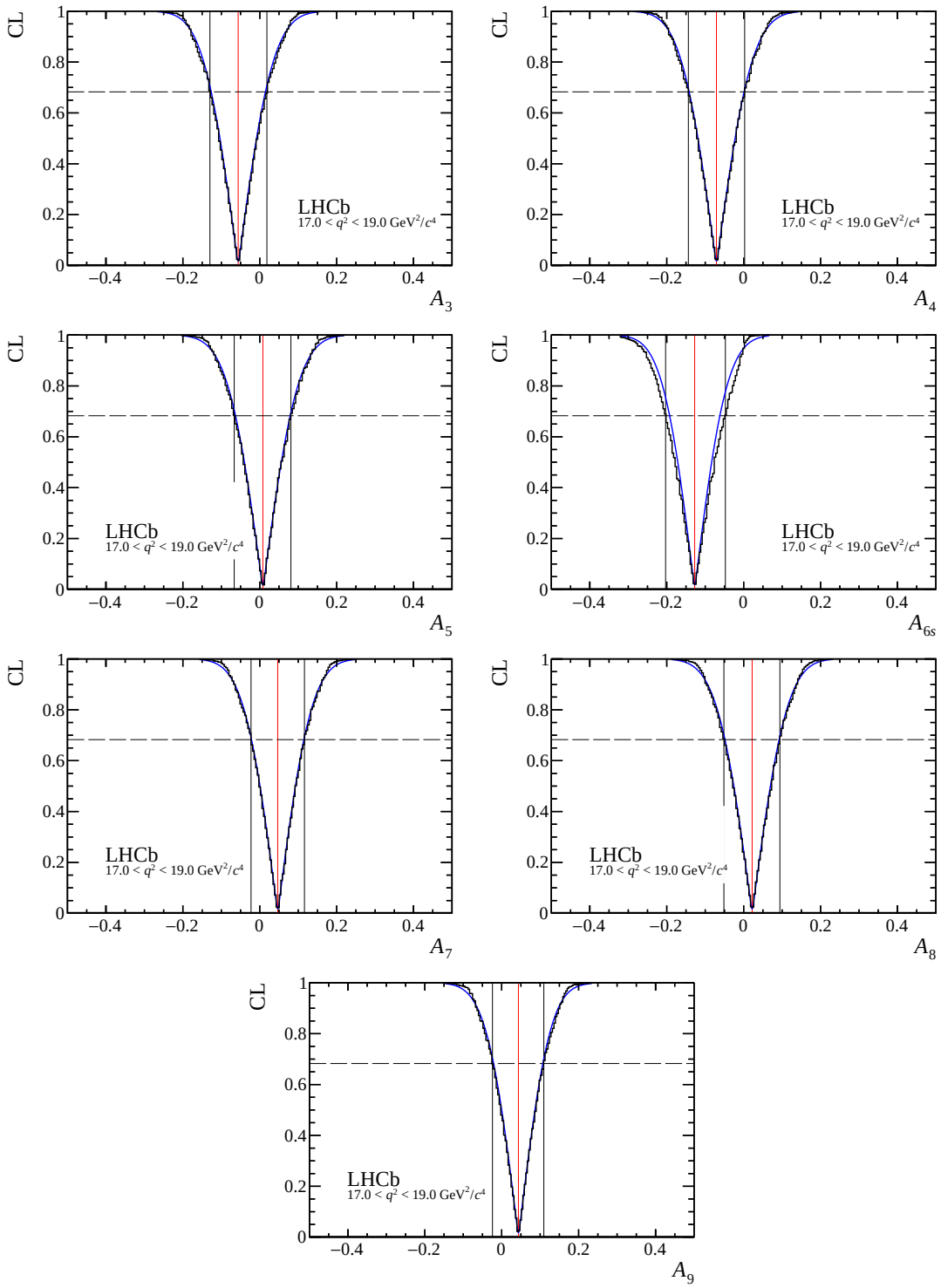

Figure 18: Confidence level (CL) obtained from a Feldman-Cousins scan using the likelihood ratio as an ordering principle (black). Nuisance parameters (including the other signal parameters) are treated with the plug-in method. The CL from a profile likelihood scan of the parameter is shown as the continuous (blue) curve. The 68% confidence interval from the Feldman-Cousins scan is indicated by the vertical lines.

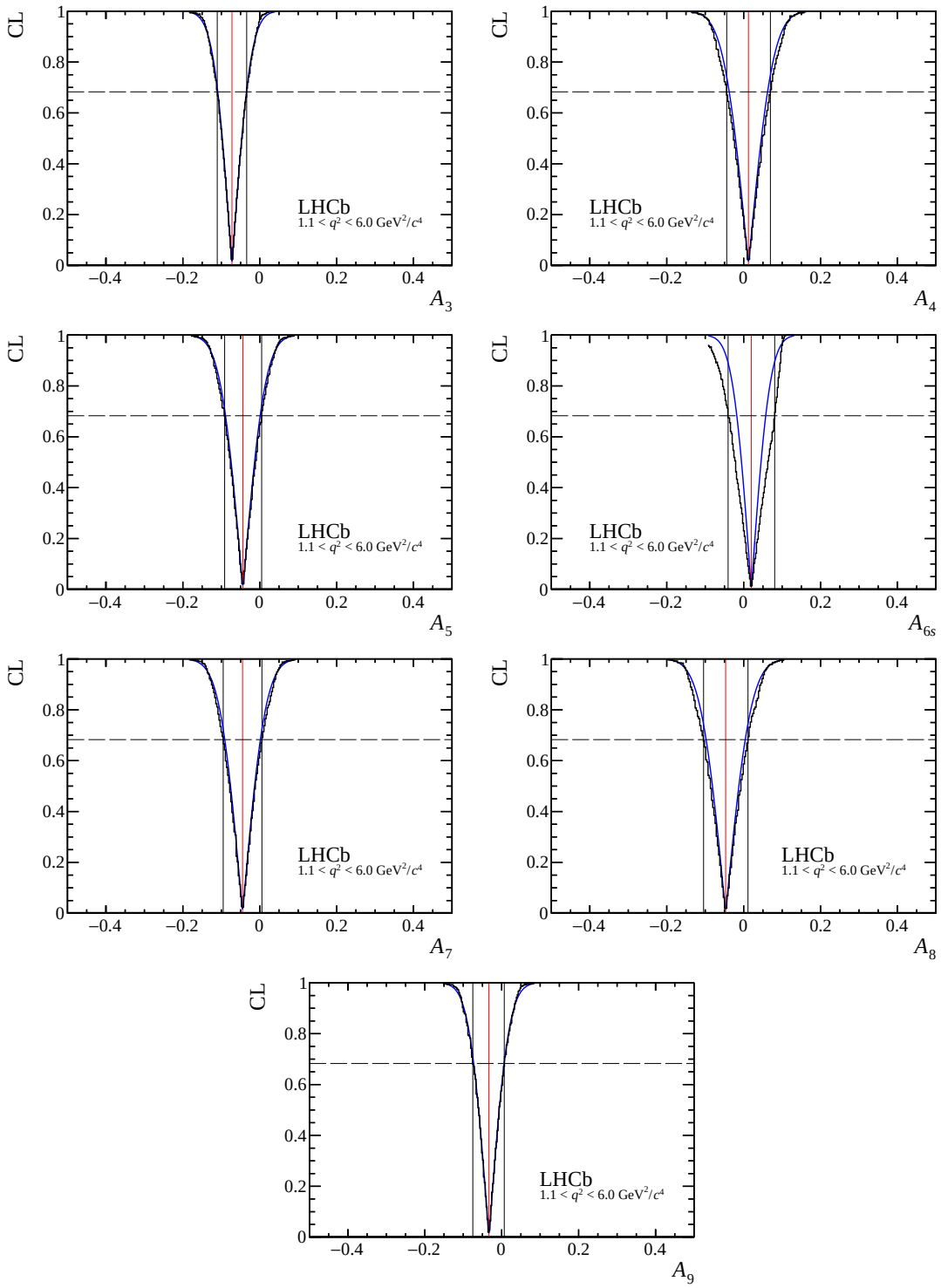

Figure 19: Confidence level (CL) obtained from a Feldman-Cousins scan using the likelihood ratio as an ordering principle (black). Nuisance parameters (including the other signal parameters) are treated with the plug-in method. The CL from a profile likelihood scan of the parameter is shown as the continuous (blue) curve. The 68% confidence interval from the Feldman-Cousins scan is indicated by the vertical lines.

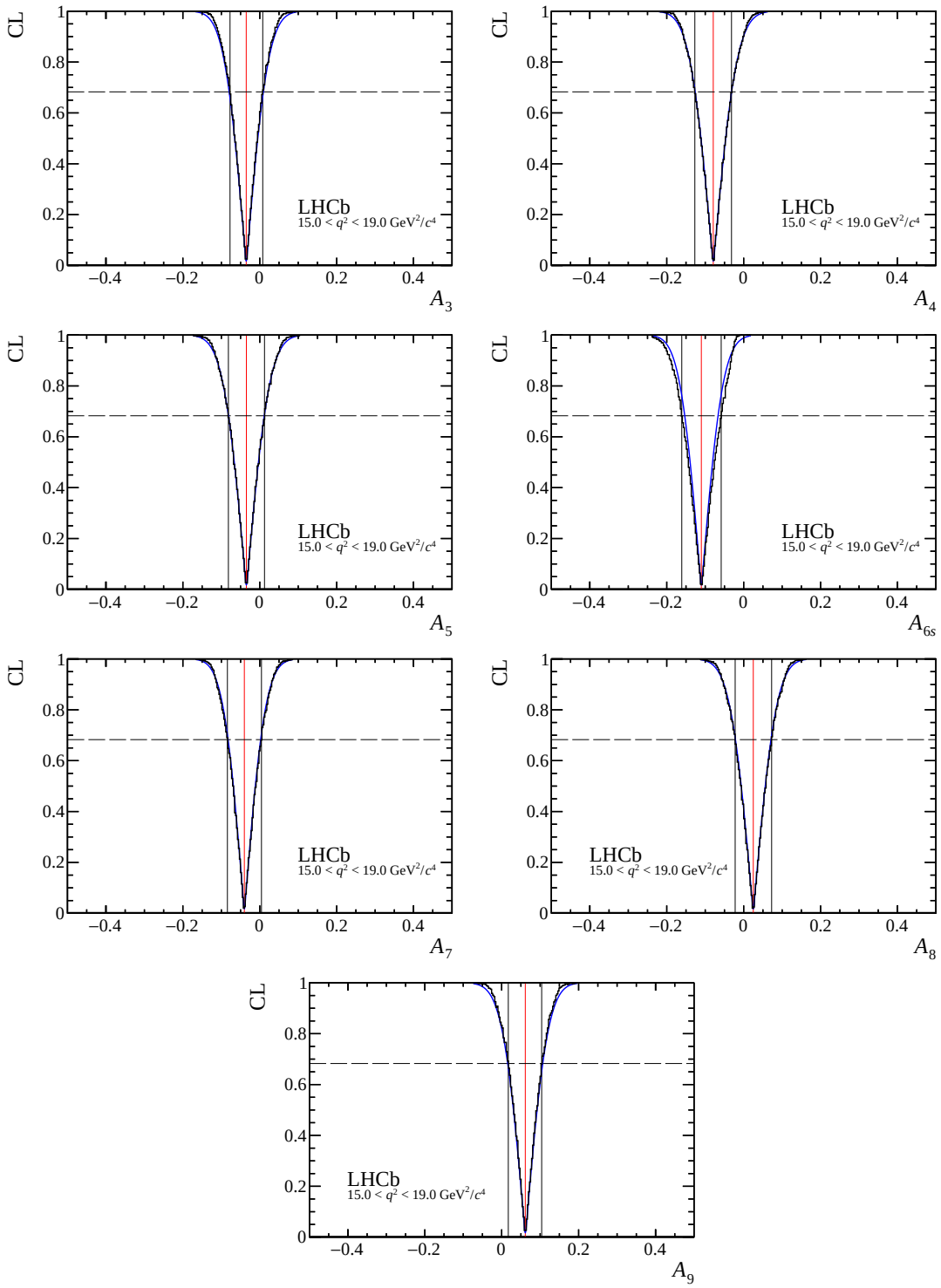

Figure 20: Confidence level (CL) obtained from a Feldman-Cousins scan using the likelihood ratio as an ordering principle (black). Nuisance parameters (including the other signal parameters) are treated with the plug-in method. The CL from a profile likelihood scan of the parameter is shown as the continuous (blue) curve. The 68% confidence interval from the Feldman-Cousins scan is indicated by the vertical lines.

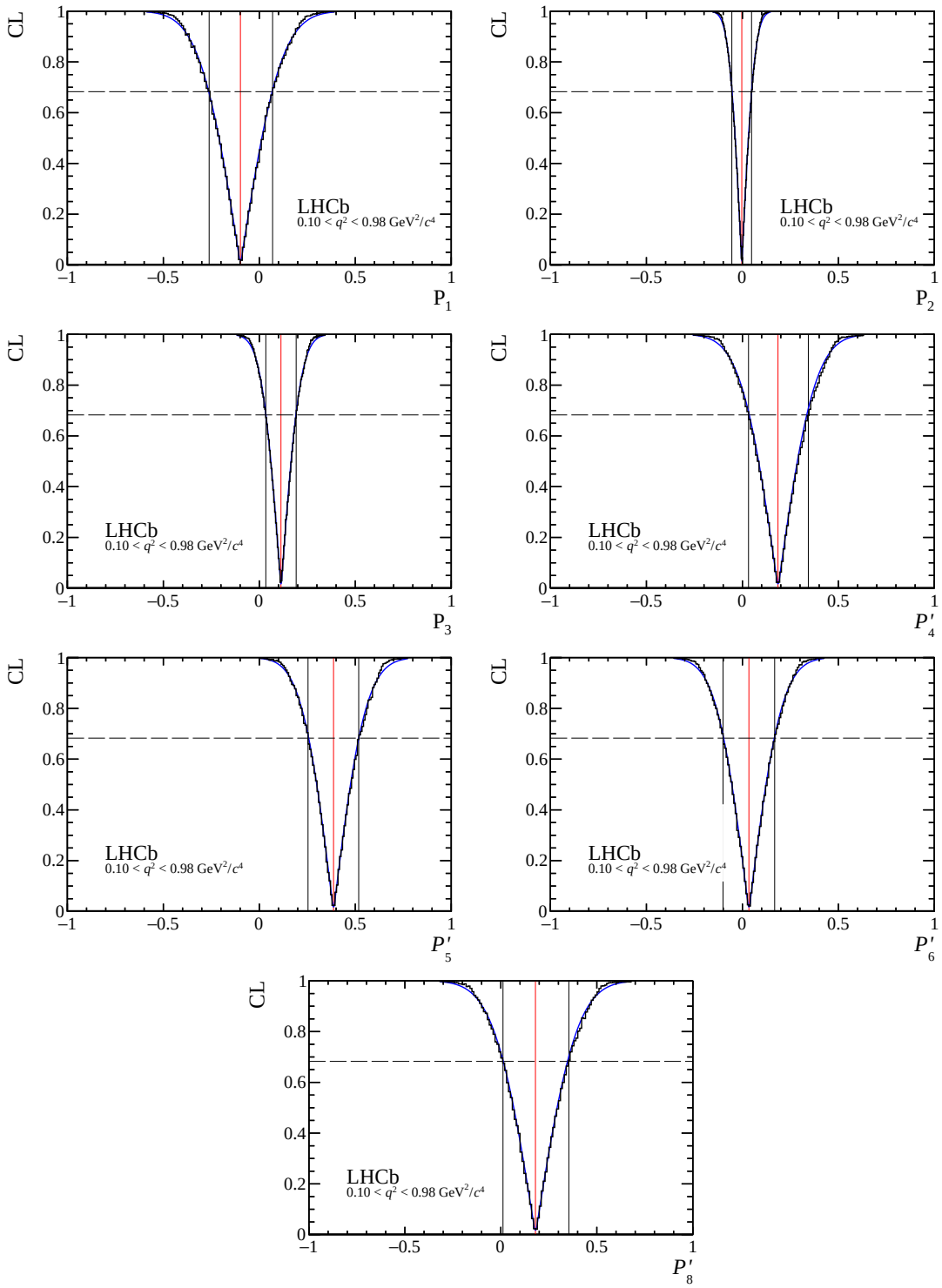

Figure 21: Confidence level (CL) obtained from a Feldman-Cousins scan using the likelihood ratio as an ordering principle (black). Nuisance parameters (including the other signal parameters) are treated with the plug-in method. The CL from a profile likelihood scan of the parameter is shown as the continuous (blue) curve. The 68% confidence interval from the Feldman-Cousins scan is indicated by the vertical lines.

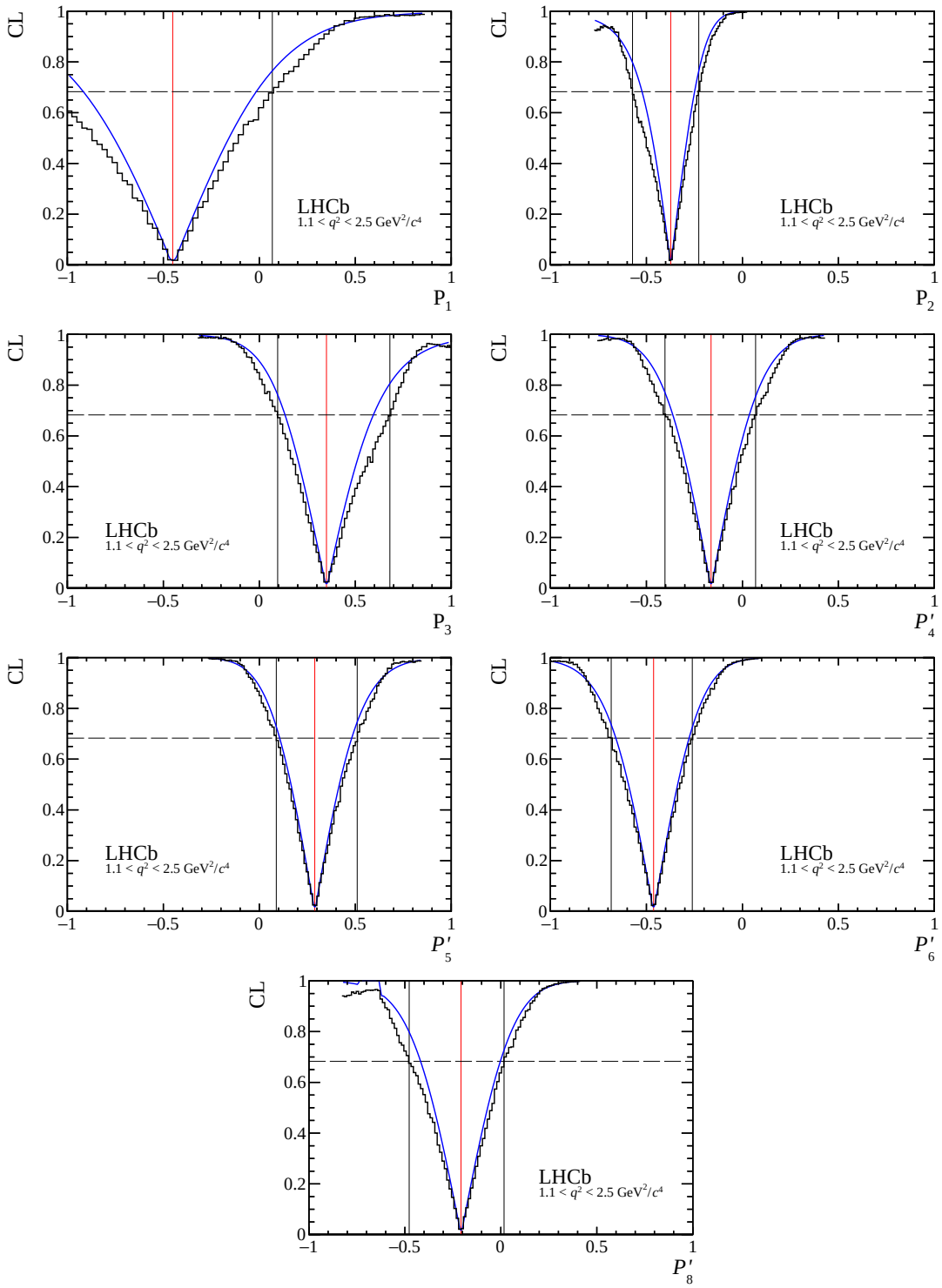

Figure 22: Confidence level (CL) obtained from a Feldman-Cousins scan using the likelihood ratio as an ordering principle (black). Nuisance parameters (including the other signal parameters) are treated with the plug-in method. The CL from a profile likelihood scan of the parameter is shown as the continuous (blue) curve. The 68% confidence interval from the Feldman-Cousins scan is indicated by the vertical lines.

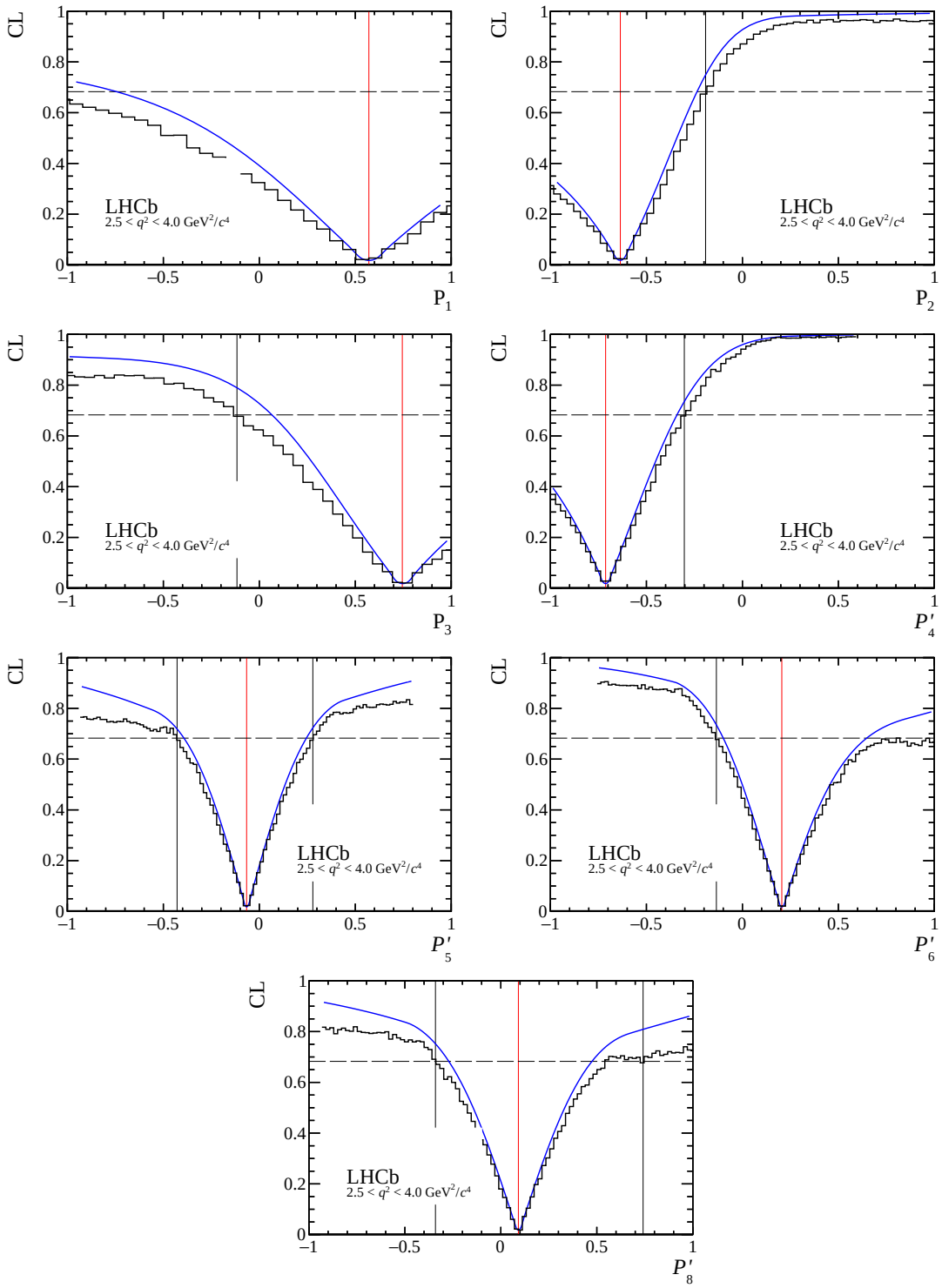

Figure 23: Confidence level (CL) obtained from a Feldman-Cousins scan using the likelihood ratio as an ordering principle (black). Nuisance parameters (including the other signal parameters) are treated with the plug-in method. The CL from a profile likelihood scan of the parameter is shown as the continuous (blue) curve. The 68% confidence interval from the Feldman-Cousins scan is indicated by the vertical lines.

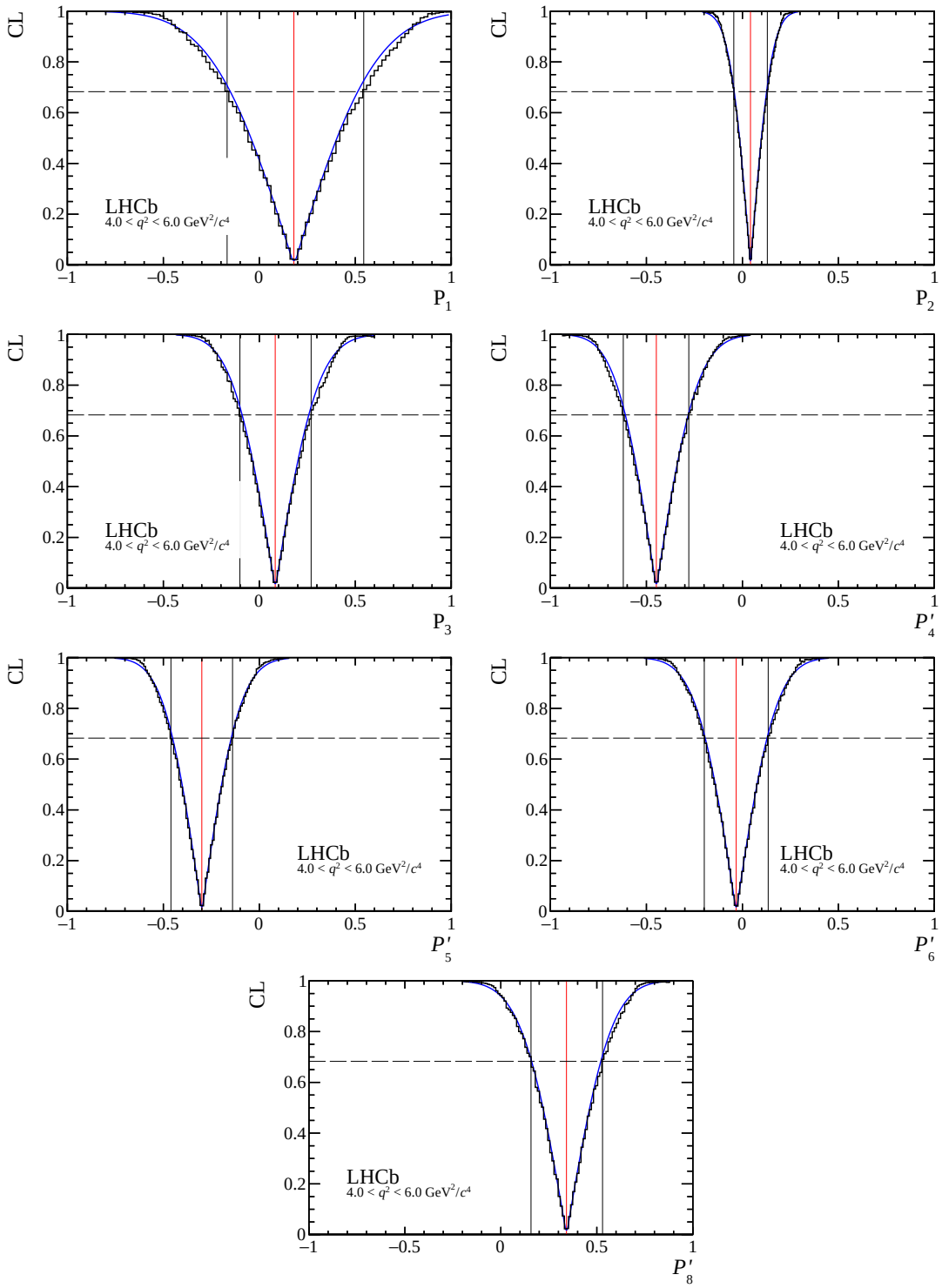

Figure 24: Confidence level (CL) obtained from a Feldman-Cousins scan using the likelihood ratio as an ordering principle (black). Nuisance parameters (including the other signal parameters) are treated with the plug-in method. The CL from a profile likelihood scan of the parameter is shown as the continuous (blue) curve. The 68% confidence interval from the Feldman-Cousins scan is indicated by the vertical lines.

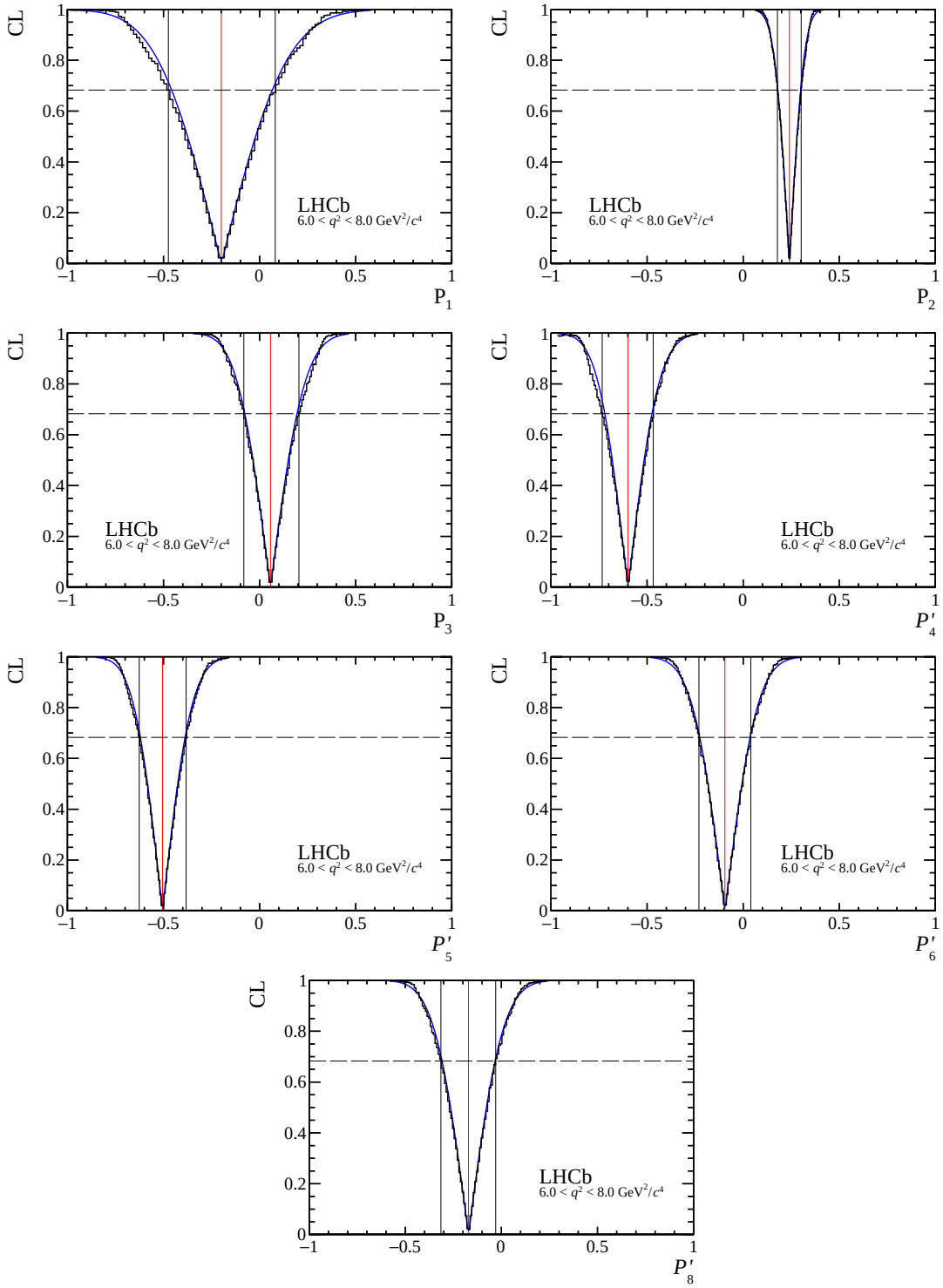

Figure 25: Confidence level (CL) obtained from a Feldman-Cousins scan using the likelihood ratio as an ordering principle (black). Nuisance parameters (including the other signal parameters) are treated with the plug-in method. The CL from a profile likelihood scan of the parameter is shown as the continuous (blue) curve. The 68% confidence interval from the Feldman-Cousins scan is indicated by the vertical lines.

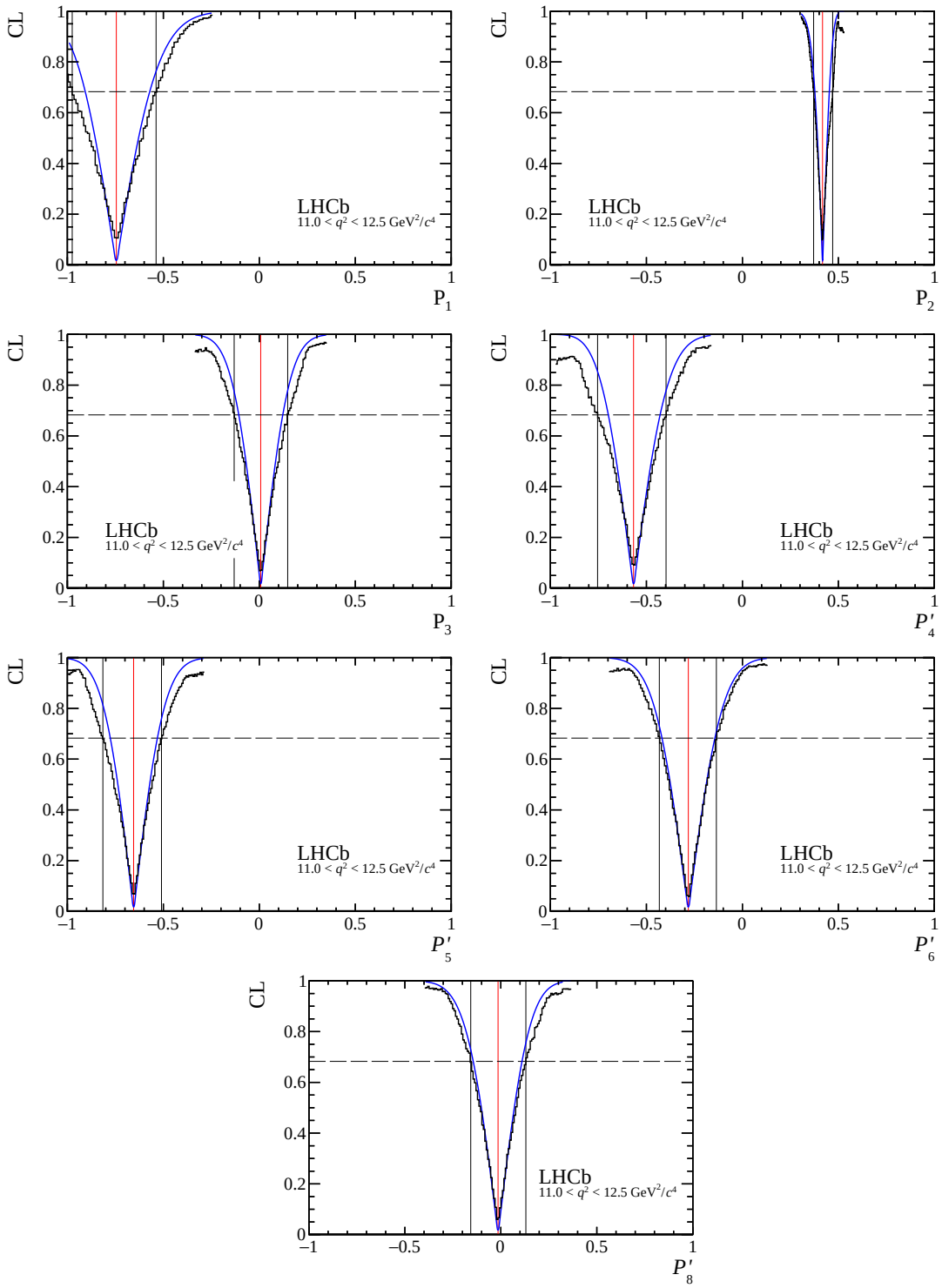

Figure 26: Confidence level (CL) obtained from a Feldman-Cousins scan using the likelihood ratio as an ordering principle (black). Nuisance parameters (including the other signal parameters) are treated with the plug-in method. The CL from a profile likelihood scan of the parameter is shown as the continuous (blue) curve. The 68% confidence interval from the Feldman-Cousins scan is indicated by the vertical lines.

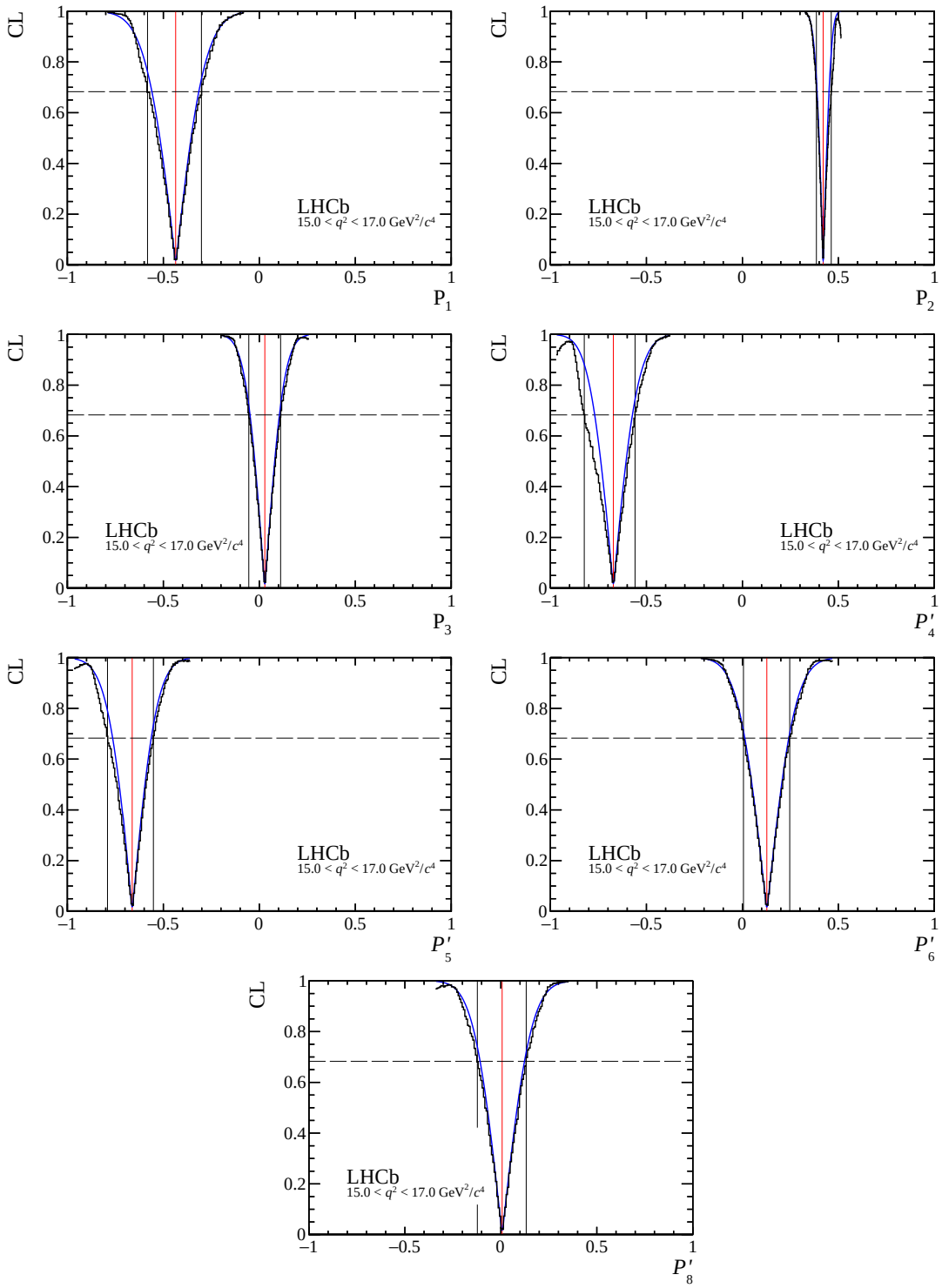

Figure 27: Confidence level (CL) obtained from a Feldman-Cousins scan using the likelihood ratio as an ordering principle (black). Nuisance parameters (including the other signal parameters) are treated with the plug-in method. The CL from a profile likelihood scan of the parameter is shown as the continuous (blue) curve. The 68% confidence interval from the Feldman-Cousins scan is indicated by the vertical lines.

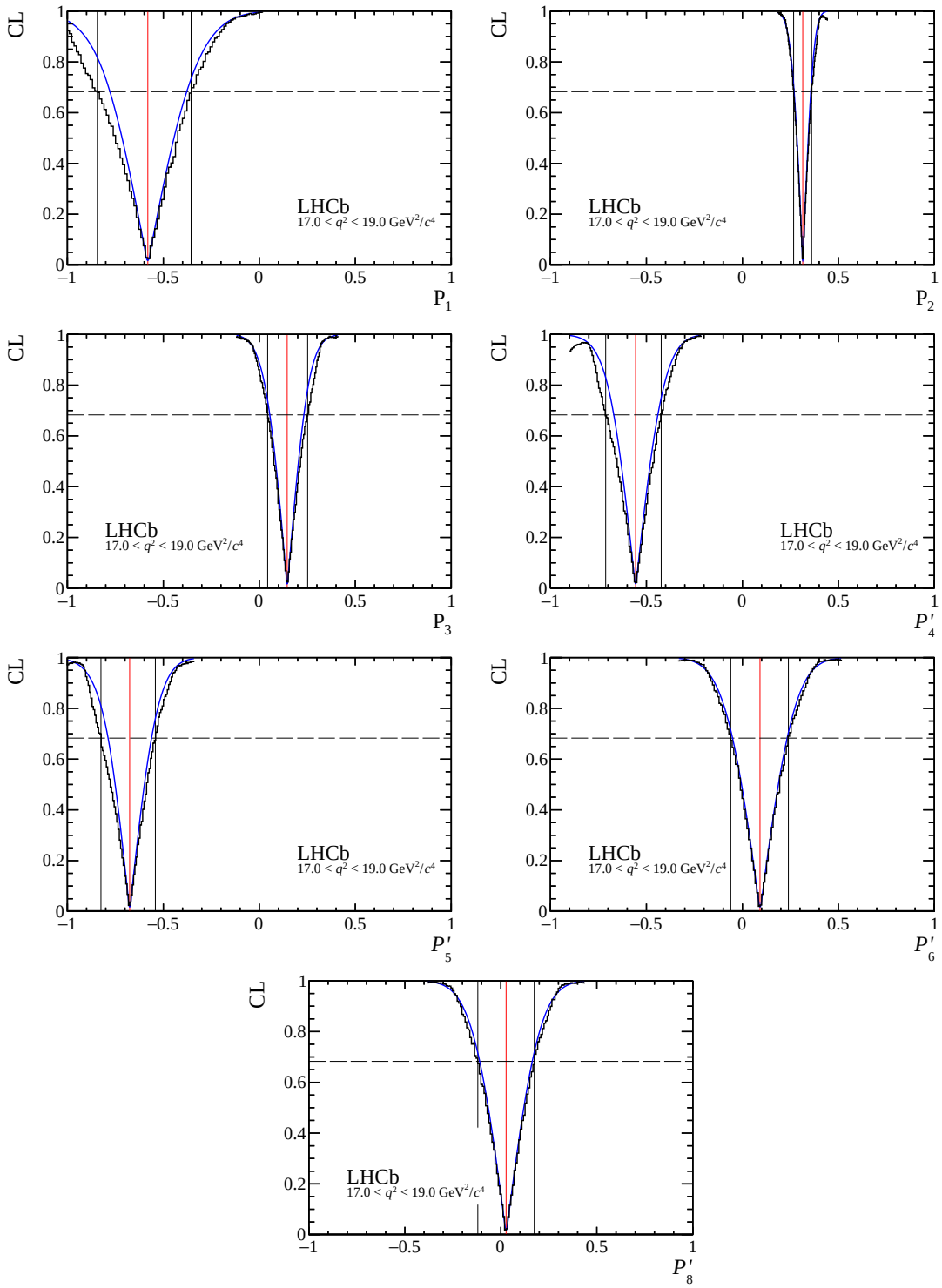

Figure 28: Confidence level (CL) obtained from a Feldman-Cousins scan using the likelihood ratio as an ordering principle (black). Nuisance parameters (including the other signal parameters) are treated with the plug-in method. The CL from a profile likelihood scan of the parameter is shown as the continuous (blue) curve. The 68% confidence interval from the Feldman-Cousins scan is indicated by the vertical lines.

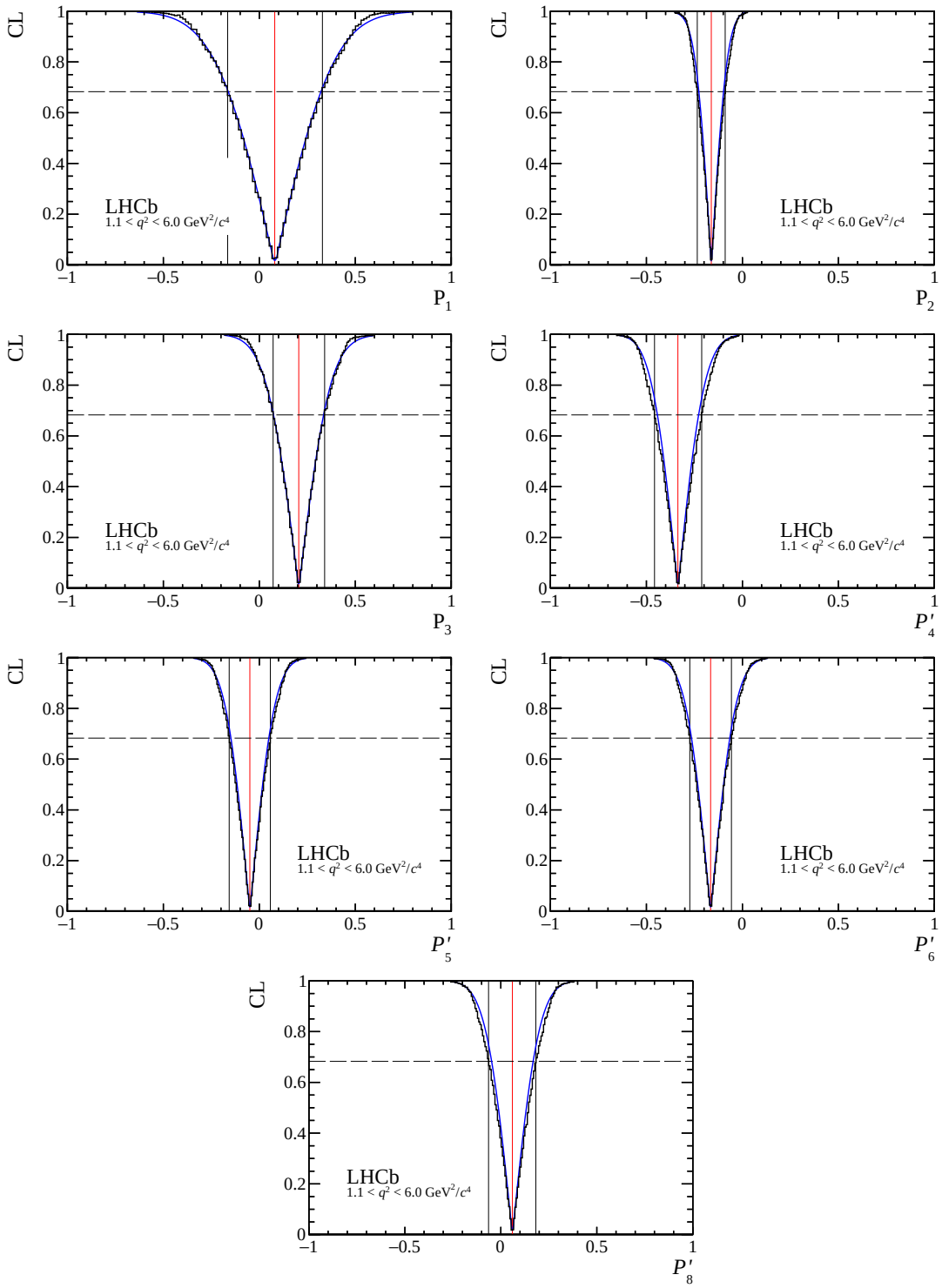

Figure 29: Confidence level (CL) obtained from a Feldman-Cousins scan using the likelihood ratio as an ordering principle (black). Nuisance parameters (including the other signal parameters) are treated with the plug-in method. The CL from a profile likelihood scan of the parameter is shown as the continuous (blue) curve. The 68% confidence interval from the Feldman-Cousins scan is indicated by the vertical lines.

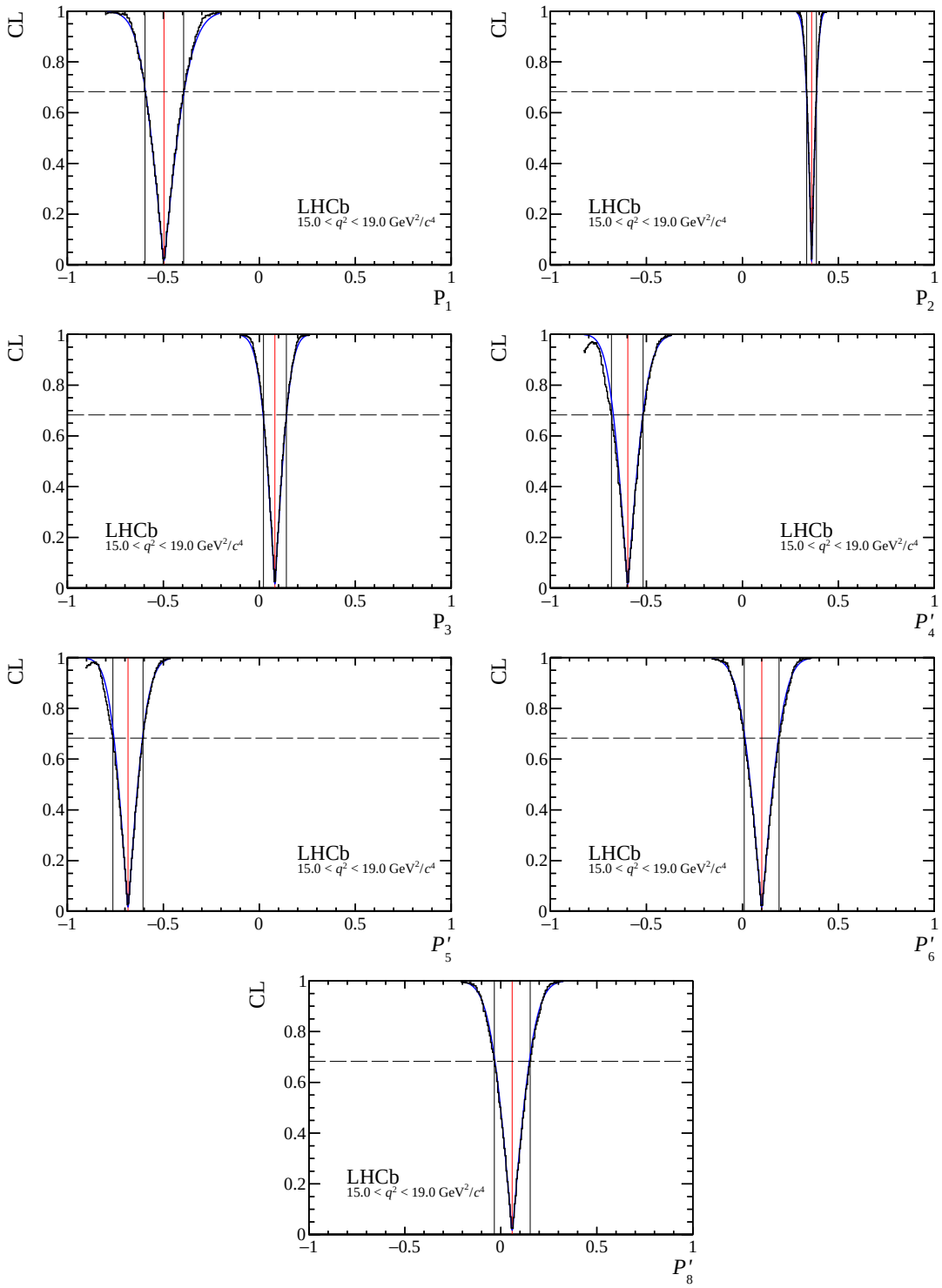

Figure 30: Confidence level (CL) obtained from a Feldman-Cousins scan using the likelihood ratio as an ordering principle (black). Nuisance parameters (including the other signal parameters) are treated with the plug-in method. The CL from a profile likelihood scan of the parameter is shown as the continuous (blue) curve. The 68% confidence interval from the Feldman-Cousins scan is indicated by the vertical lines.

2 Bootstrap distributions for the angular moments

Figures 31–75 show the distribution of the observables obtained by a bootstrapping technique. The *CP*-averaged observables and *CP* asymmetries are distributed as a normal distribution about the values measured in the dataset. The $P_i^{(\prime)}$ observables depend on the *CP*-averaged observables in a non-linear way. Consequently, these observables are not normally distributed. The shaded region in the figures corresponds to the quoted 68% confidence interval. Candidates with non-physical values of $F_{\rm L}$ ($F_{\rm L} < 0$ or $F_{\rm L} > 1$) are not shown.

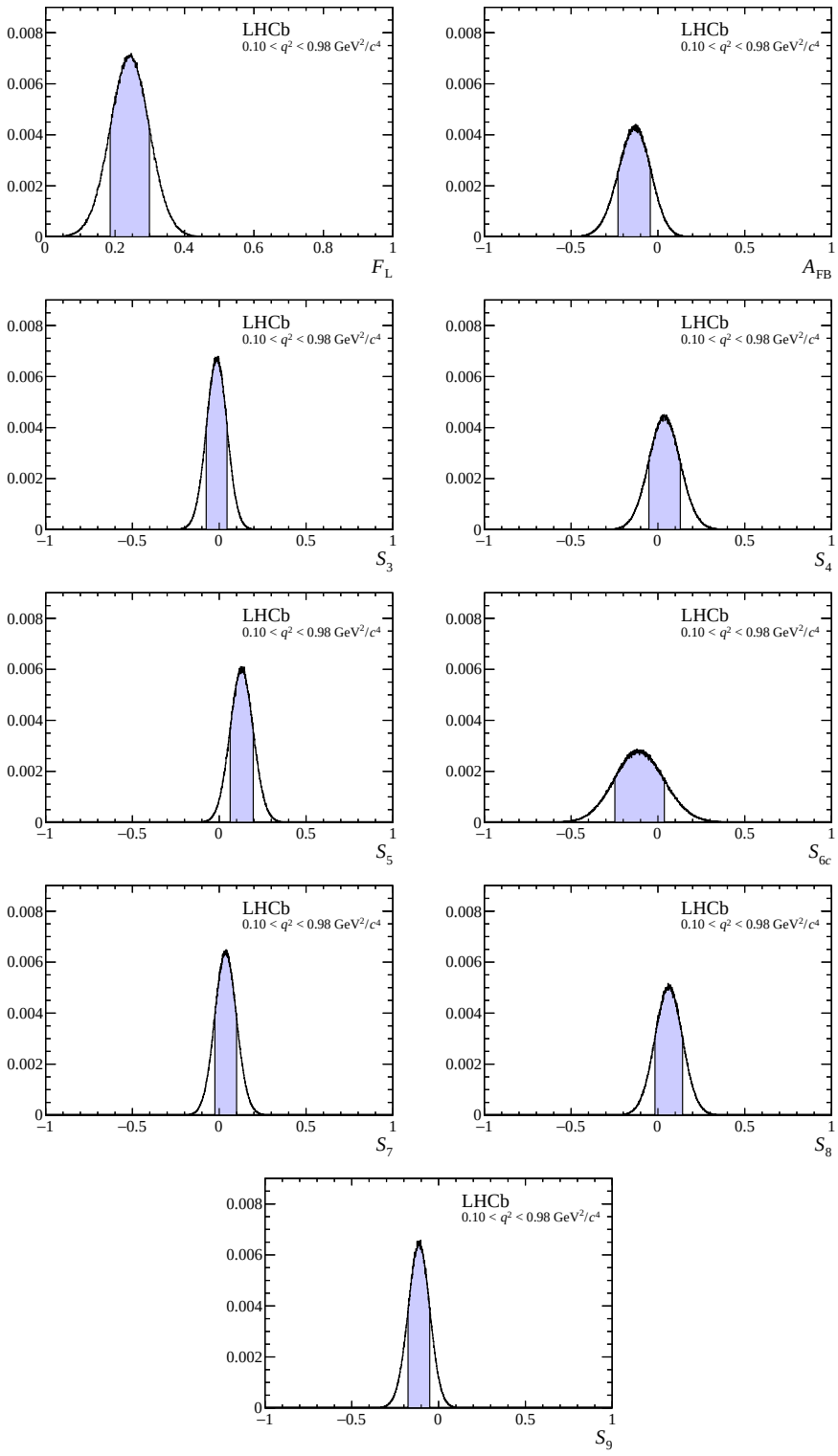

Figure 31: Distribution of pseudoexperiments obtained by applying a bootstrapping technique to the moment analysis. The 68% confidence interval on the angular observable is indicated by the shaded region.

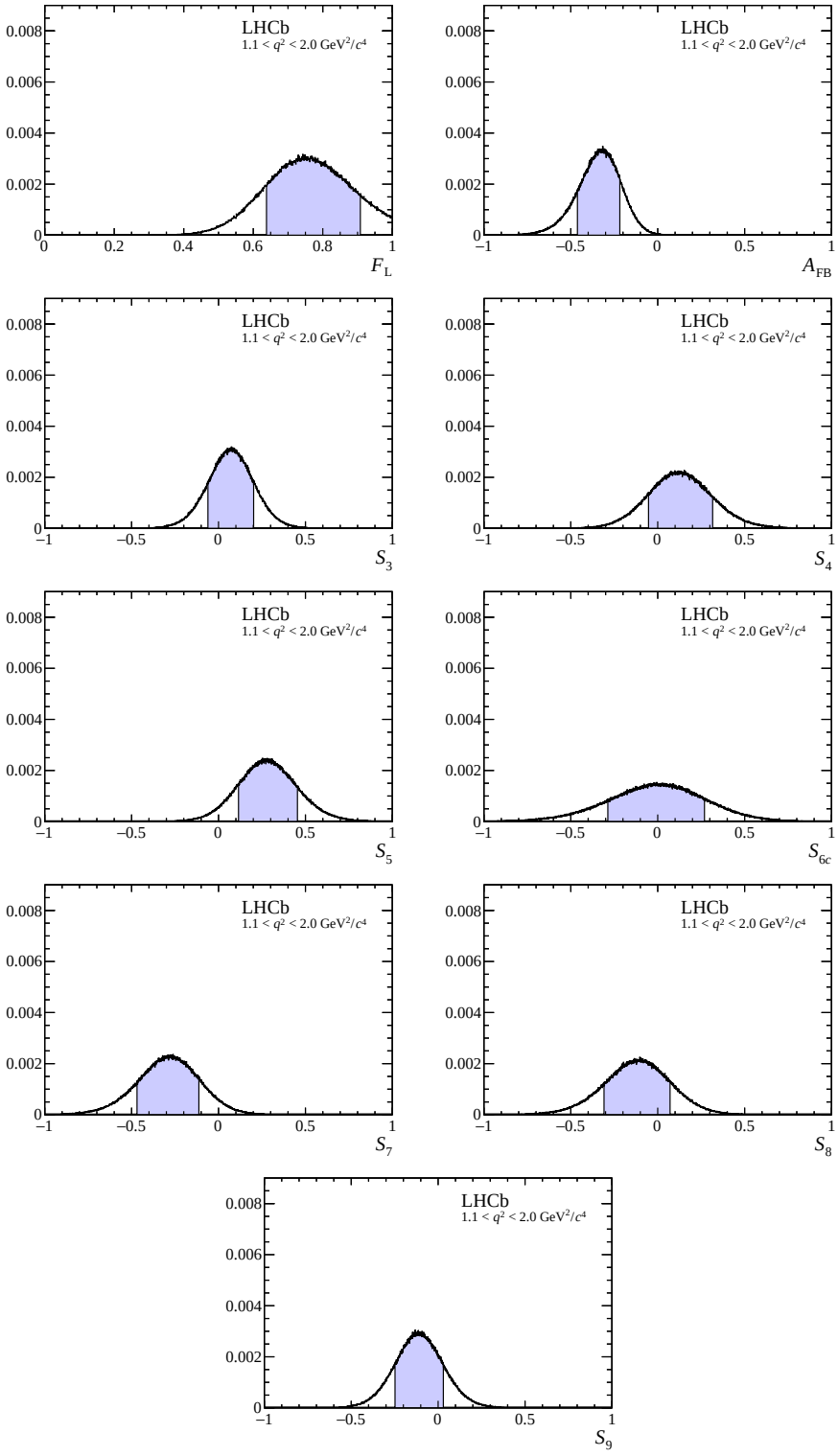

Figure 32: Distribution of pseudoexperiments obtained by applying a bootstrapping technique to the moment analysis. The 68% confidence interval on the angular observable is indicated by the shaded region.

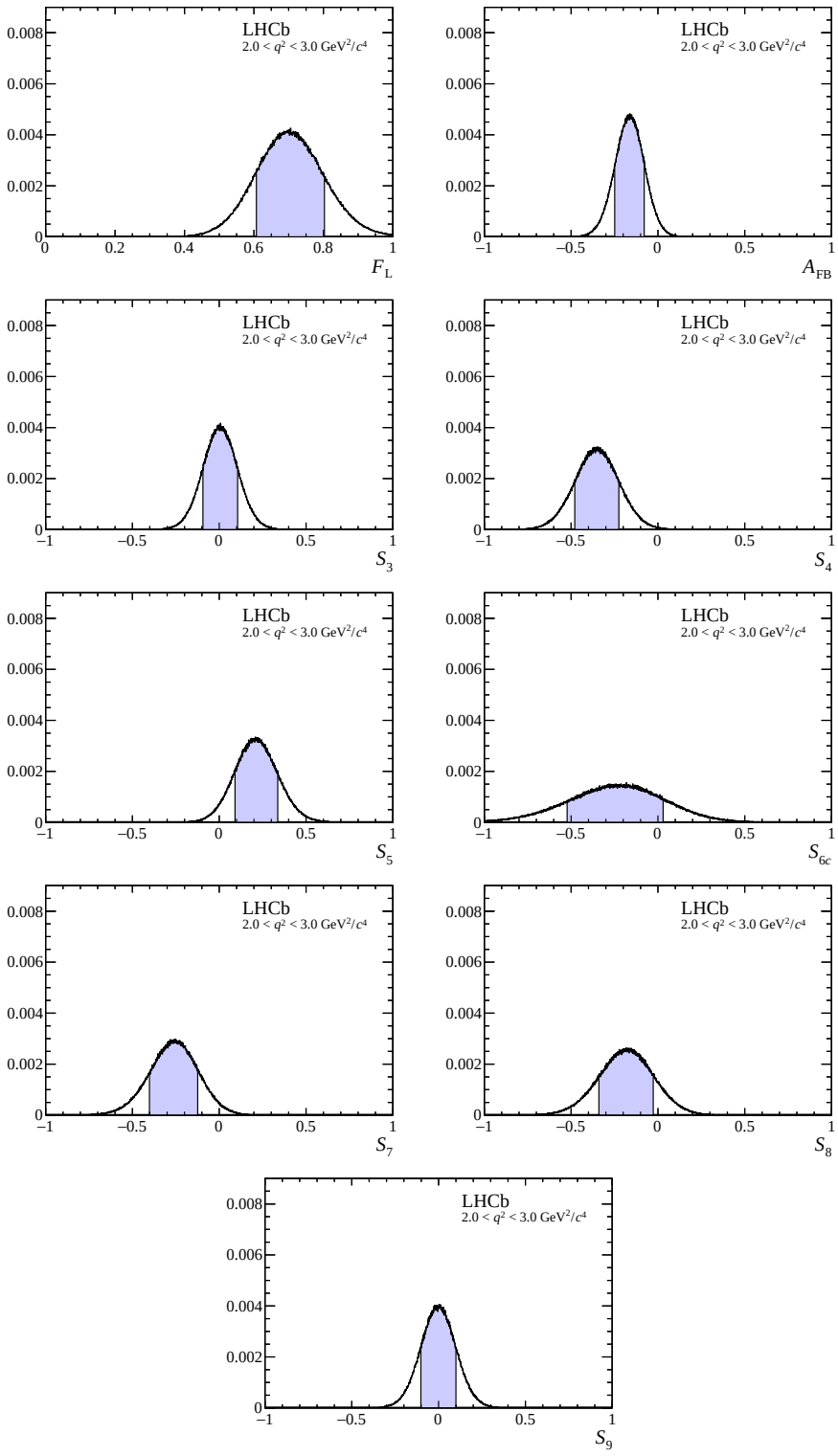

Figure 33: Distribution of pseudoexperiments obtained by applying a bootstrapping technique to the moment analysis. The 68% confidence interval on the angular observable is indicated by the shaded region.

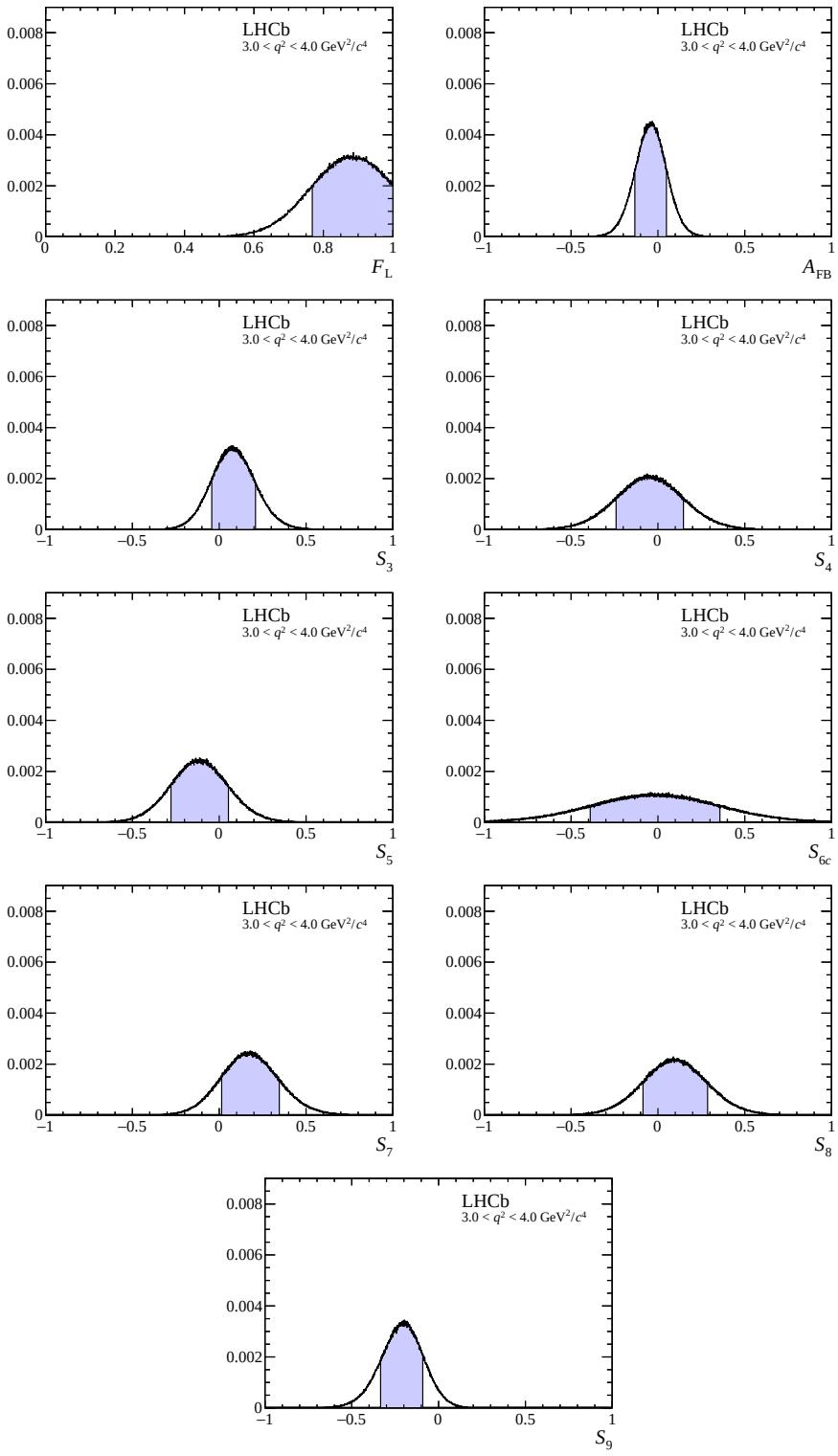

Figure 34: Distribution of pseudoexperiments obtained by applying a bootstrapping technique to the moment analysis. The 68% confidence interval on the angular observable is indicated by the shaded region.

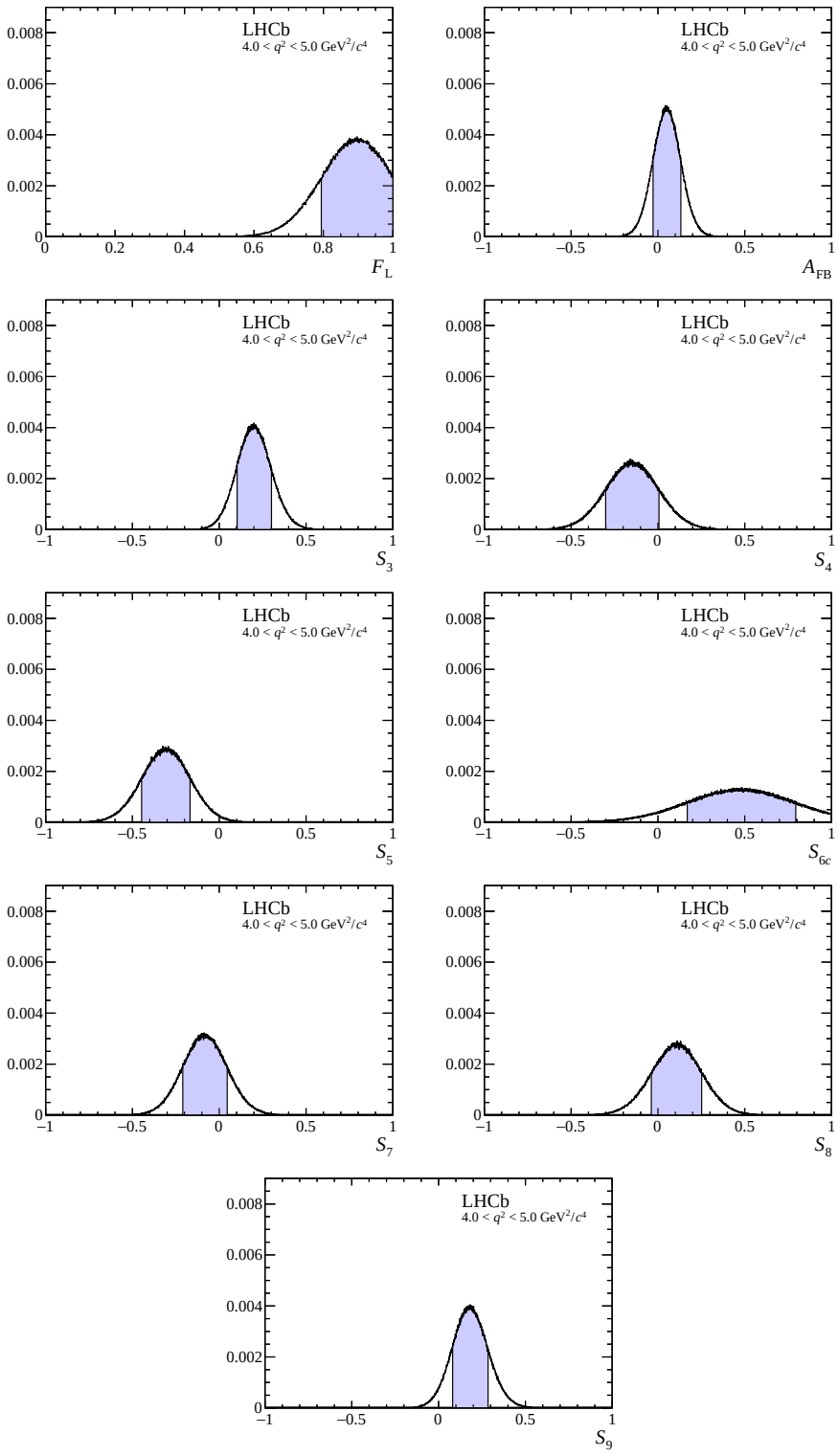

Figure 35: Distribution of pseudoexperiments obtained by applying a bootstrapping technique to the moment analysis. The 68% confidence interval on the angular observable is indicated by the shaded region.

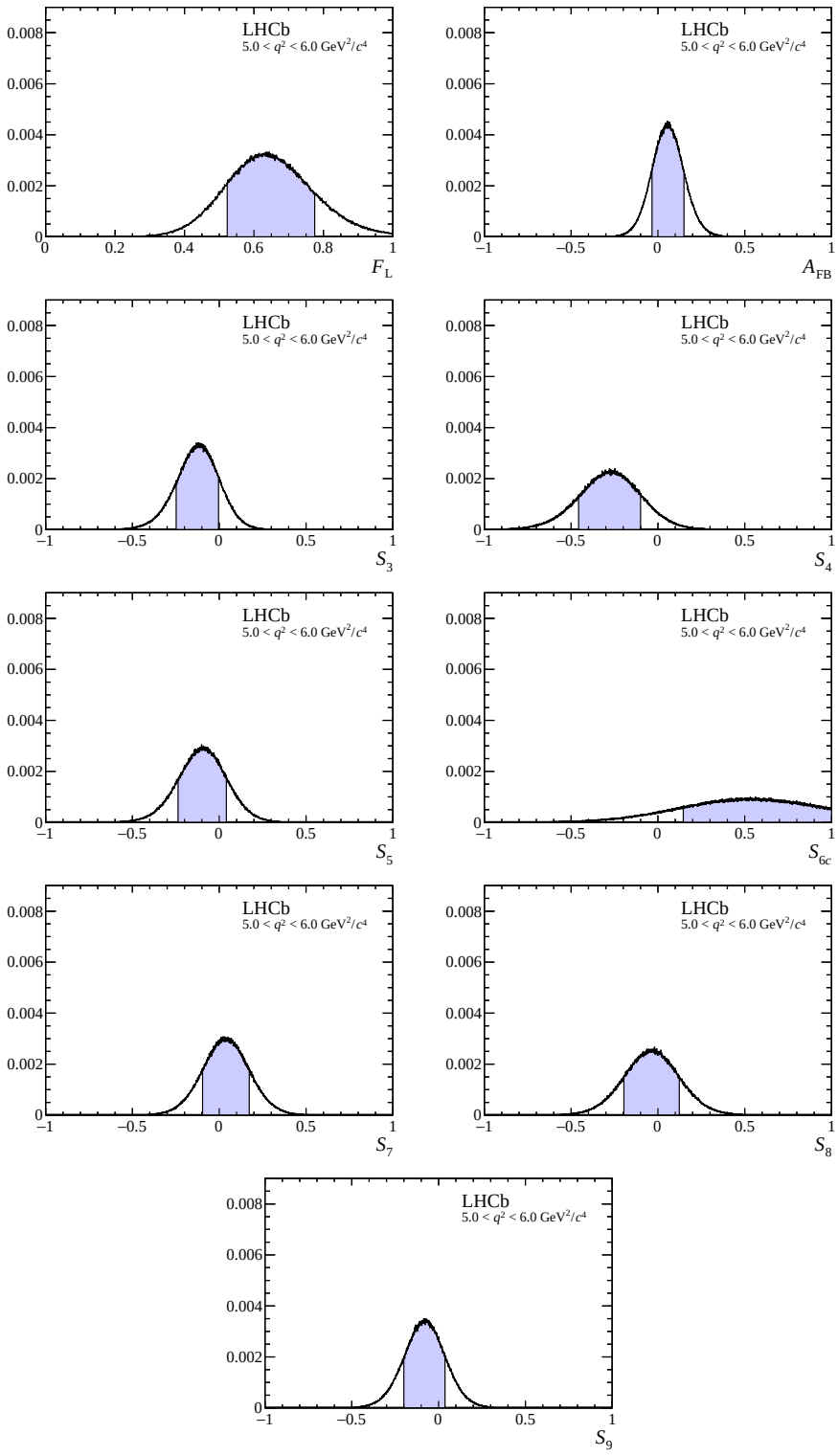

Figure 36: Distribution of pseudoexperiments obtained by applying a bootstrapping technique to the moment analysis. The 68% confidence interval on the angular observable is indicated by the shaded region.

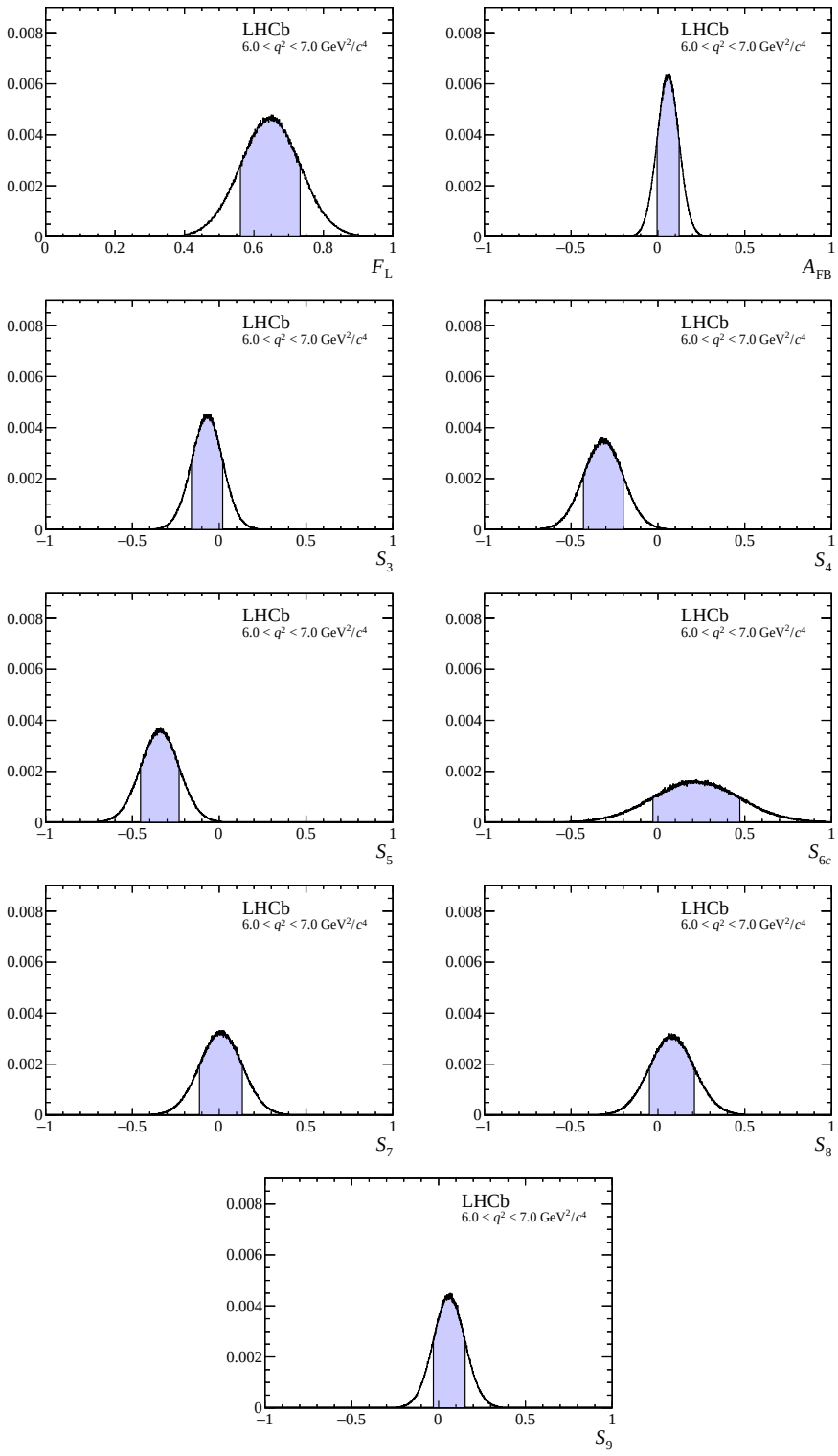

Figure 37: Distribution of pseudoexperiments obtained by applying a bootstrapping technique to the moment analysis. The 68% confidence interval on the angular observable is indicated by the shaded region.

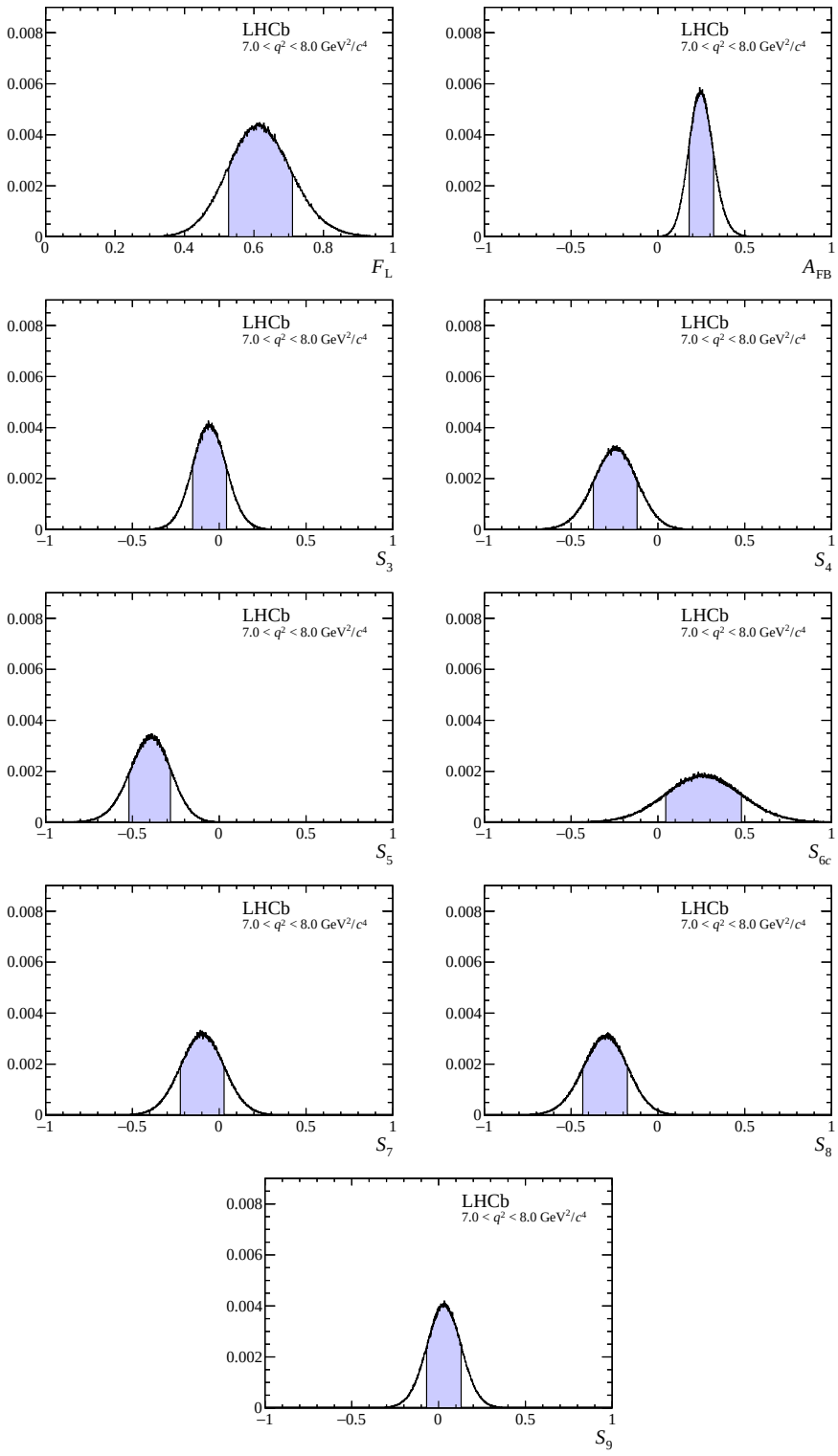

Figure 38: Distribution of pseudoexperiments obtained by applying a bootstrapping technique to the moment analysis. The 68% confidence interval on the angular observable is indicated by the shaded region.

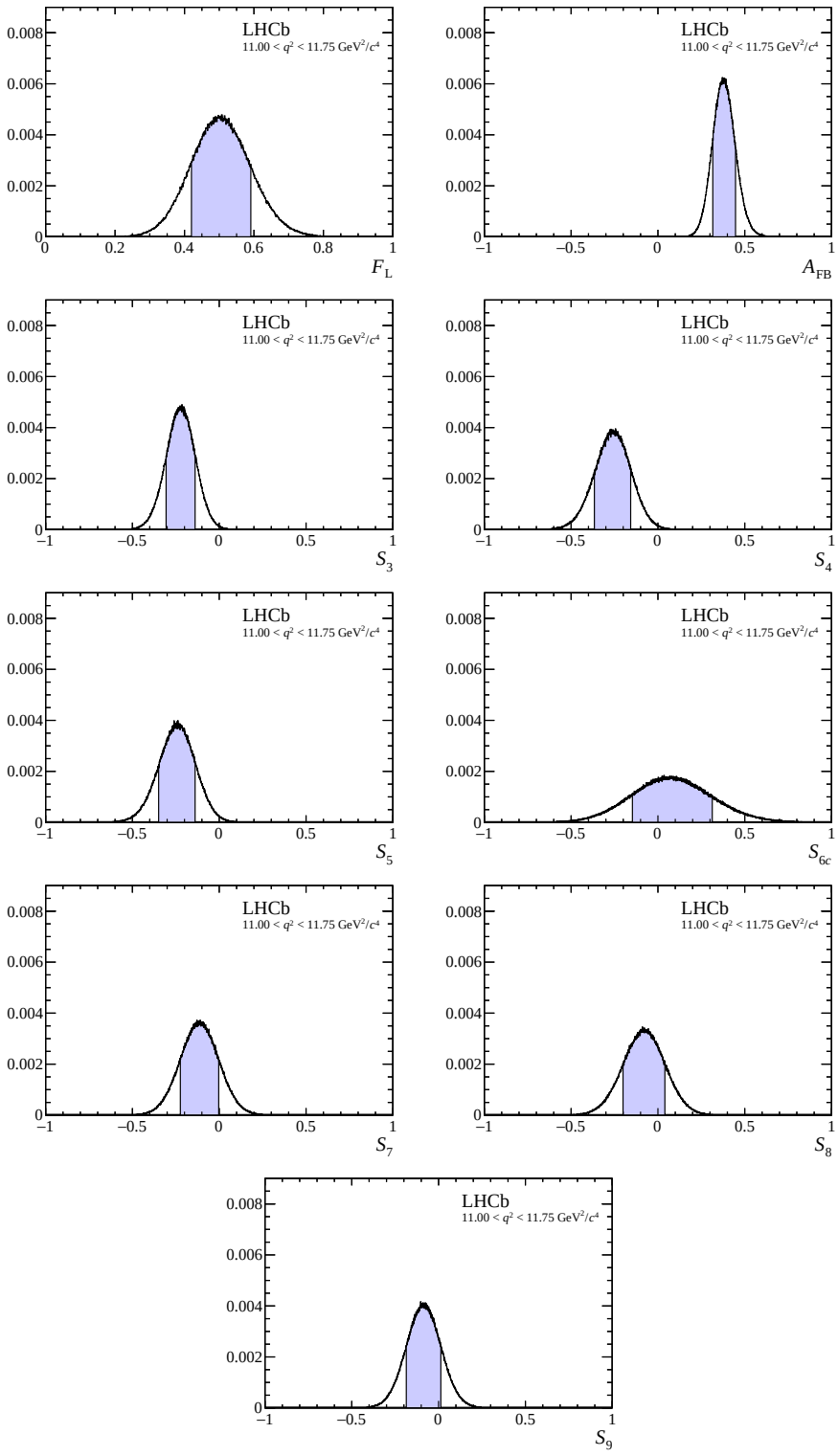

Figure 39: Distribution of pseudoexperiments obtained by applying a bootstrapping technique to the moment analysis. The 68% confidence interval on the angular observable is indicated by the shaded region.

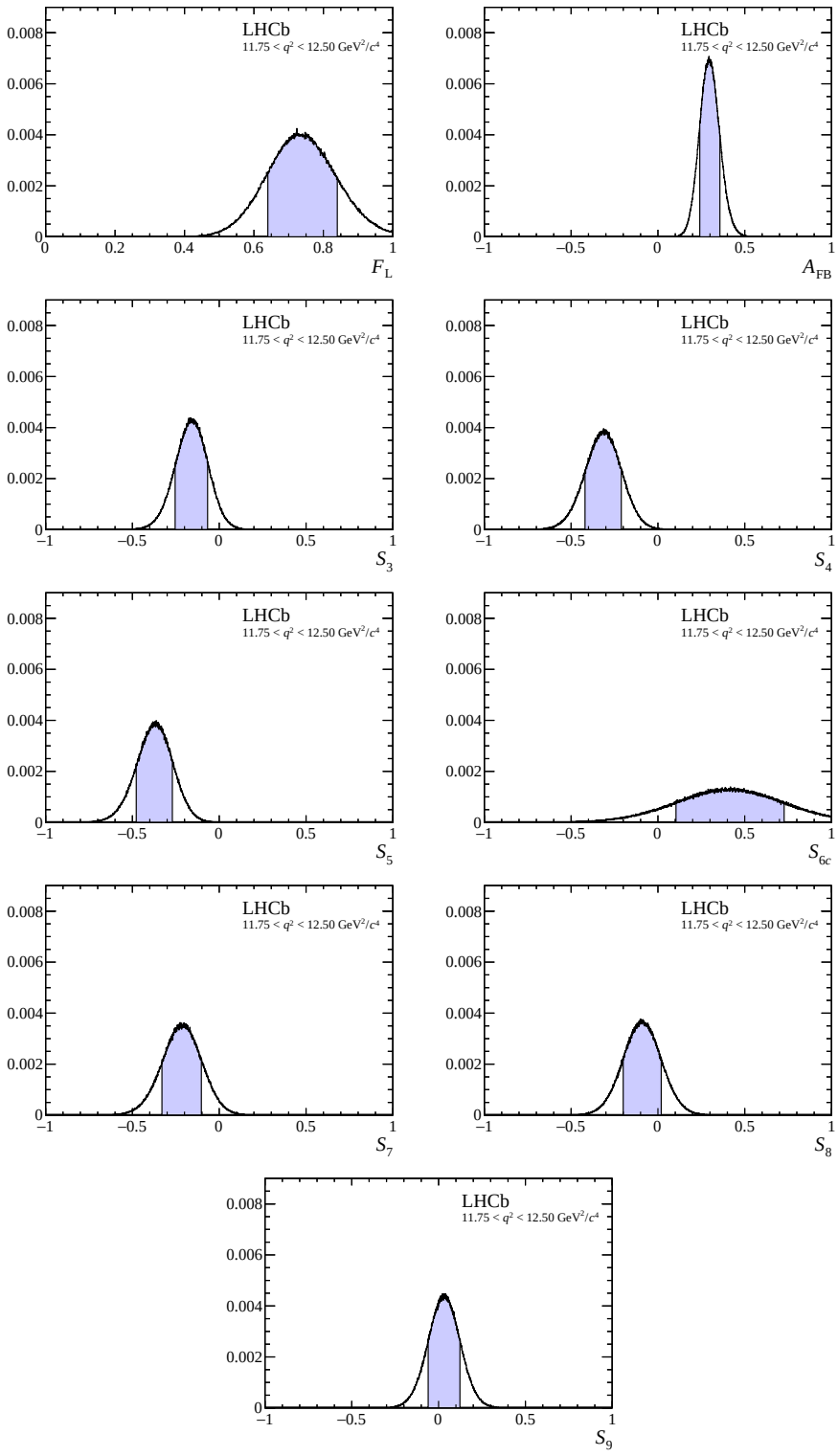

Figure 40: Distribution of pseudoexperiments obtained by applying a bootstrapping technique to the moment analysis. The 68% confidence interval on the angular observable is indicated by the shaded region.

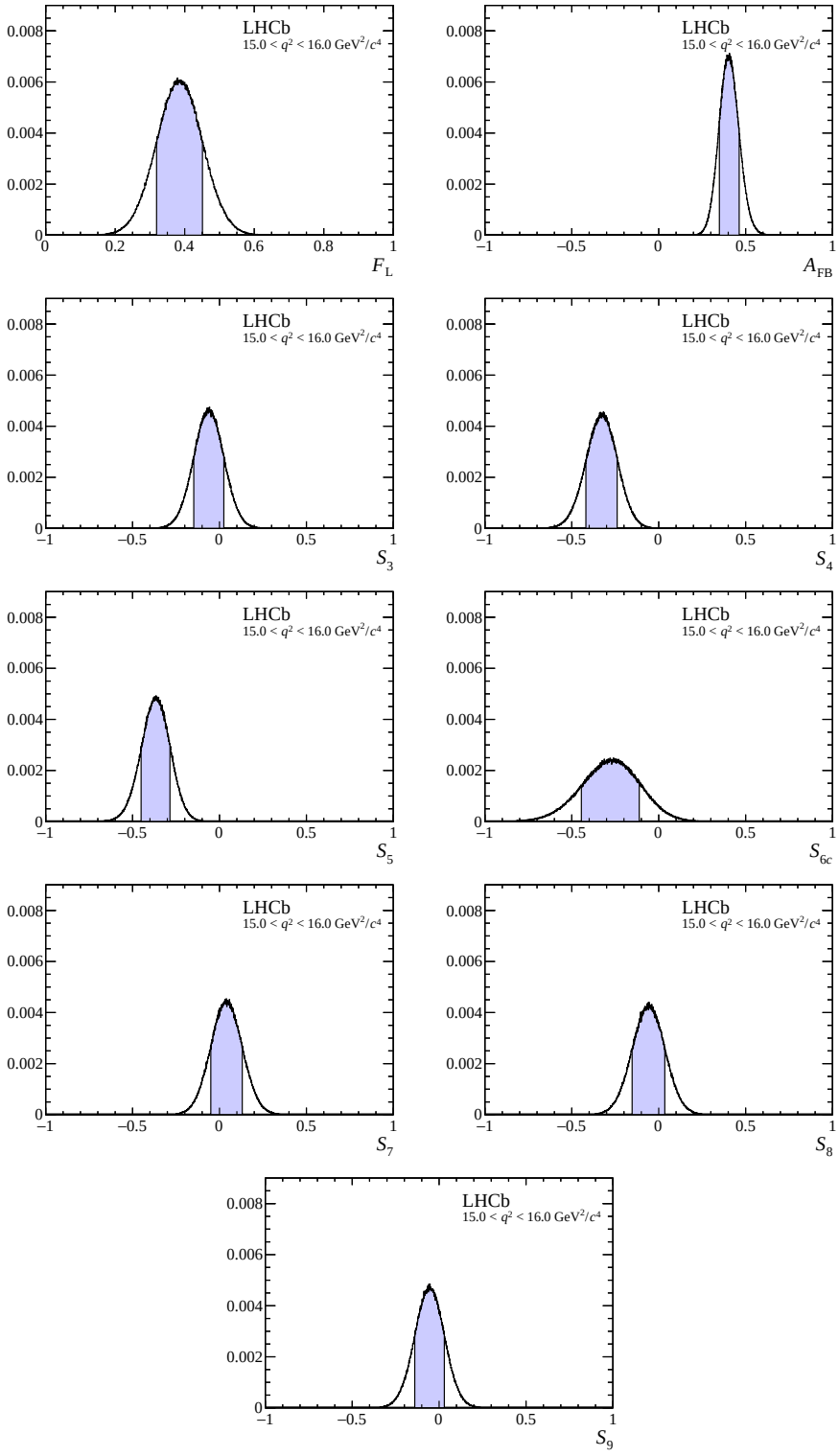

Figure 41: Distribution of pseudoexperiments obtained by applying a bootstrapping technique to the moment analysis. The 68% confidence interval on the angular observable is indicated by the shaded region.

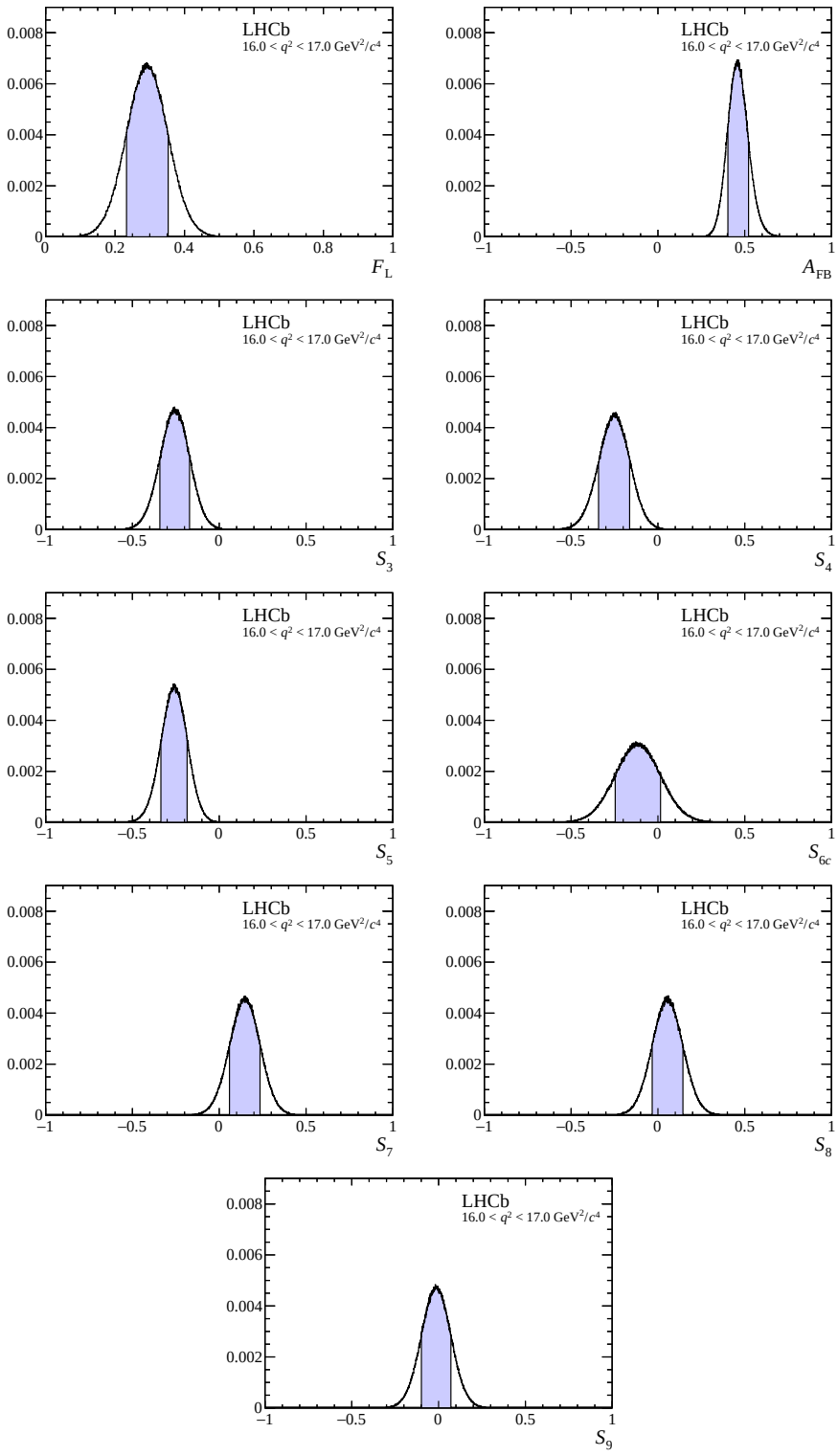

Figure 42: Distribution of pseudoexperiments obtained by applying a bootstrapping technique to the moment analysis. The 68% confidence interval on the angular observable is indicated by the shaded region.

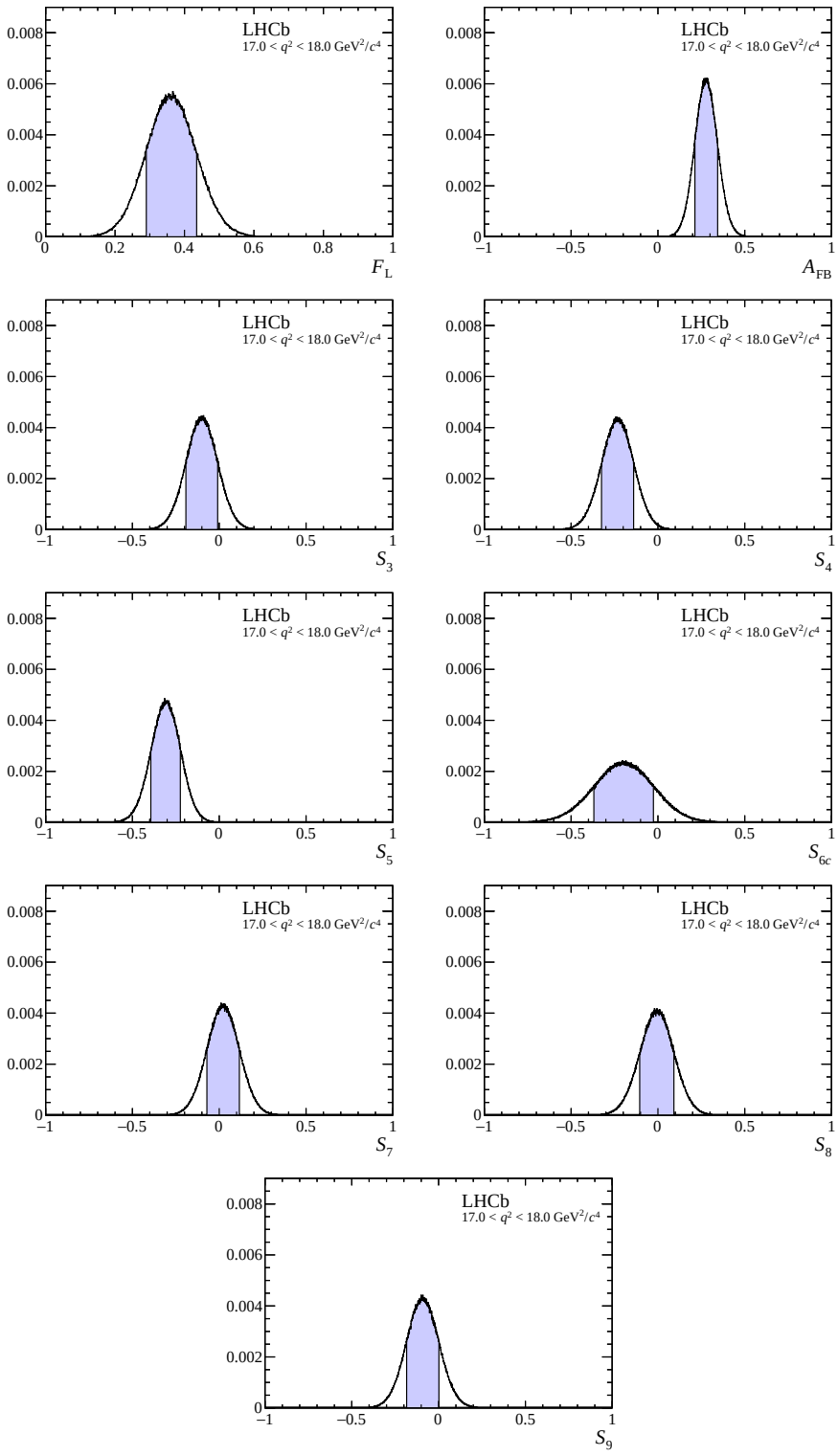

Figure 43: Distribution of pseudoexperiments obtained by applying a bootstrapping technique to the moment analysis. The 68% confidence interval on the angular observable is indicated by the shaded region.

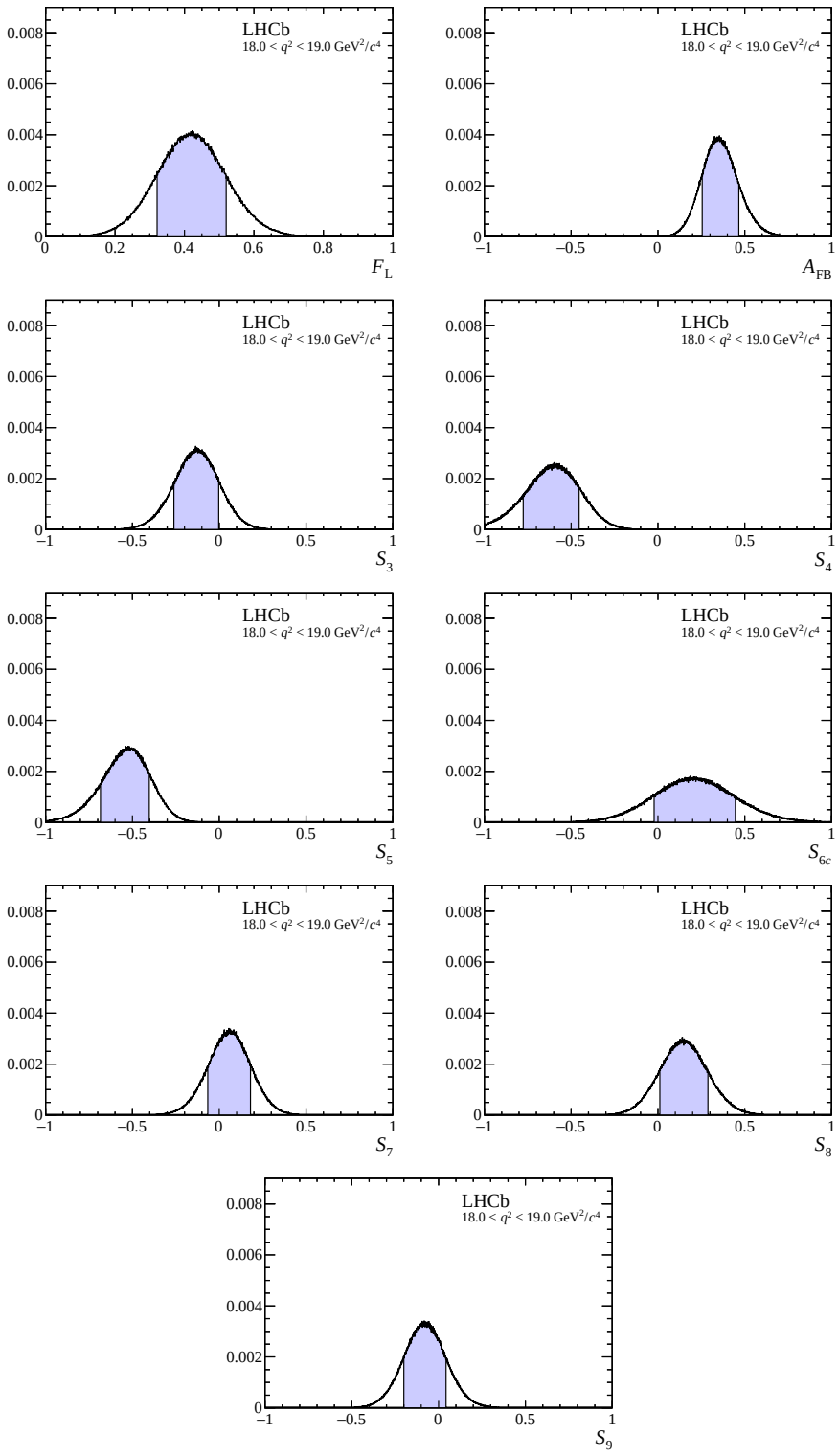

Figure 44: Distribution of pseudoexperiments obtained by applying a bootstrapping technique to the moment analysis. The 68% confidence interval on the angular observable is indicated by the shaded region.

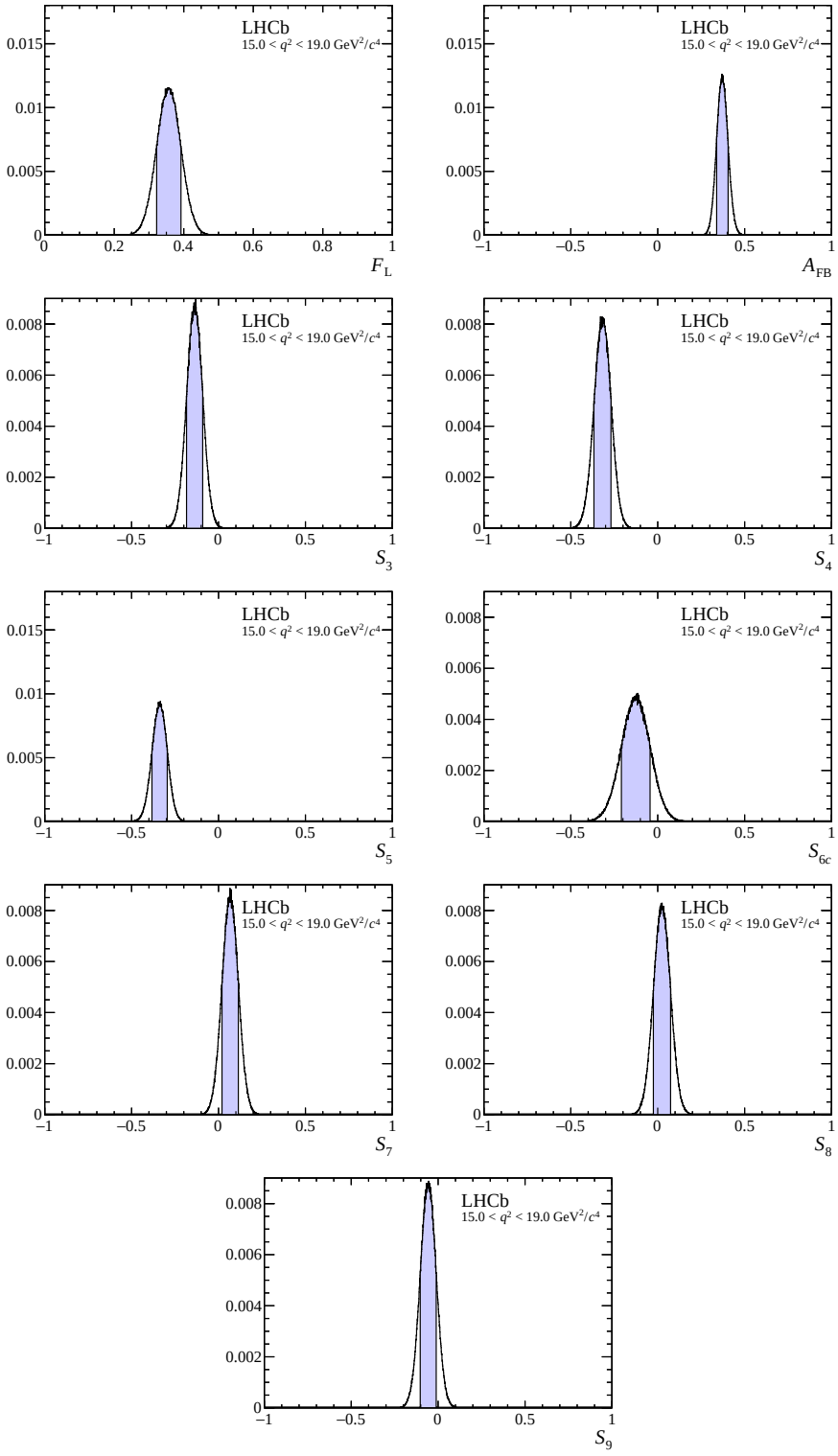

Figure 45: Distribution of pseudoexperiments obtained by applying a bootstrapping technique to the moment analysis. The 68% confidence interval on the angular observable is indicated by the shaded region.

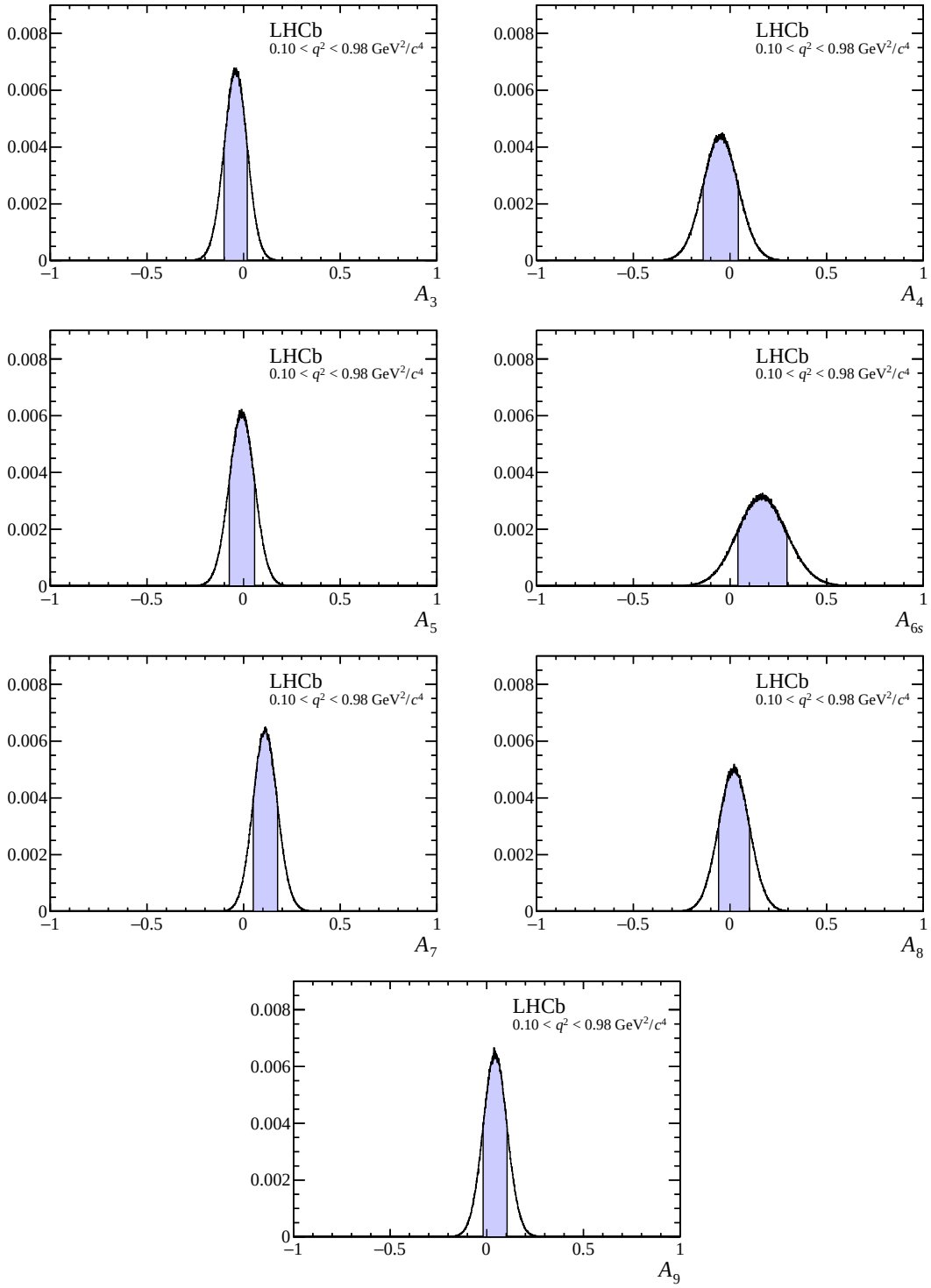

Figure 46: Distribution of pseudoexperiments obtained by applying a bootstrapping technique to the moment analysis. The 68% confidence interval on the angular observable is indicated by the shaded region.

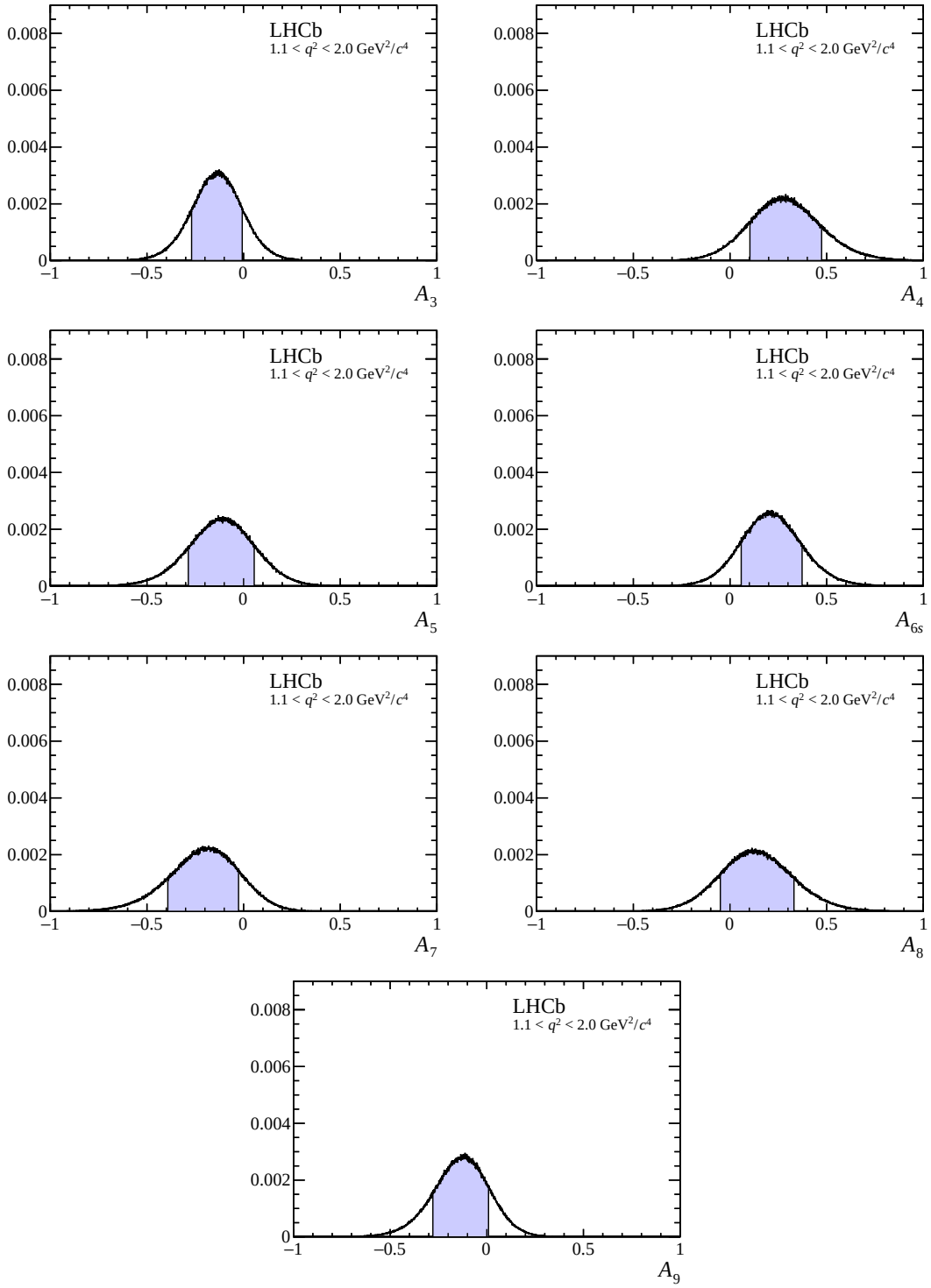

Figure 47: Distribution of pseudoexperiments obtained by applying a bootstrapping technique to the moment analysis. The 68% confidence interval on the angular observable is indicated by the shaded region.

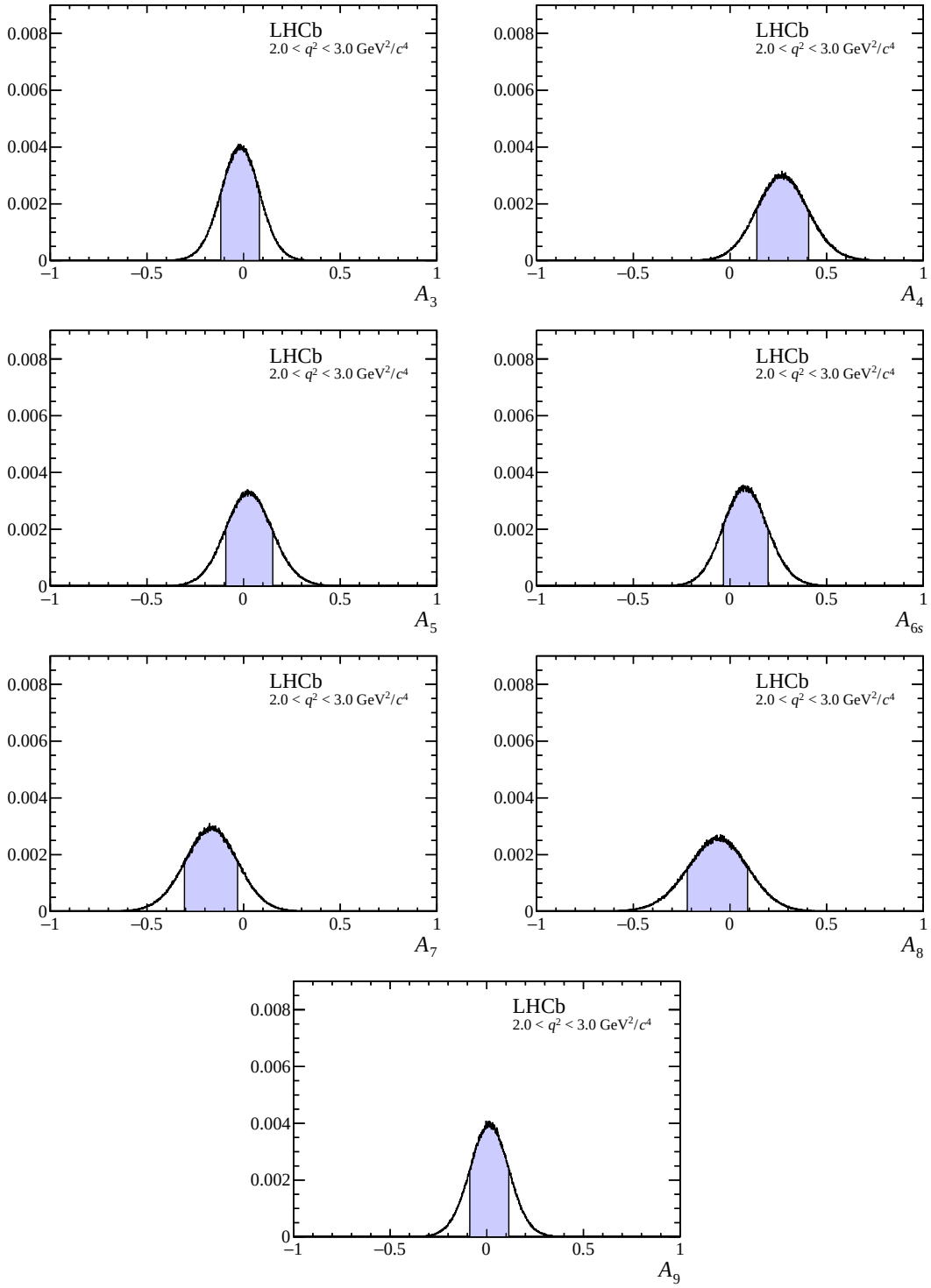

Figure 48: Distribution of pseudoexperiments obtained by applying a bootstrapping technique to the moment analysis. The 68% confidence interval on the angular observable is indicated by the shaded region.

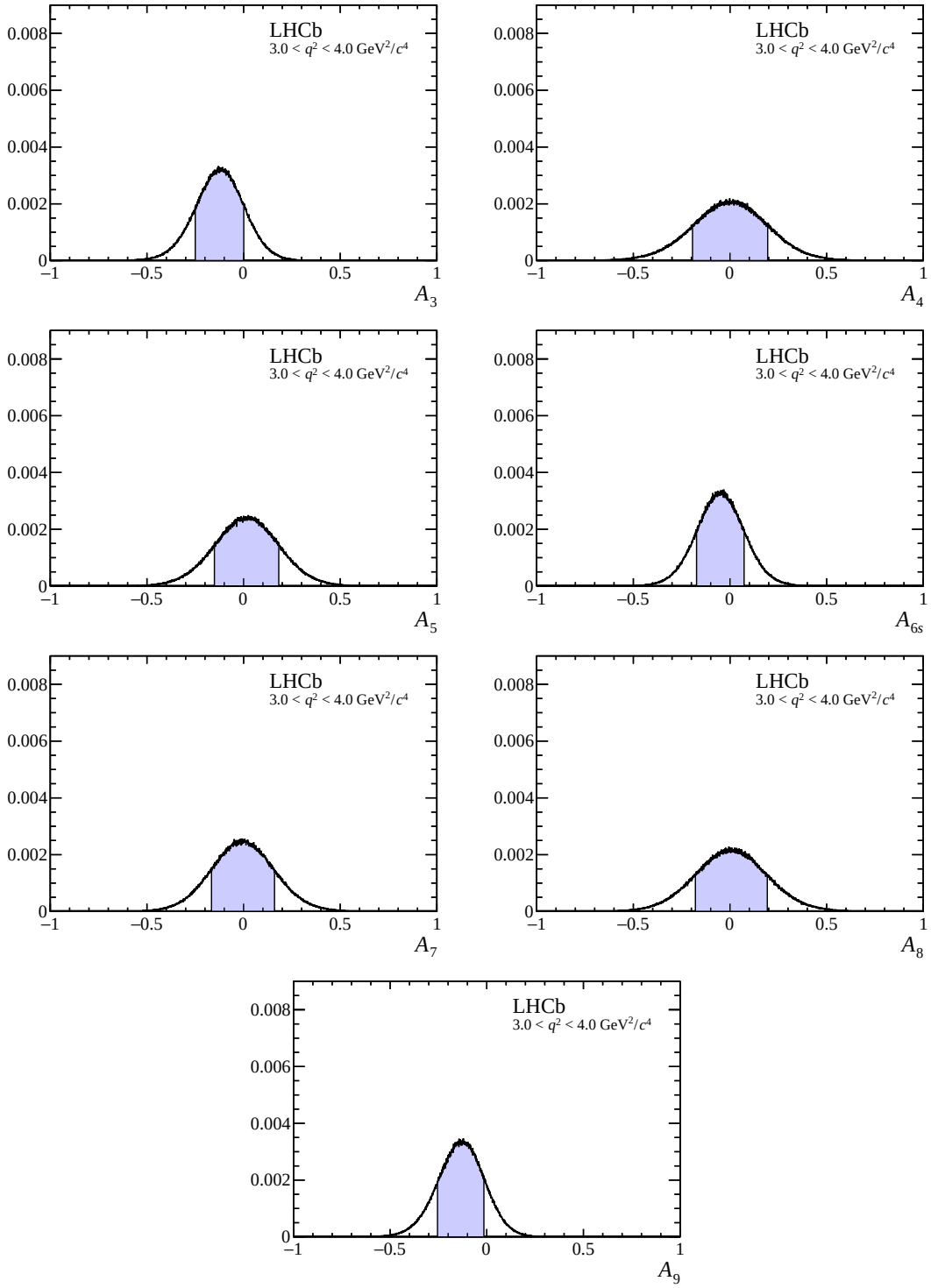

Figure 49: Distribution of pseudoexperiments obtained by applying a bootstrapping technique to the moment analysis. The 68% confidence interval on the angular observable is indicated by the shaded region.

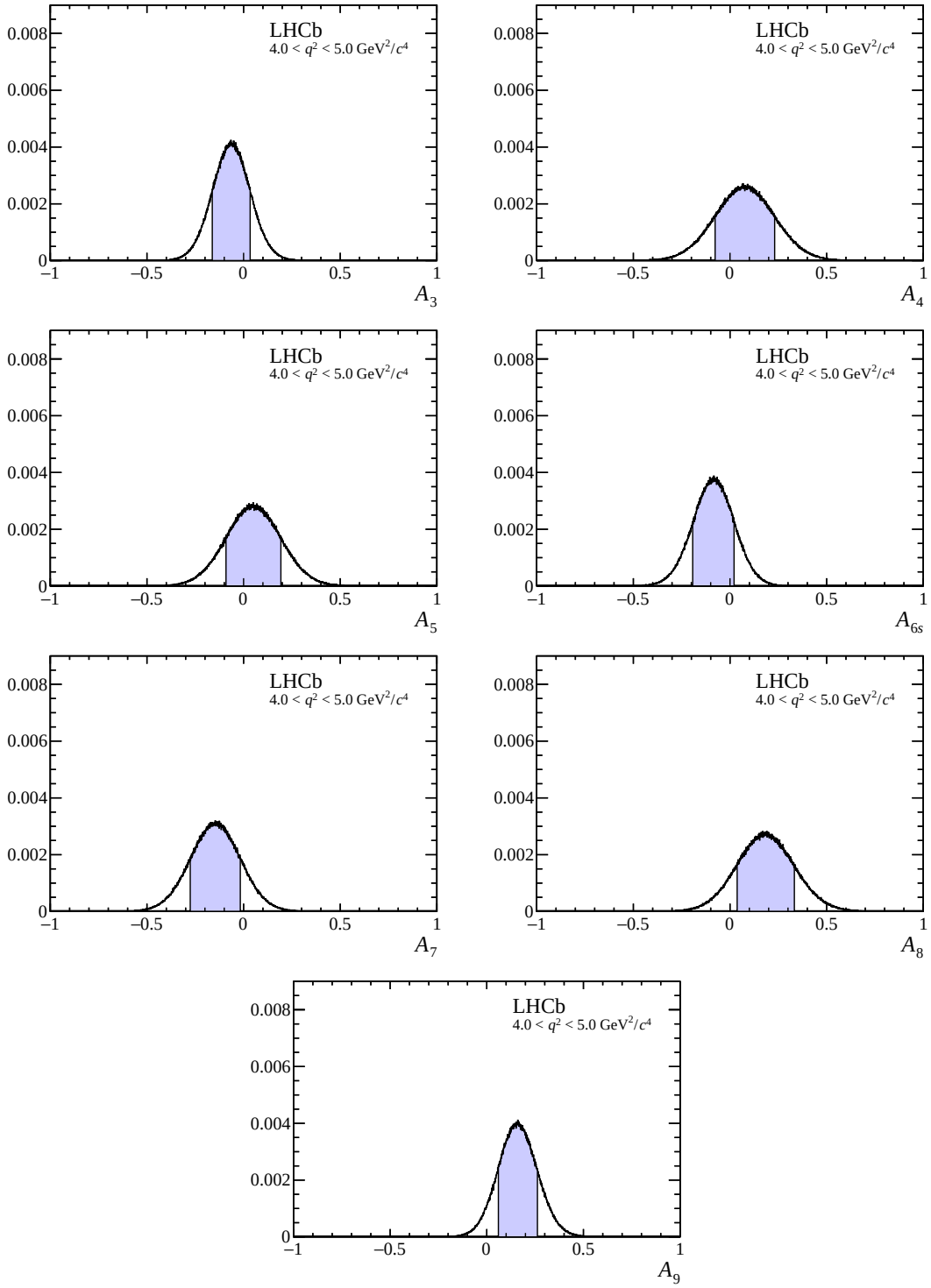

Figure 50: Distribution of pseudoexperiments obtained by applying a bootstrapping technique to the moment analysis. The 68% confidence interval on the angular observable is indicated by the shaded region.

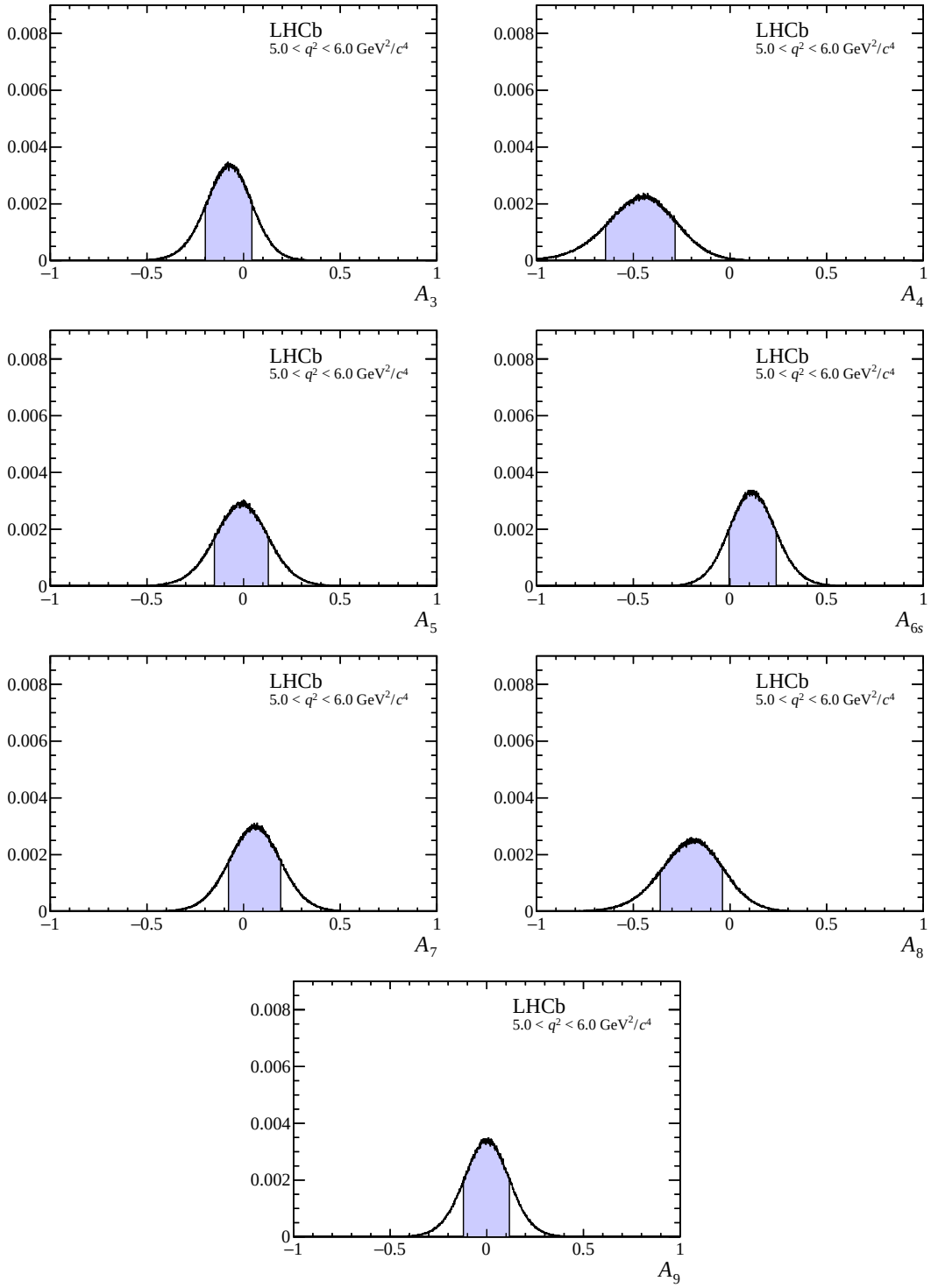

Figure 51: Distribution of pseudoexperiments obtained by applying a bootstrapping technique to the moment analysis. The 68% confidence interval on the angular observable is indicated by the shaded region.

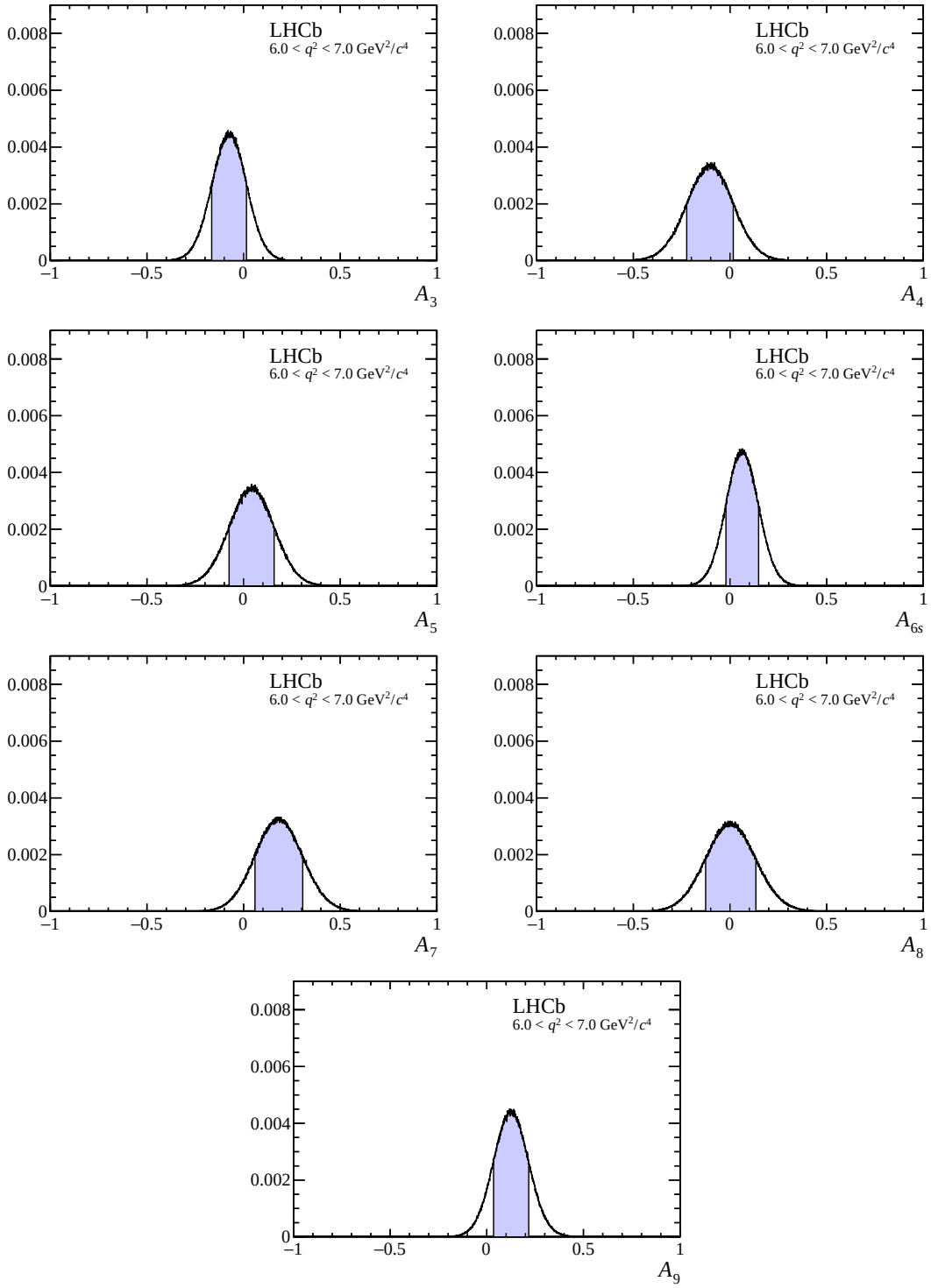

Figure 52: Distribution of pseudoexperiments obtained by applying a bootstrapping technique to the moment analysis. The 68% confidence interval on the angular observable is indicated by the shaded region.

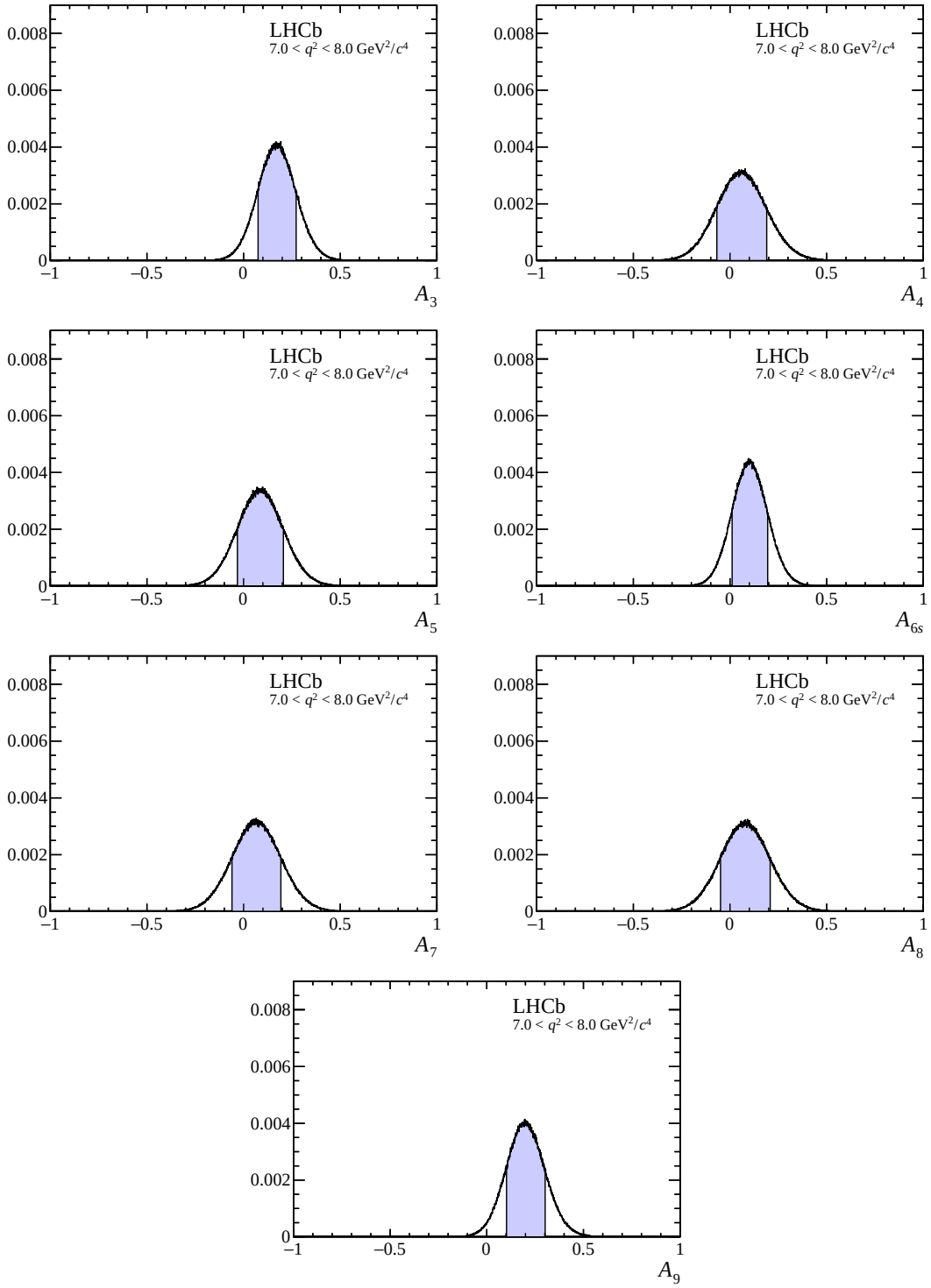

Figure 53: Distribution of pseudoexperiments obtained by applying a bootstrapping technique to the moment analysis. The 68% confidence interval on the angular observable is indicated by the shaded region.

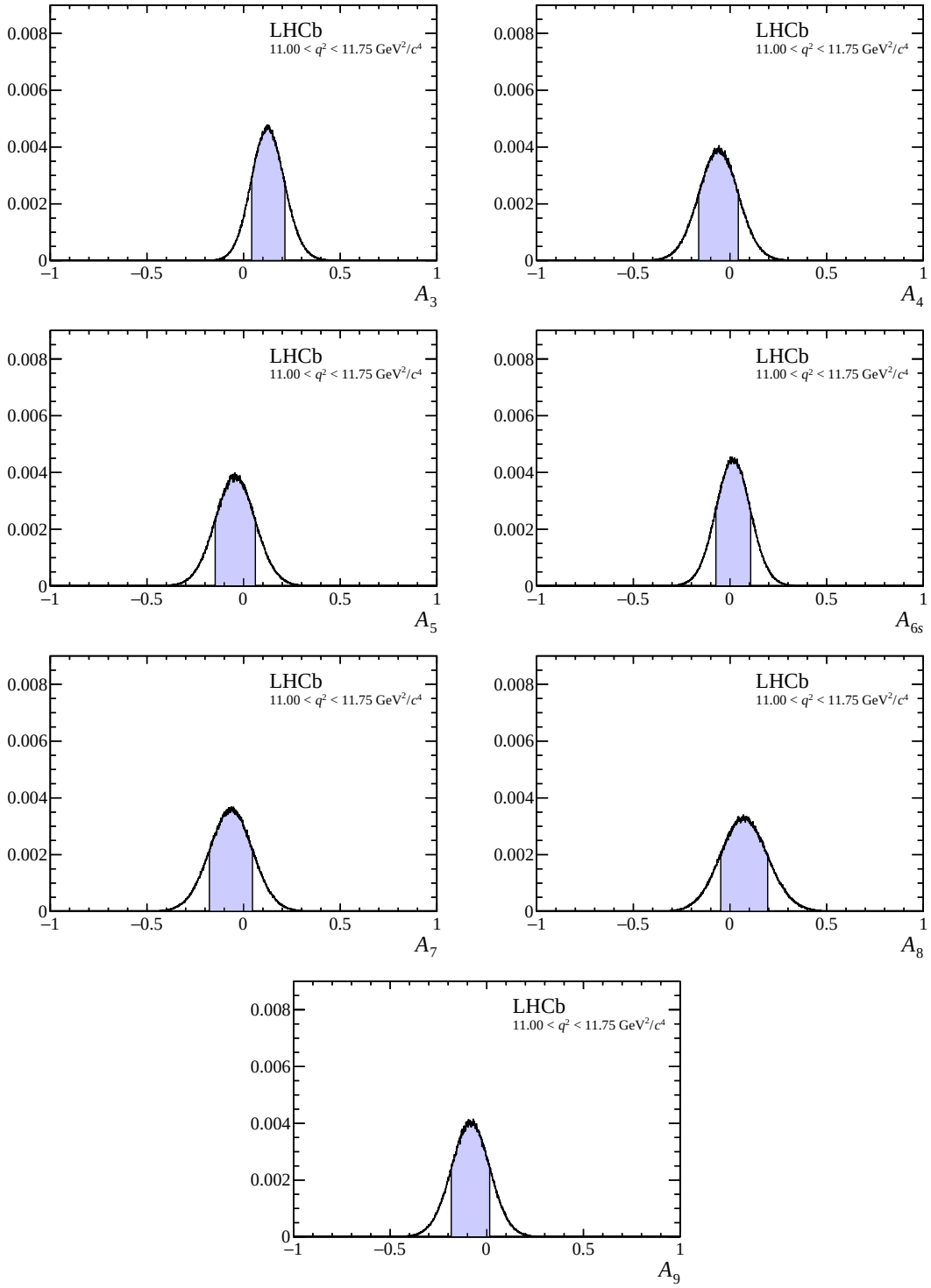

Figure 54: Distribution of pseudoexperiments obtained by applying a bootstrapping technique to the moment analysis. The 68% confidence interval on the angular observable is indicated by the shaded region.

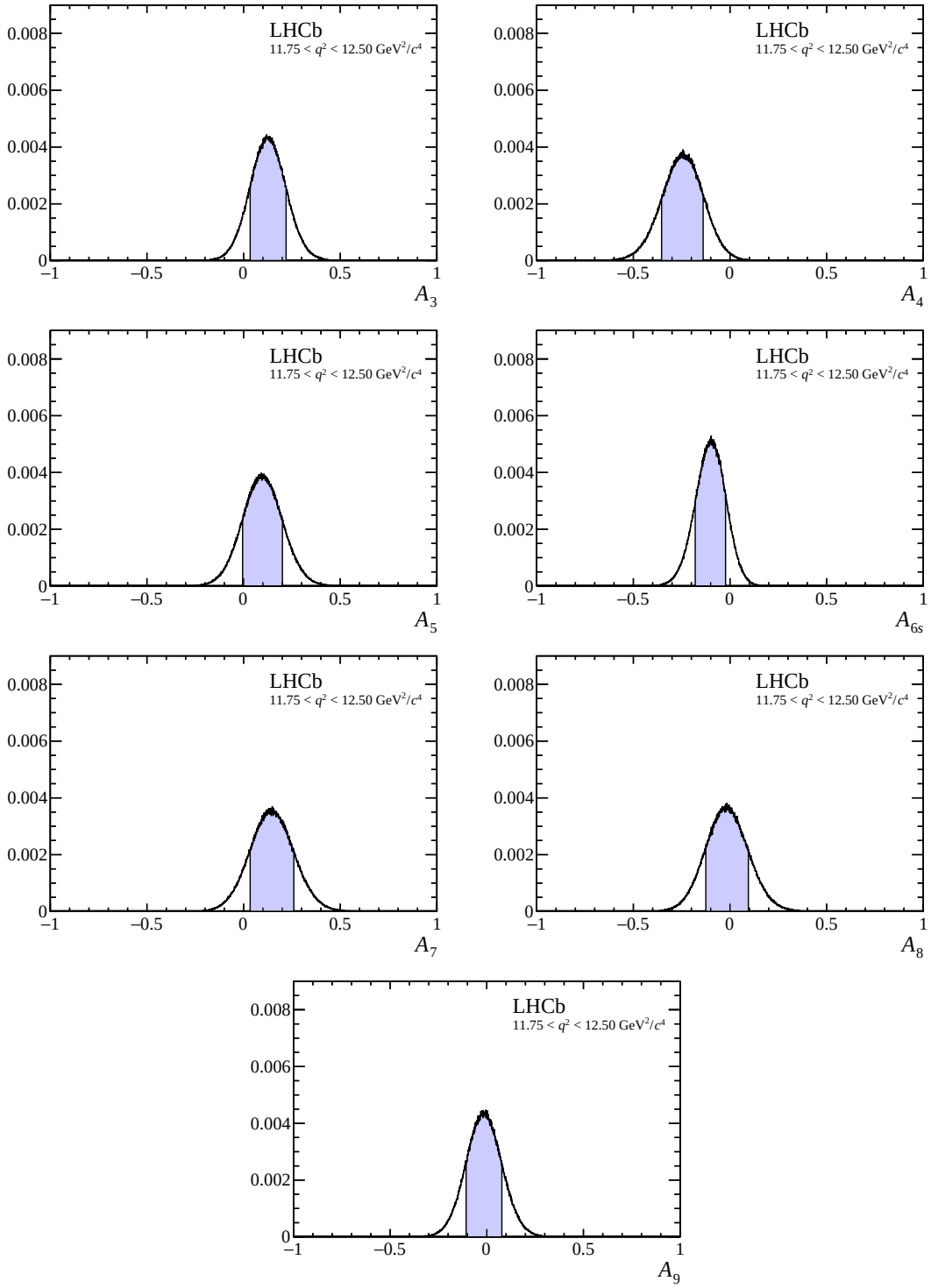

Figure 55: Distribution of pseudoexperiments obtained by applying a bootstrapping technique to the moment analysis. The 68% confidence interval on the angular observable is indicated by the shaded region.

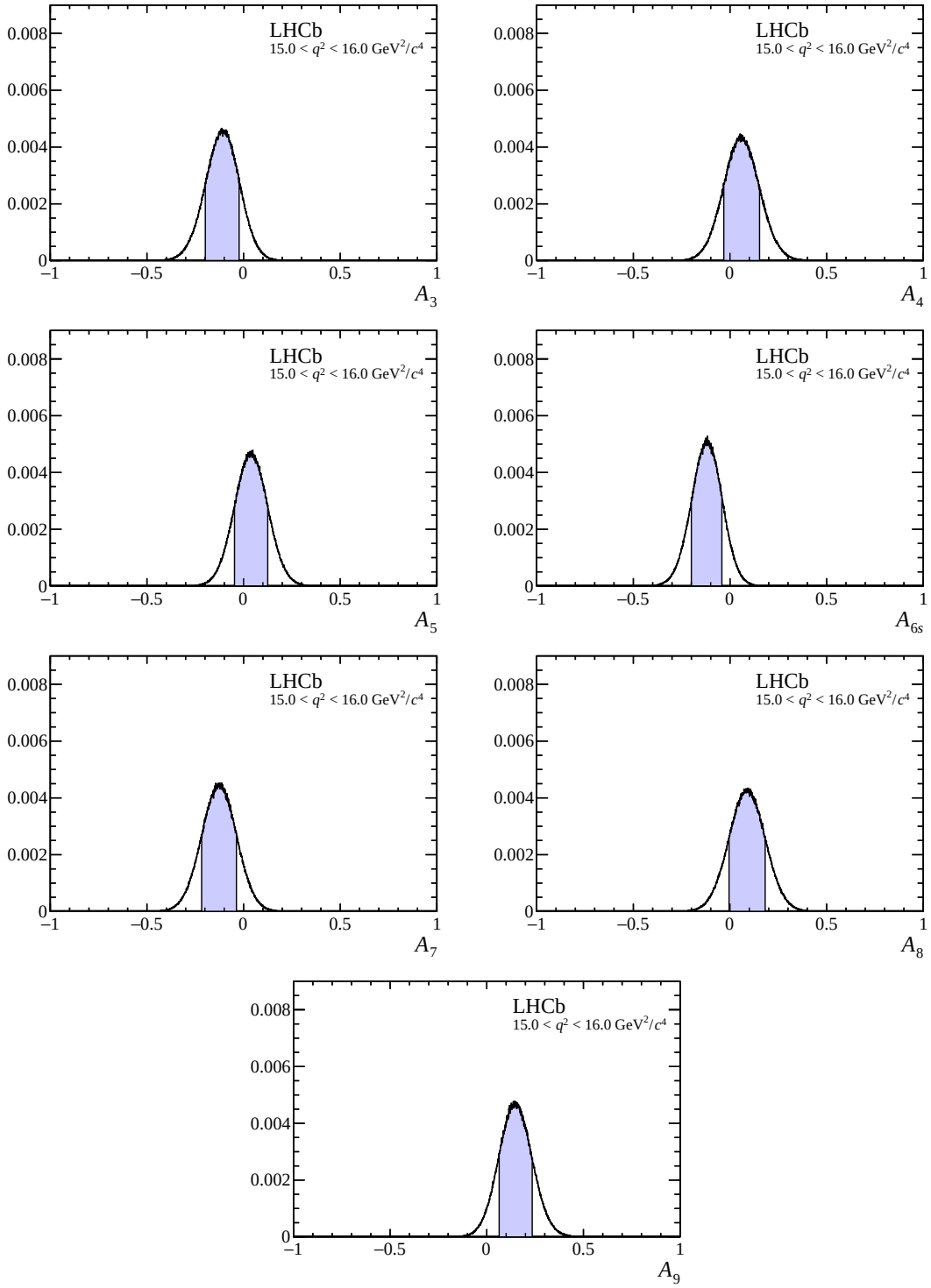

Figure 56: Distribution of pseudoexperiments obtained by applying a bootstrapping technique to the moment analysis. The 68% confidence interval on the angular observable is indicated by the shaded region.

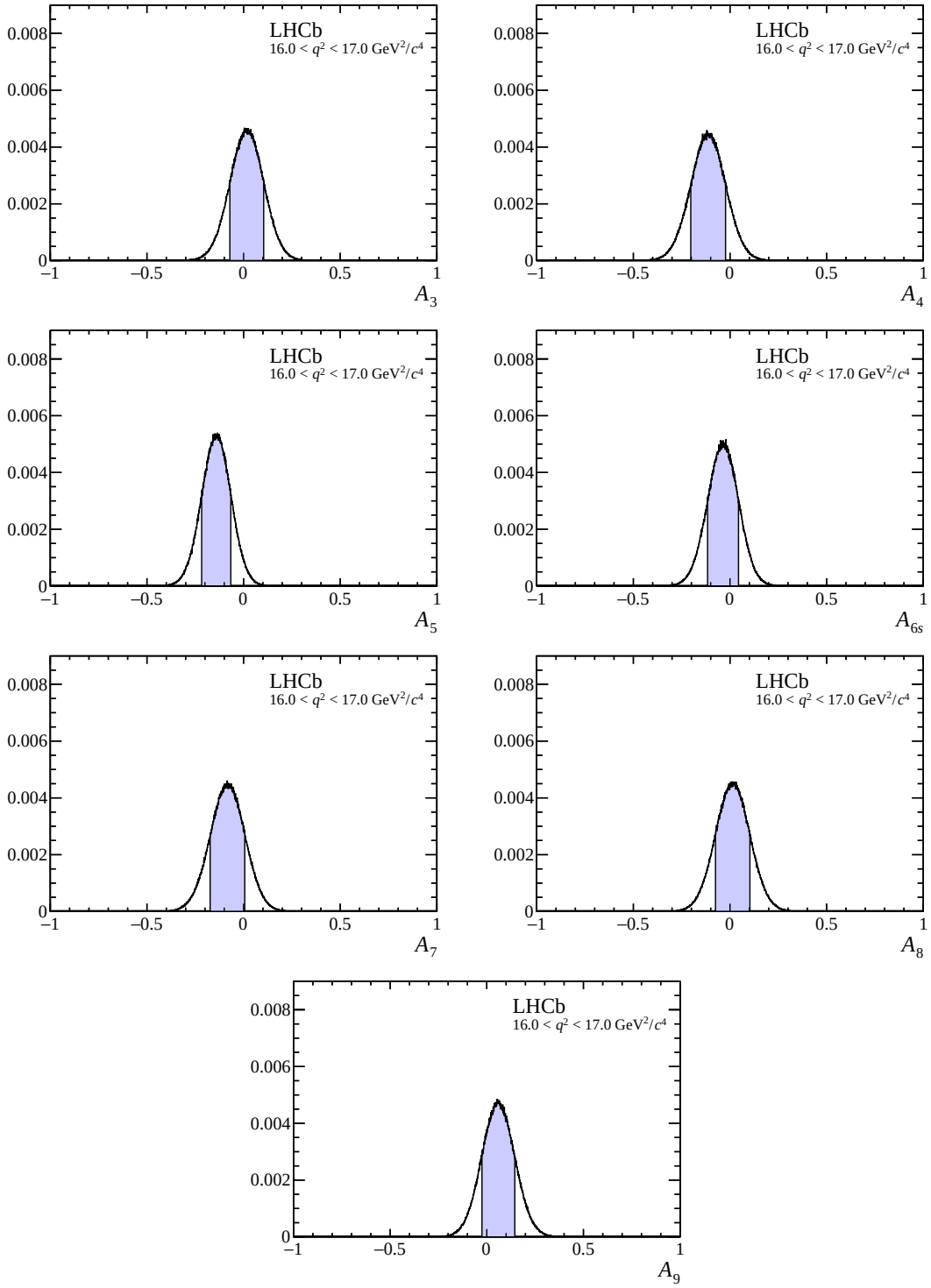

Figure 57: Distribution of pseudoexperiments obtained by applying a bootstrapping technique to the moment analysis. The 68% confidence interval on the angular observable is indicated by the shaded region.

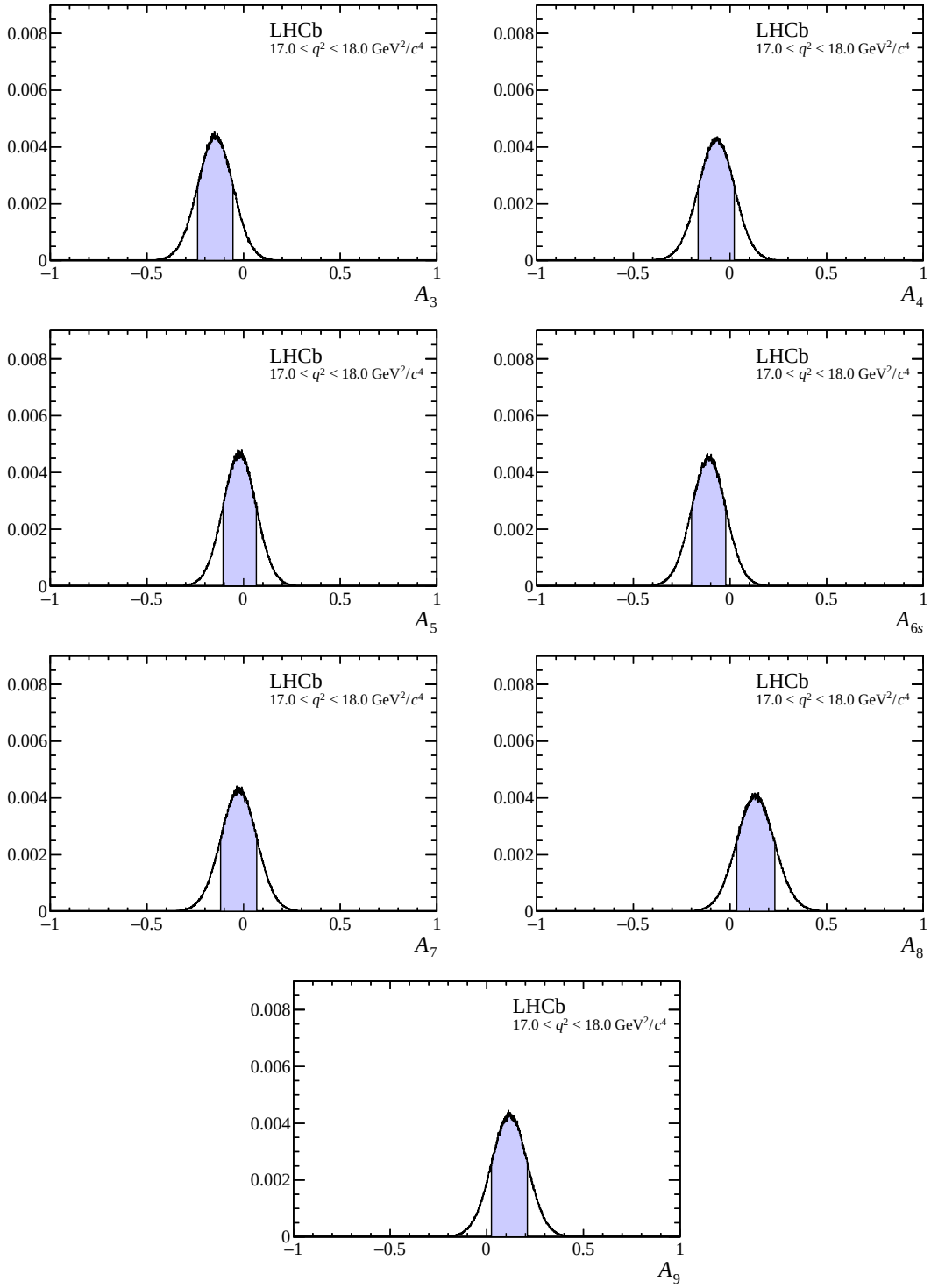

Figure 58: Distribution of pseudoexperiments obtained by applying a bootstrapping technique to the moment analysis. The 68% confidence interval on the angular observable is indicated by the shaded region.

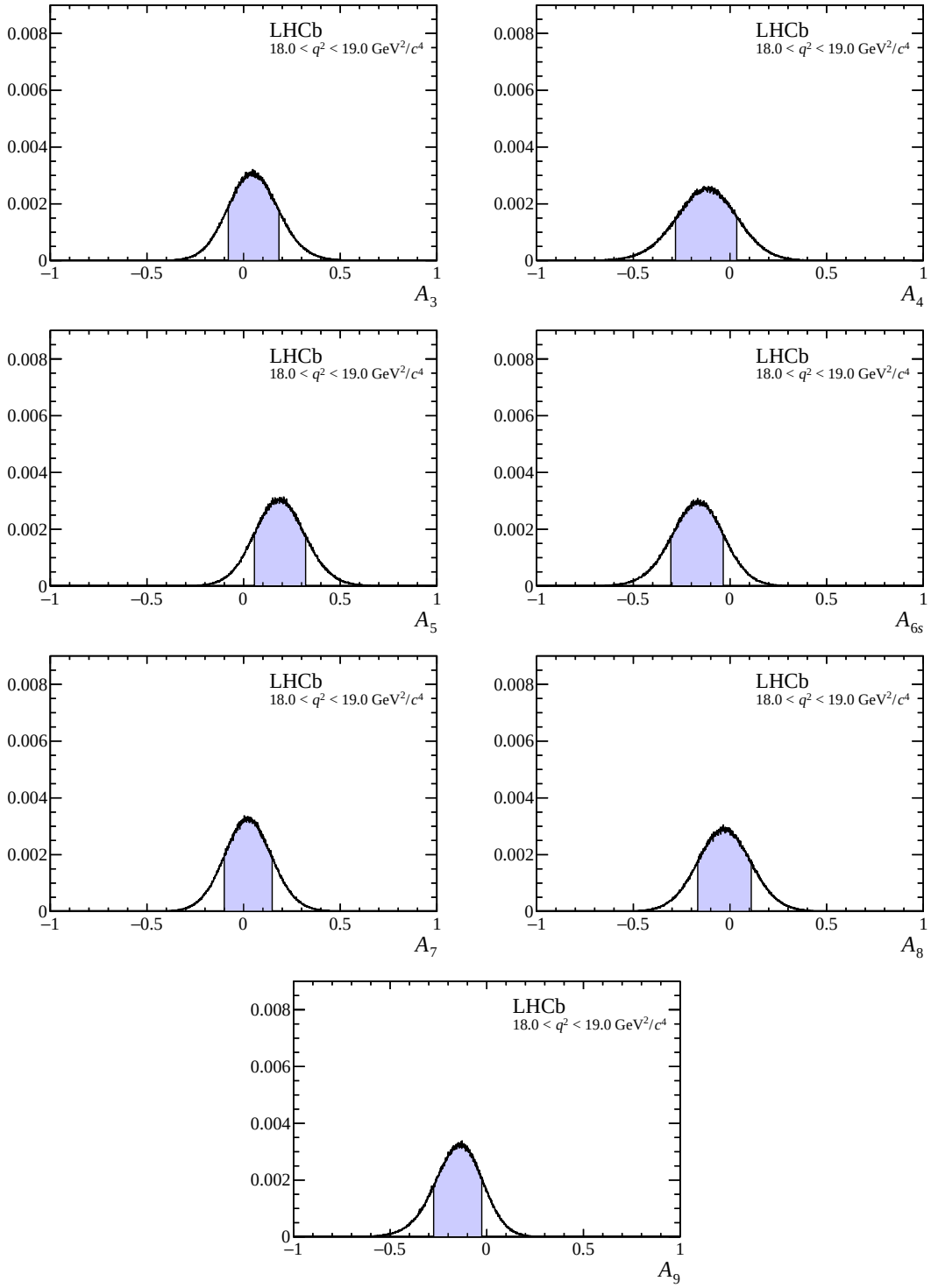

Figure 59: Distribution of pseudoexperiments obtained by applying a bootstrapping technique to the moment analysis. The 68% confidence interval on the angular observable is indicated by the shaded region.

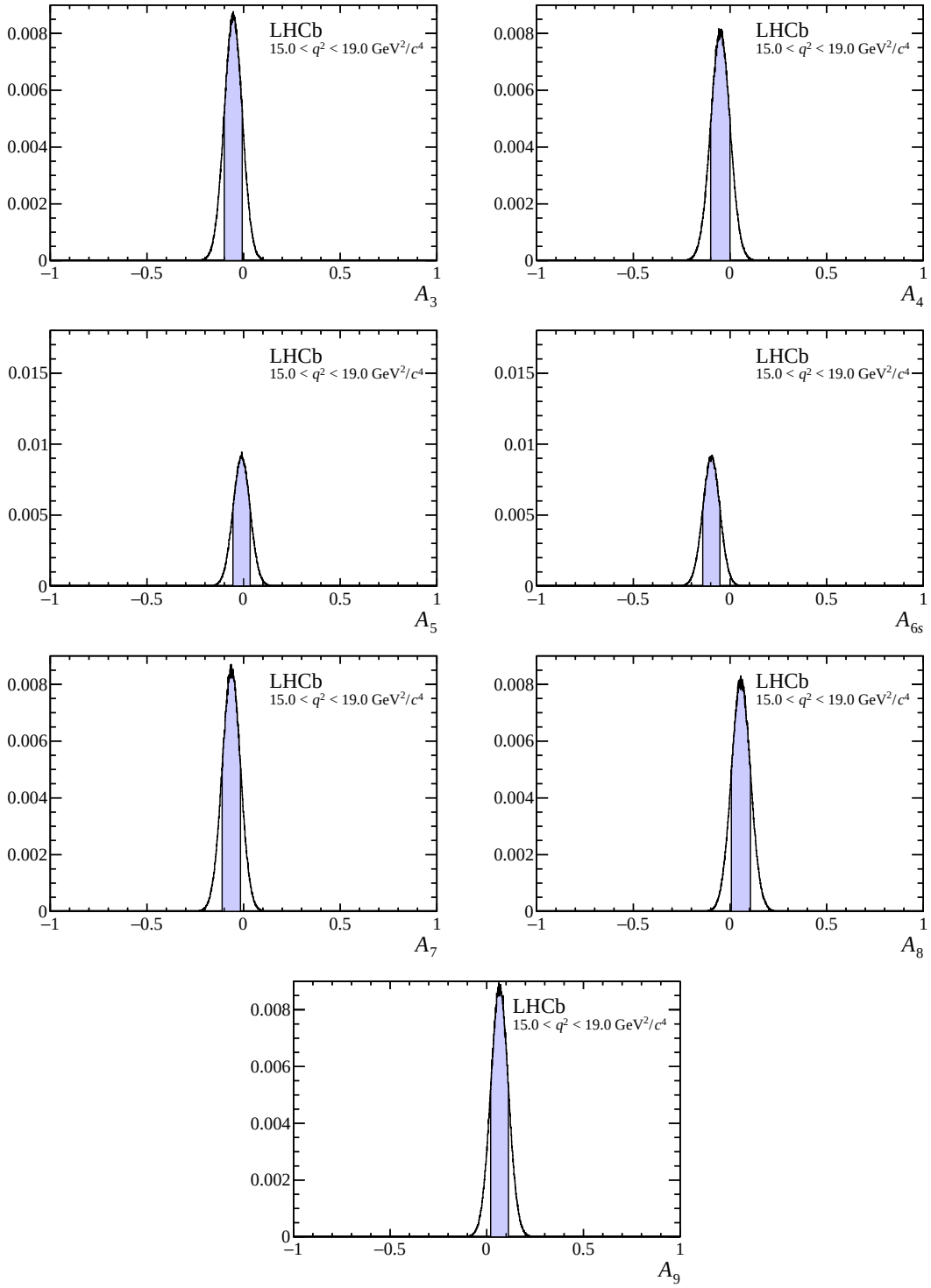

Figure 60: Distribution of pseudoexperiments obtained by applying a bootstrapping technique to the moment analysis. The 68% confidence interval on the angular observable is indicated by the shaded region.

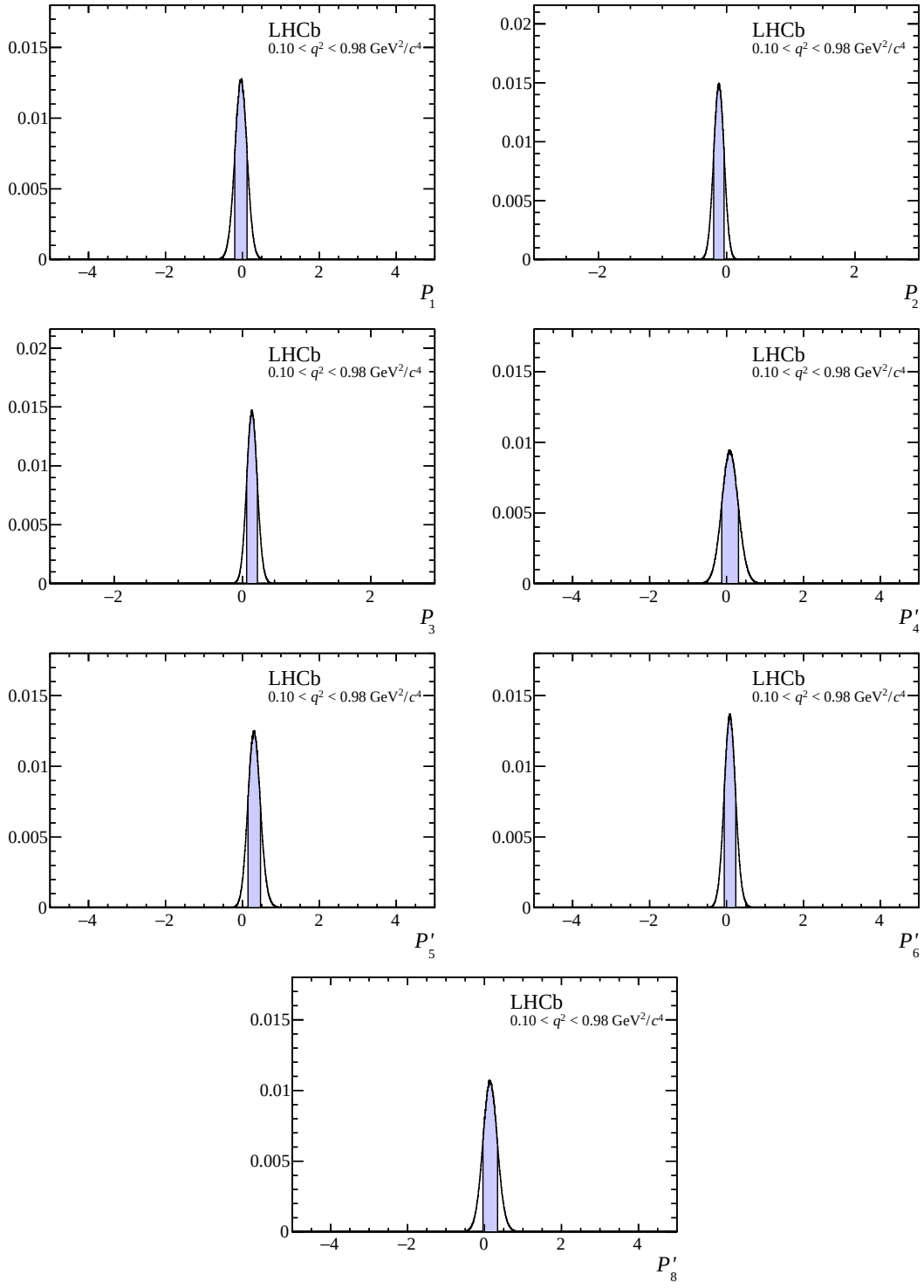

Figure 61: Distribution of pseudoexperiments obtained by applying a bootstrapping technique to the moment analysis. The 68% confidence interval on the angular observable is indicated by the shaded region.

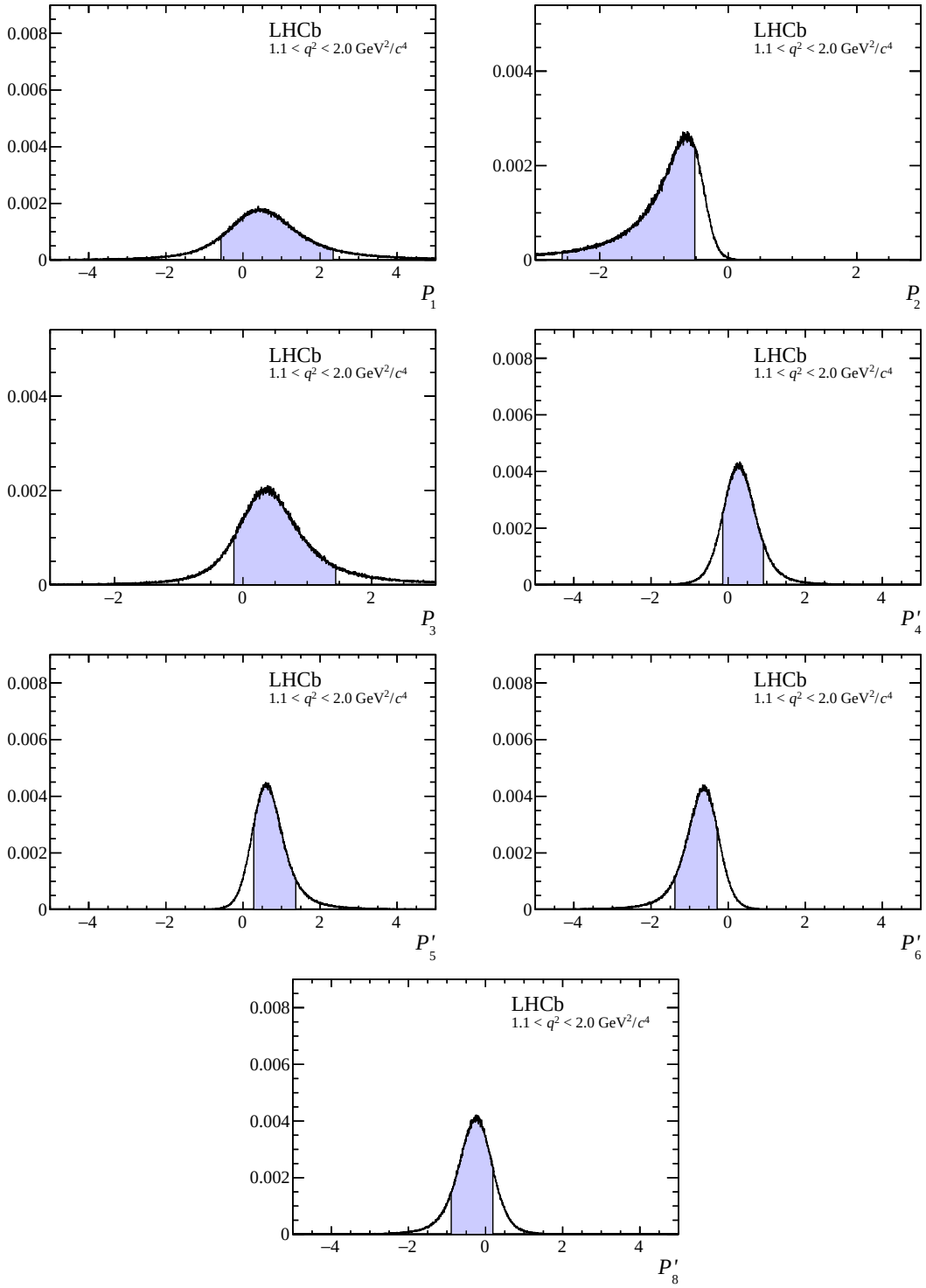

Figure 62: Distribution of pseudoexperiments obtained by applying a bootstrapping technique to the moment analysis. The 68% confidence interval on the angular observable is indicated by the shaded region.

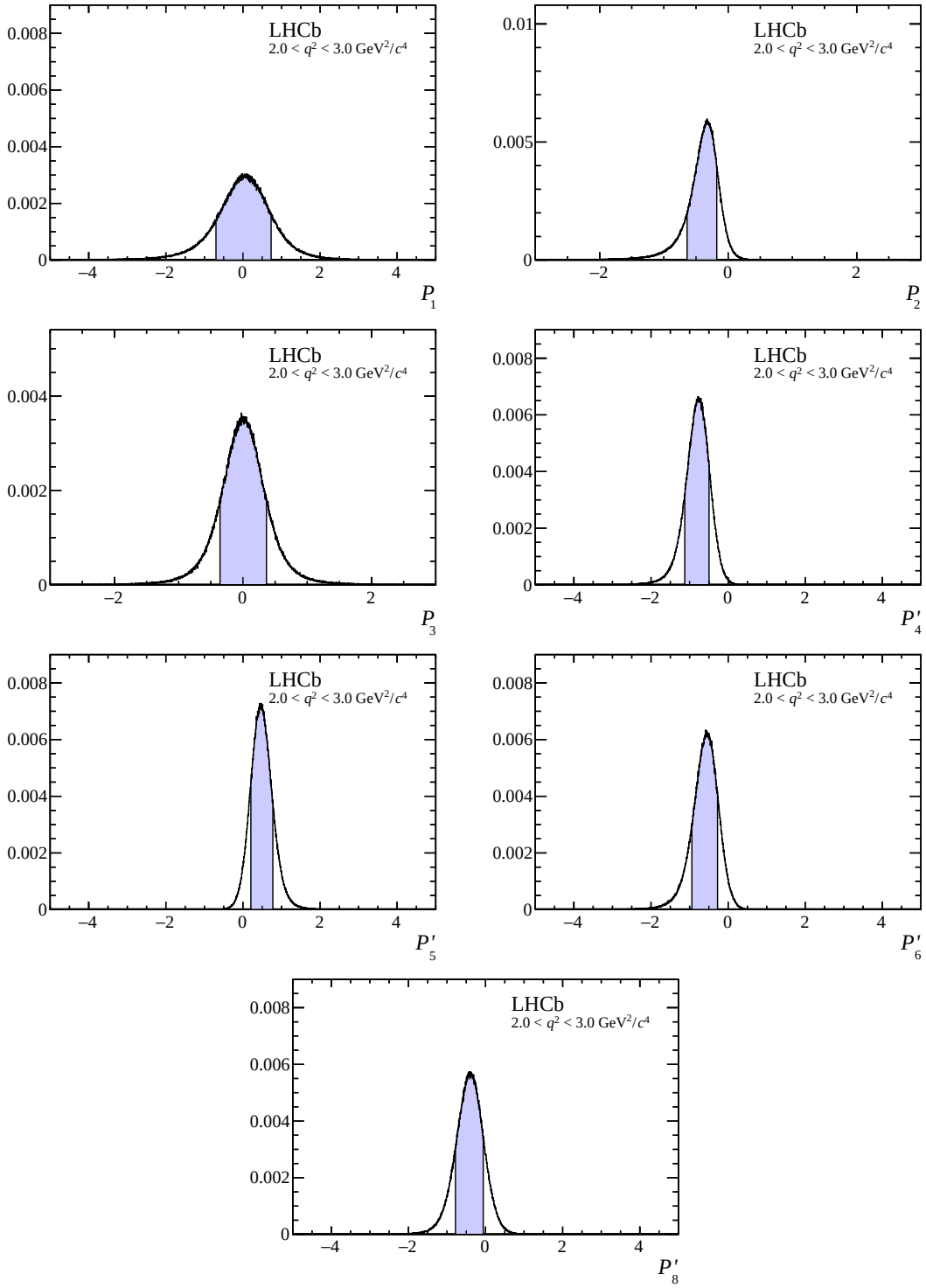

Figure 63: Distribution of pseudoexperiments obtained by applying a bootstrapping technique to the moment analysis. The 68% confidence interval on the angular observable is indicated by the shaded region.

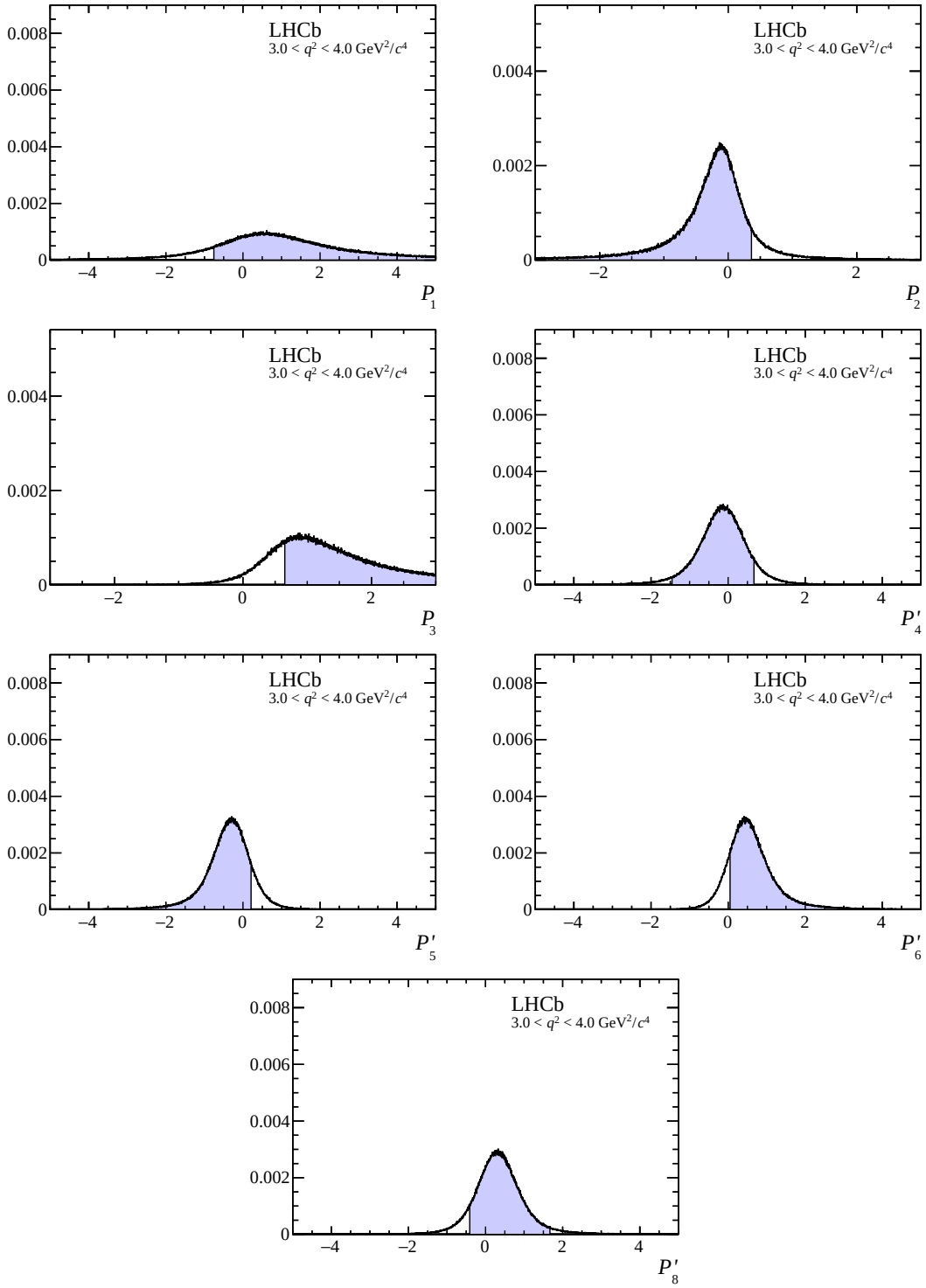

Figure 64: Distribution of pseudoexperiments obtained by applying a bootstrapping technique to the moment analysis. The 68% confidence interval on the angular observable is indicated by the shaded region.

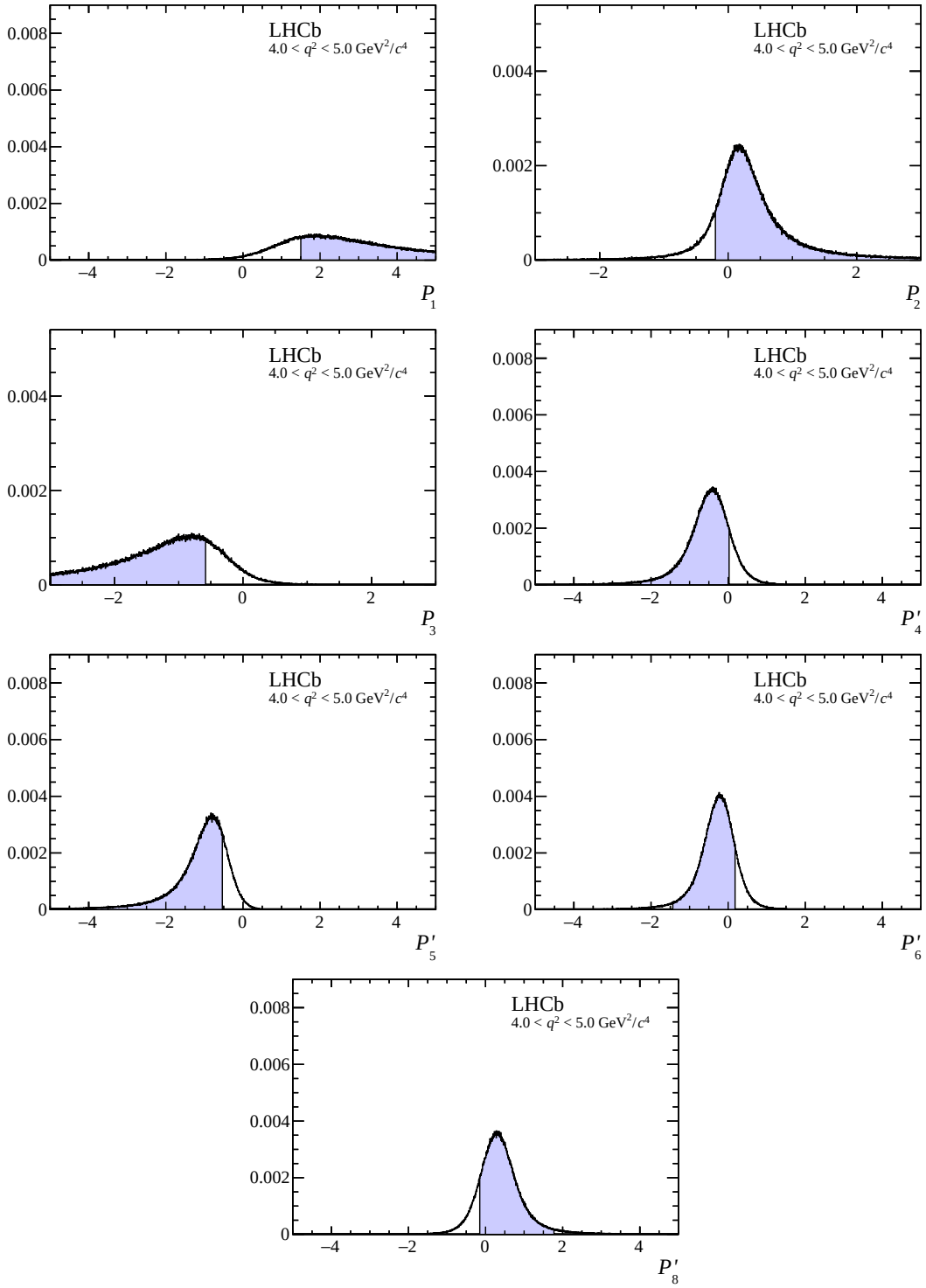

Figure 65: Distribution of pseudoexperiments obtained by applying a bootstrapping technique to the moment analysis. The 68% confidence interval on the angular observable is indicated by the shaded region.

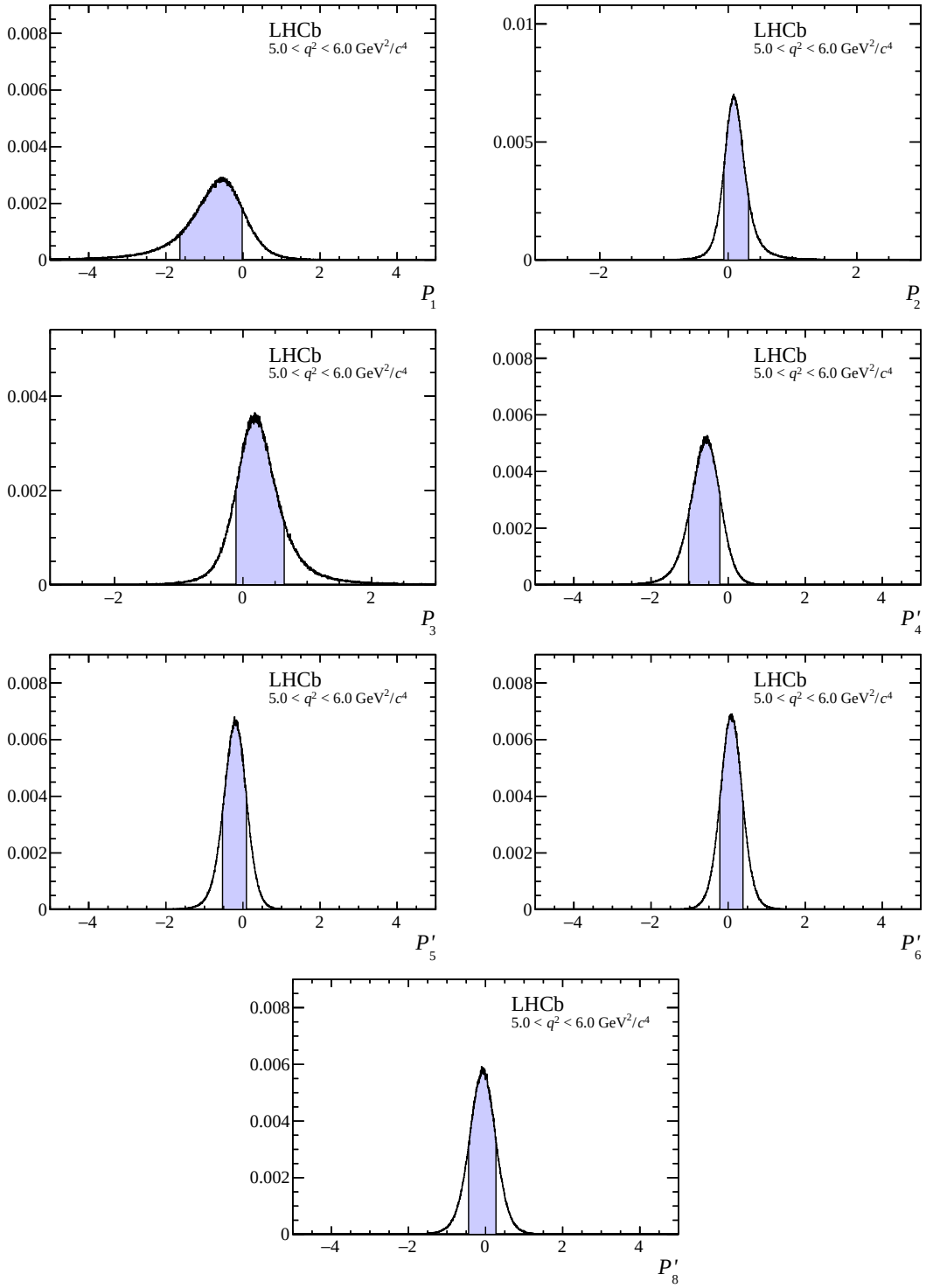

Figure 66: Distribution of pseudoexperiments obtained by applying a bootstrapping technique to the moment analysis. The 68% confidence interval on the angular observable is indicated by the shaded region.

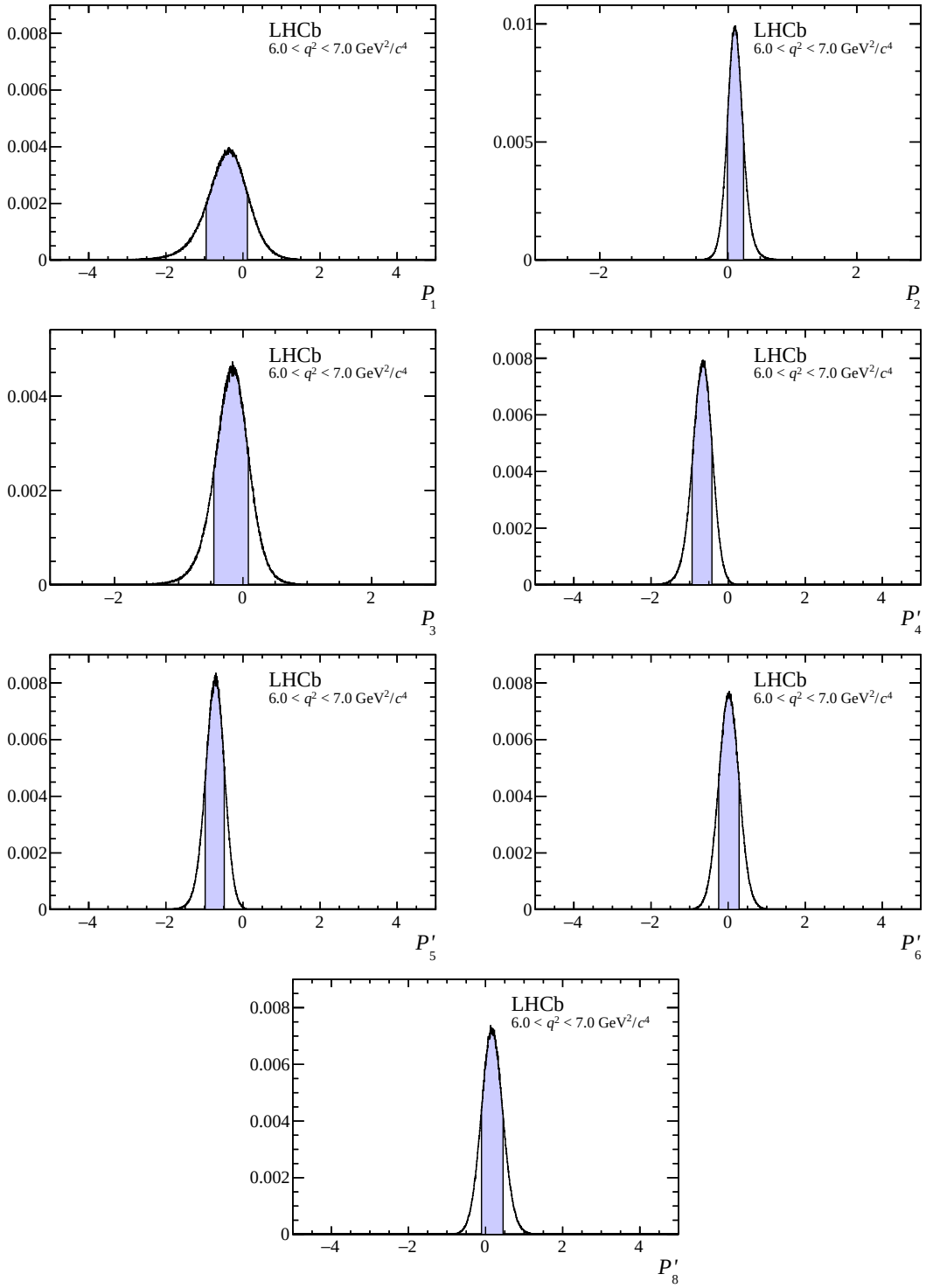

Figure 67: Distribution of pseudoexperiments obtained by applying a bootstrapping technique to the moment analysis. The 68% confidence interval on the angular observable is indicated by the shaded region.

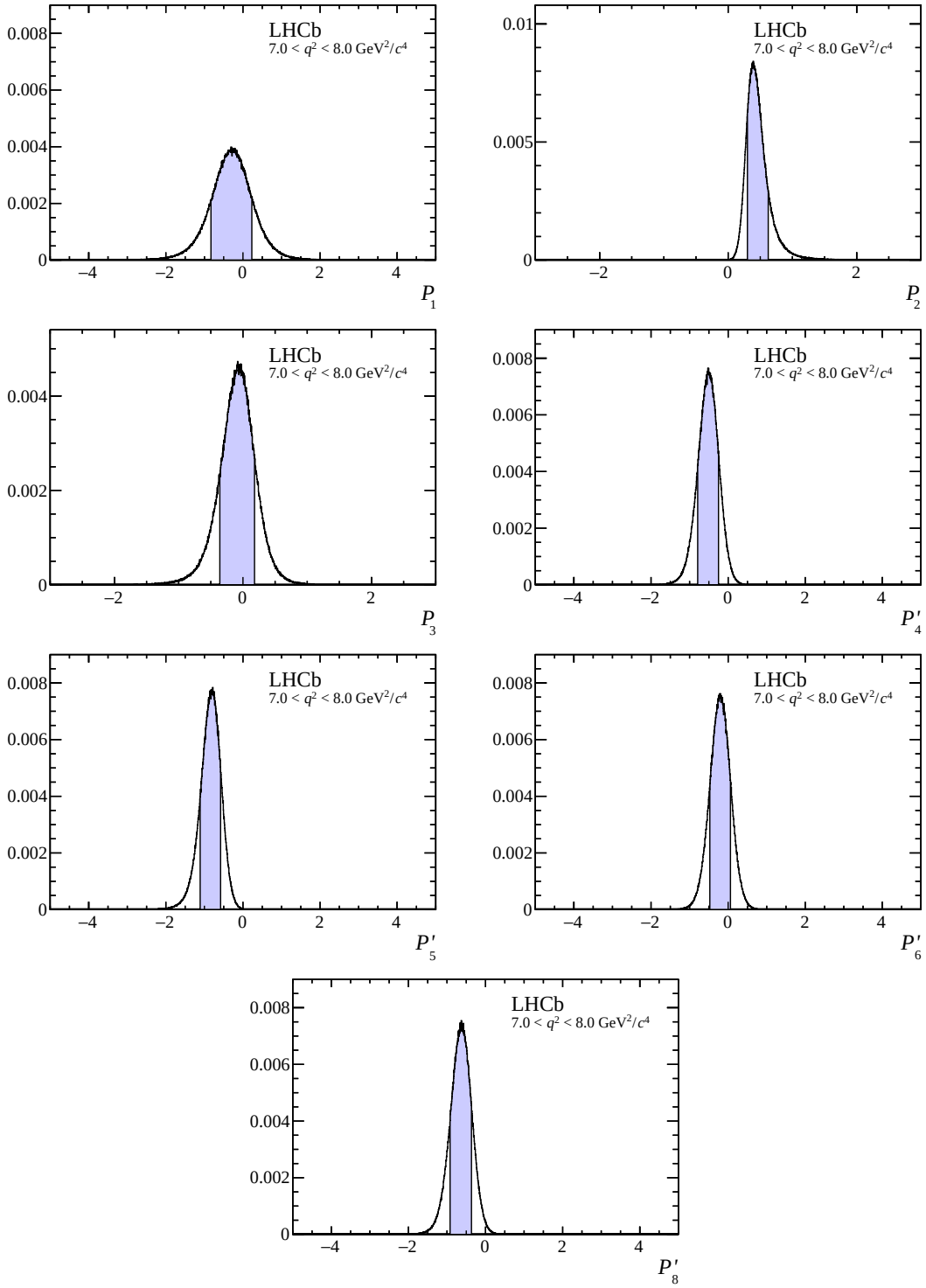

Figure 68: Distribution of pseudoexperiments obtained by applying a bootstrapping technique to the moment analysis. The 68% confidence interval on the angular observable is indicated by the shaded region.

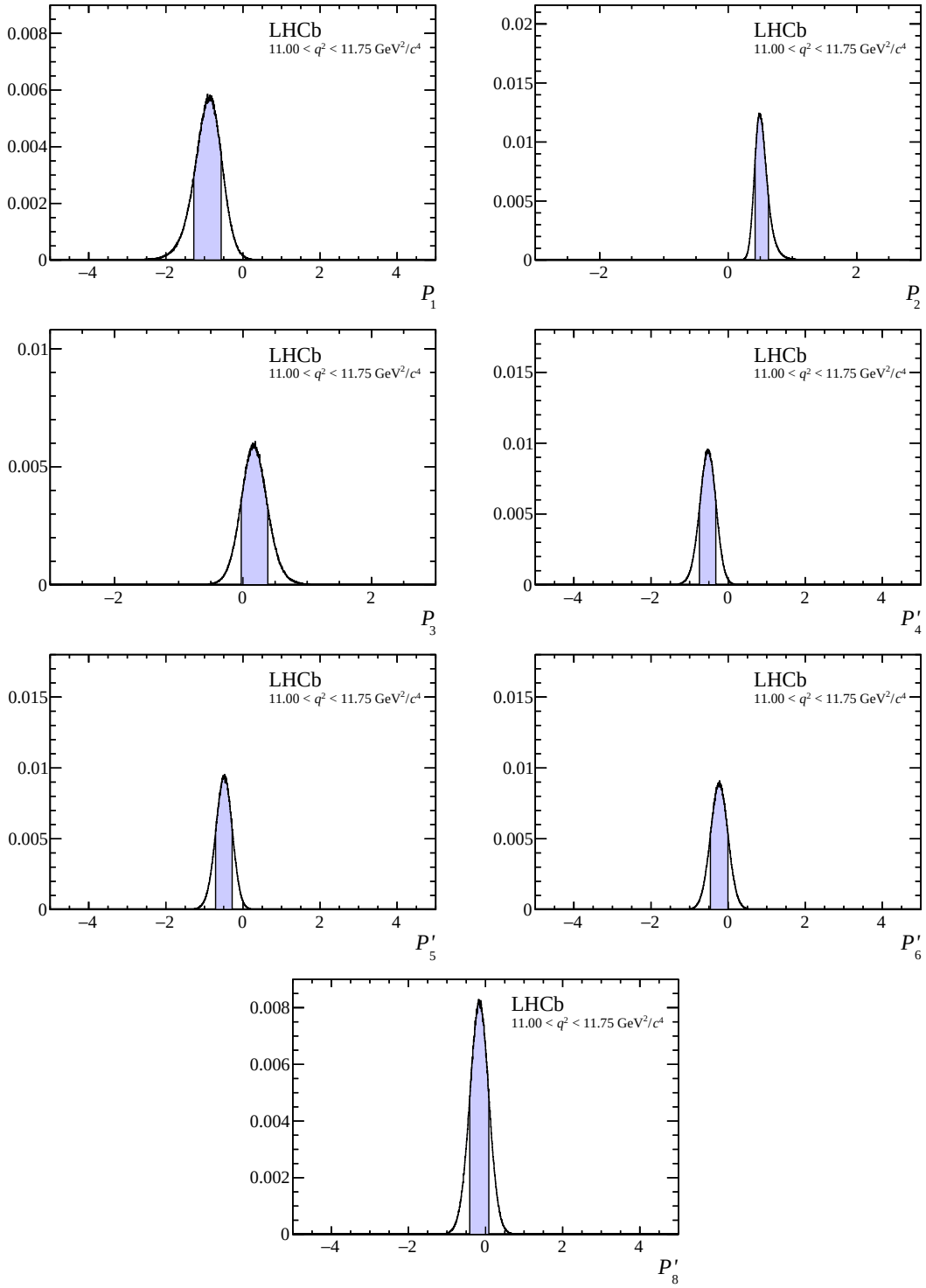

Figure 69: Distribution of pseudoexperiments obtained by applying a bootstrapping technique to the moment analysis. The 68% confidence interval on the angular observable is indicated by the shaded region.

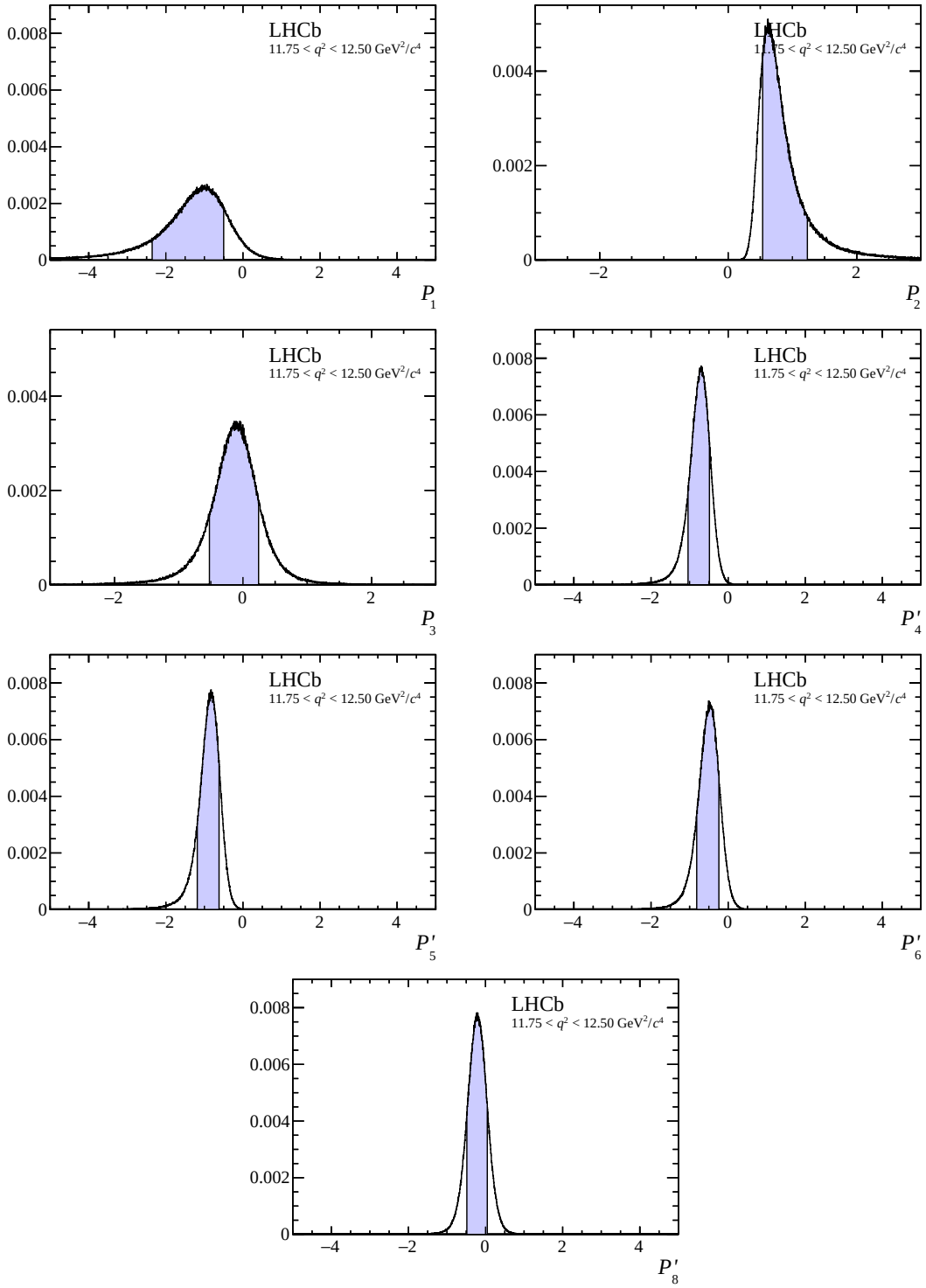

Figure 70: Distribution of pseudoexperiments obtained by applying a bootstrapping technique to the moment analysis. The 68% confidence interval on the angular observable is indicated by the shaded region.

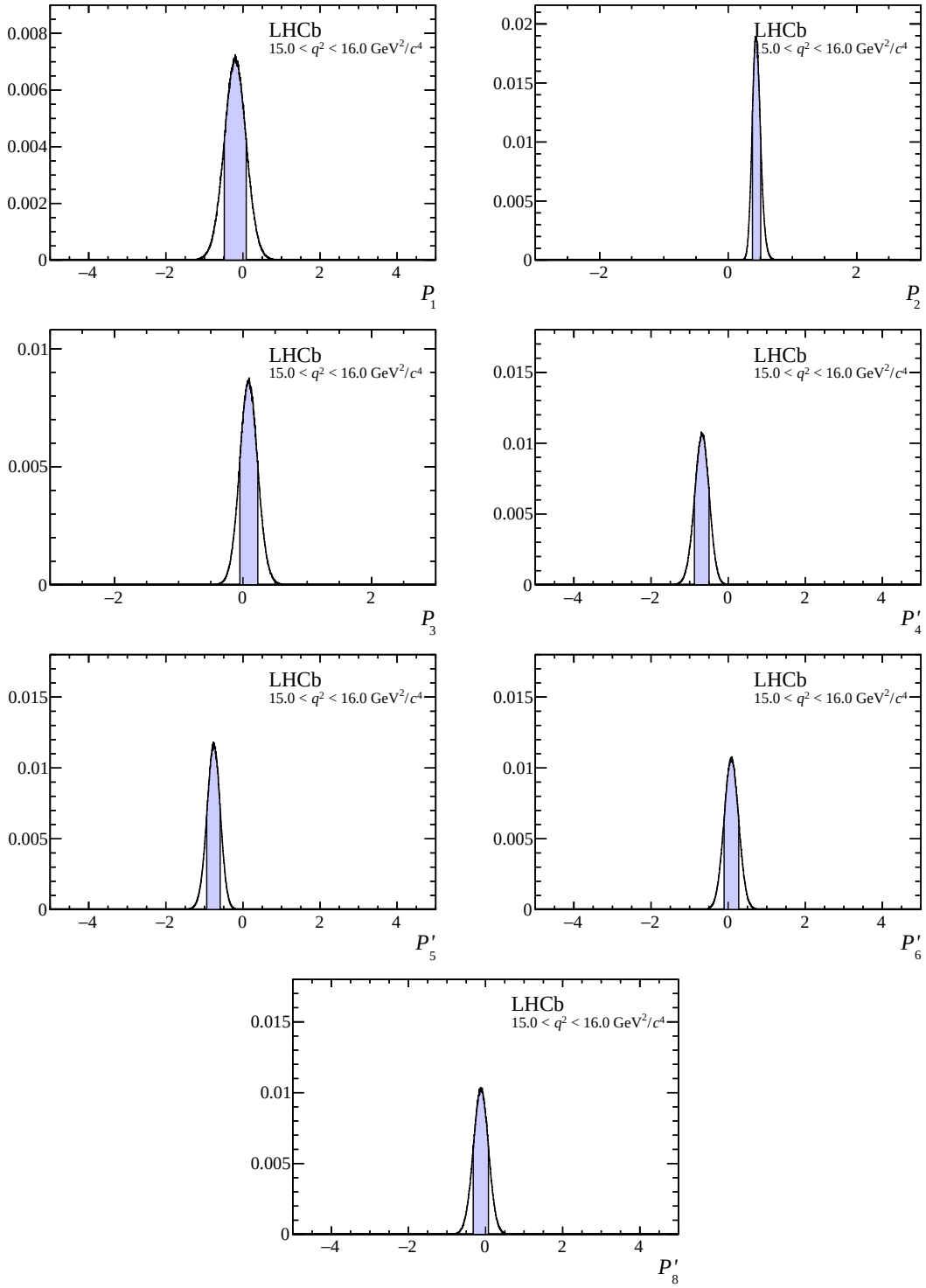

Figure 71: Distribution of pseudoexperiments obtained by applying a bootstrapping technique to the moment analysis. The 68% confidence interval on the angular observable is indicated by the shaded region.

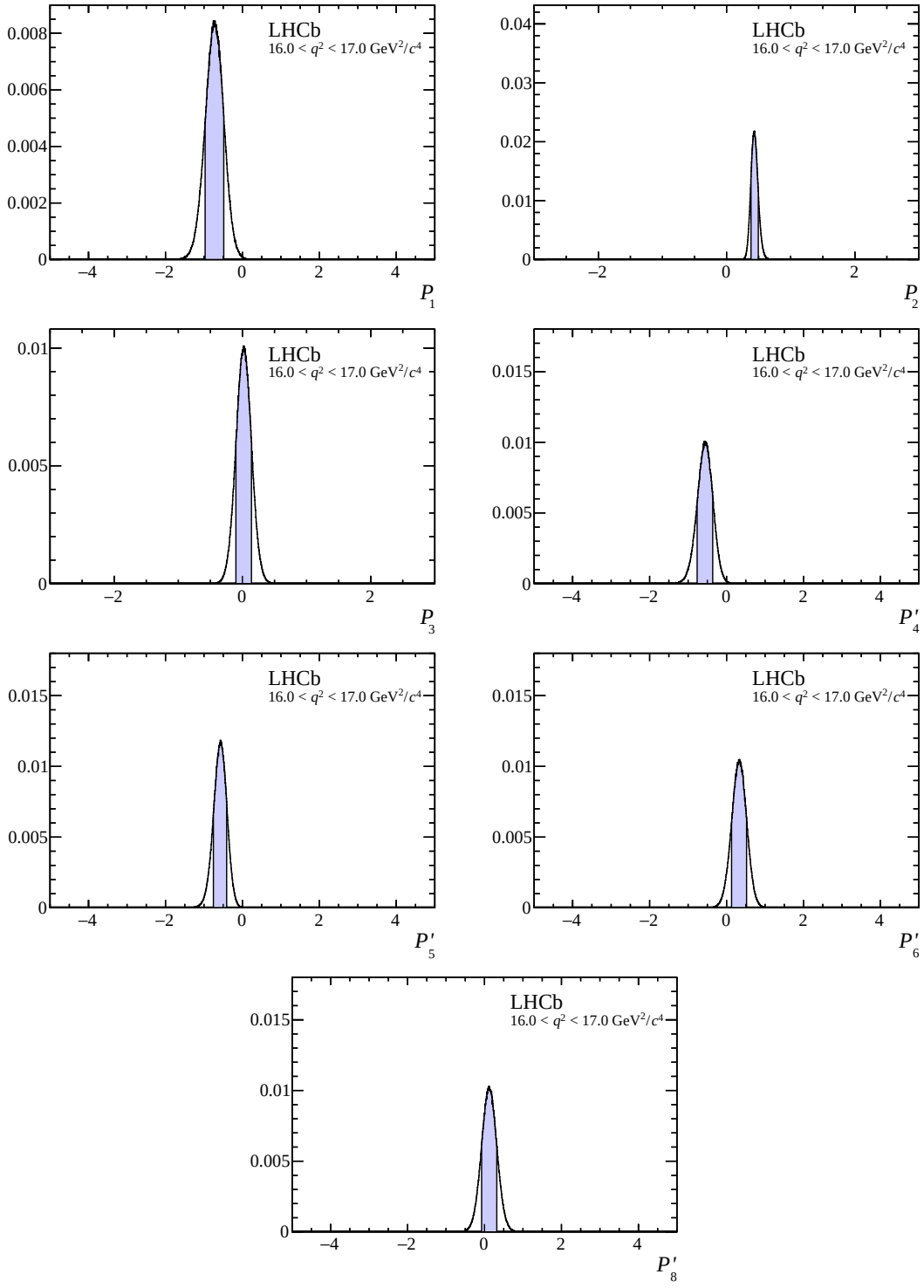

Figure 72: Distribution of pseudoexperiments obtained by applying a bootstrapping technique to the moment analysis. The 68% confidence interval on the angular observable is indicated by the shaded region.

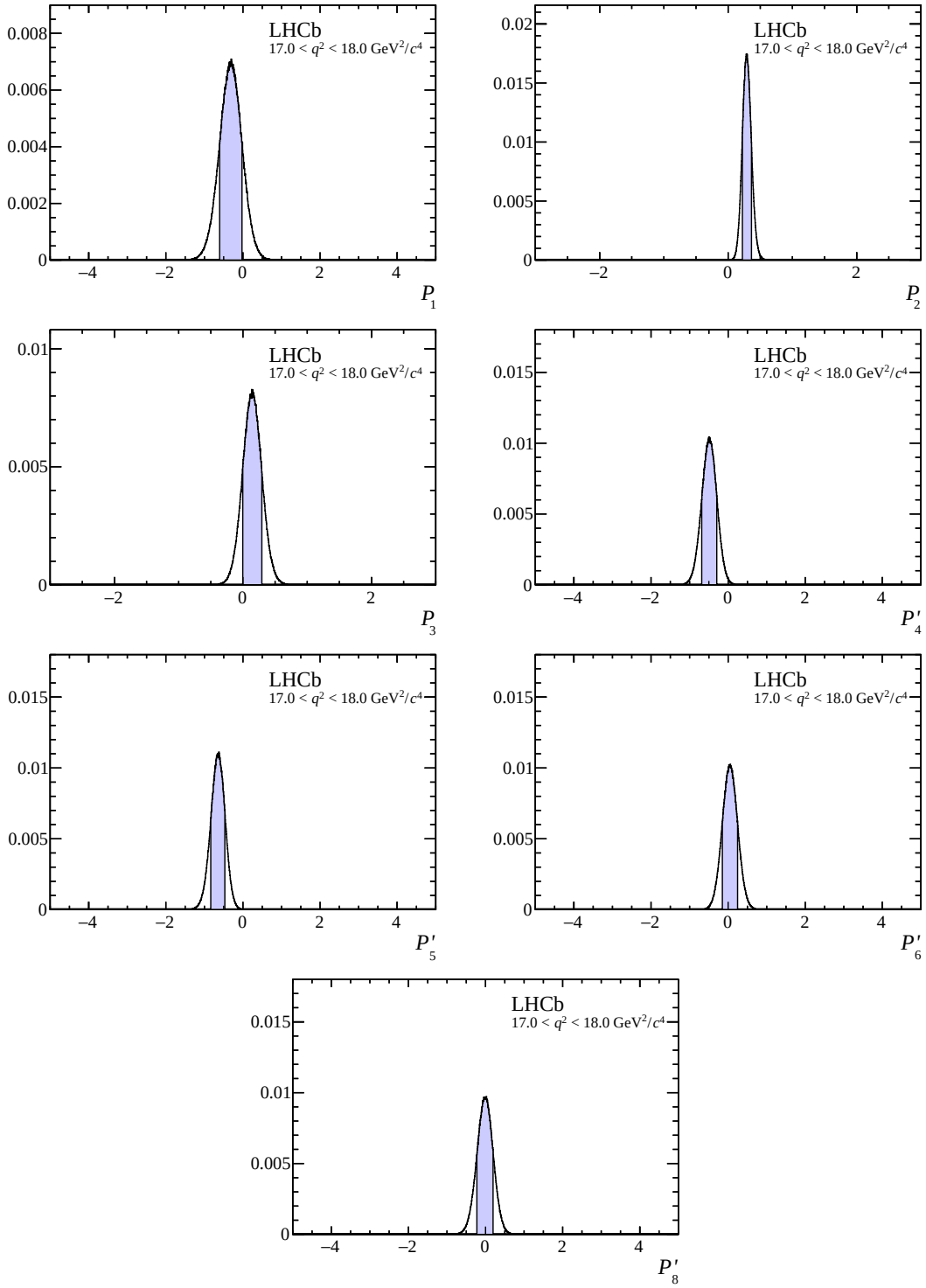

Figure 73: Distribution of pseudoexperiments obtained by applying a bootstrapping technique to the moment analysis. The 68% confidence interval on the angular observable is indicated by the shaded region.

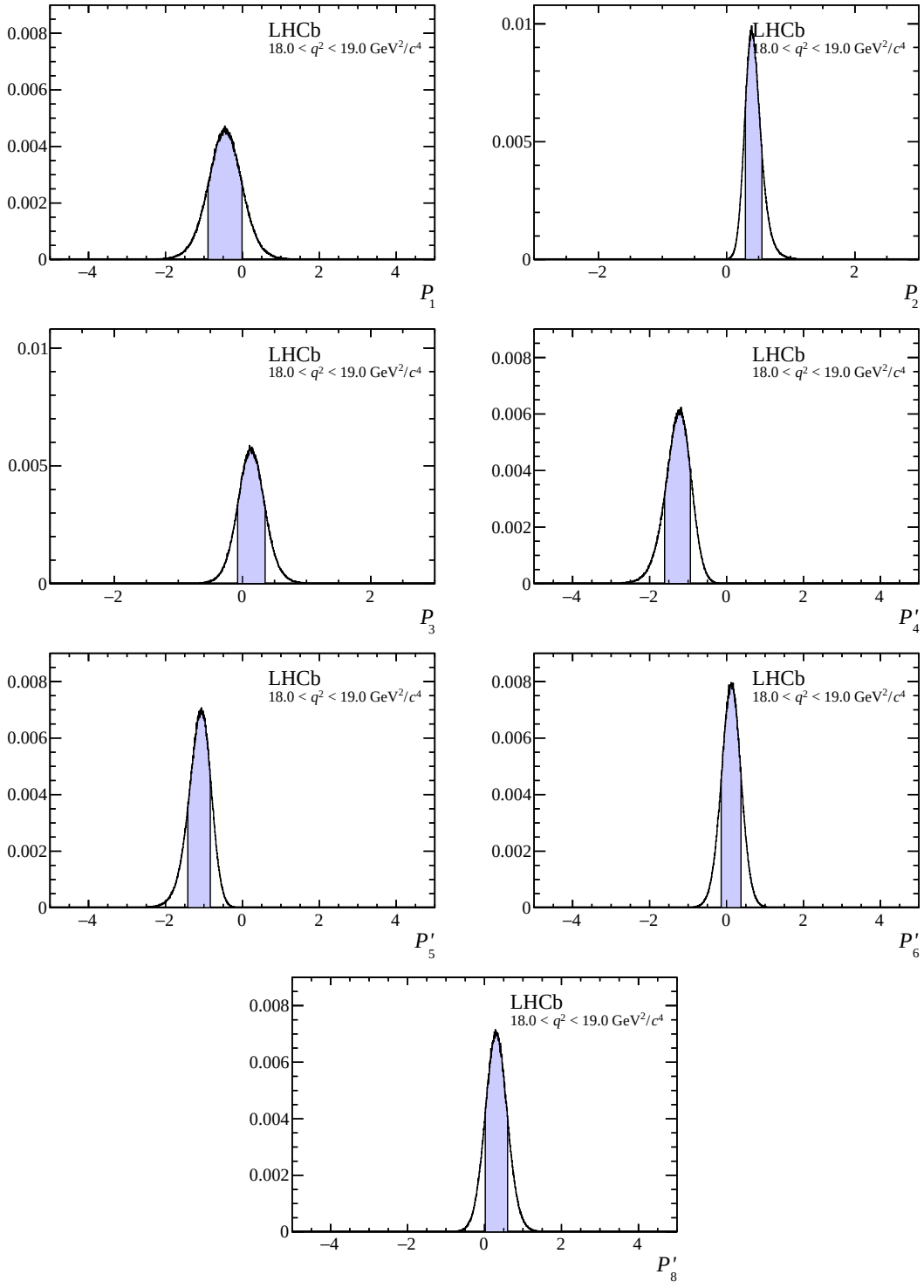

Figure 74: Distribution of pseudoexperiments obtained by applying a bootstrapping technique to the moment analysis. The 68% confidence interval on the angular observable is indicated by the shaded region.

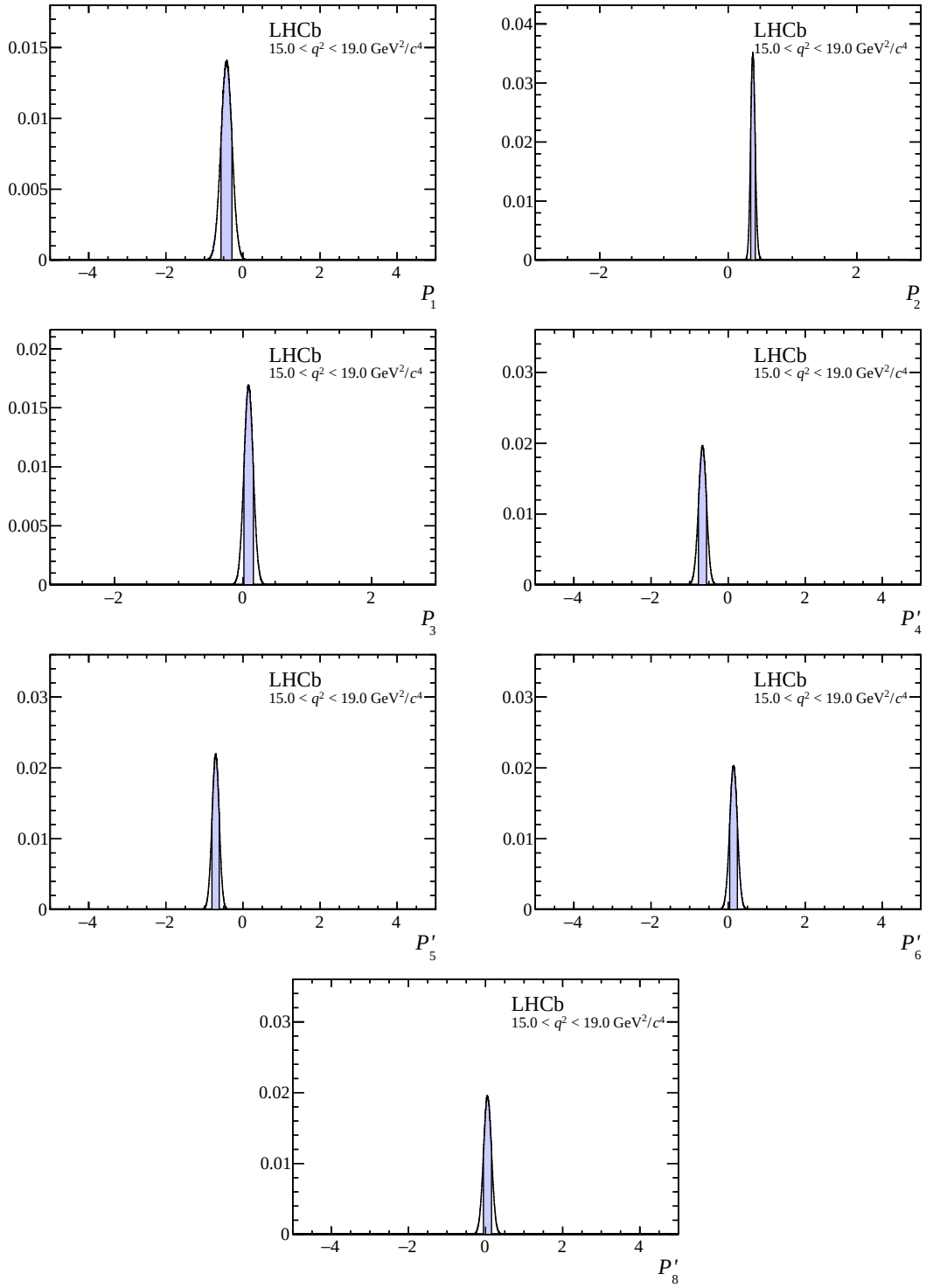

Figure 75: Distribution of pseudoexperiments obtained by applying a bootstrapping technique to the moment analysis. The 68% confidence interval on the angular observable is indicated by the shaded region.

3 Comparison of the likelihood fit, the method of moments and the amplitude fit

A comparison of the values of the *CP*-averaged and *CP*-asymmetric angular observables obtained using the likelihood fit and the method of moments is presented in Figs. 76 and 77. In general, good agreement between the two methods is observed. Since two different statistical estimators have been used, perfect agreement is not expected. Pseudoexperiments confirm that the observed level of agreement is as expected. A comparison of the optimised observables between the likelihood fit and the method of moments is shown in Fig. 78. Finally, a comparison of $A_{\rm FB}$, S_4 and S_5 determined as a function of q^2 from the amplitude fit and in bins of q^2 from the likelihood fit and method of moments is shown in Fig. 79. For the *CP*-averaged observables, predictions based on the prescription of Ref. [3] are shown for the regions $0.1 < q^2 < 6.0\,{\rm GeV}^2/c^4$ and $15.0 < q^2 < 19.0\,{\rm GeV}^2/c^4$. No predictions are made for the region close to the narrow $c\overline{c}$ resonances, the J/ψ and $\psi(2S)$, where many of the assumptions that go into the SM predictions are thought to be invalid. Reference [3] does not make predictions for the $S_{7,8,9}$ and the A_i observables. These observables are all expected to be close to zero in the SM. For the optimised observables, predictions from Ref. [4] are shown using form factors from Ref. [5]. The SM predictions are restricted to the q^2 range $q^2 < 8.0\,{\rm GeV}^2/c^4$.

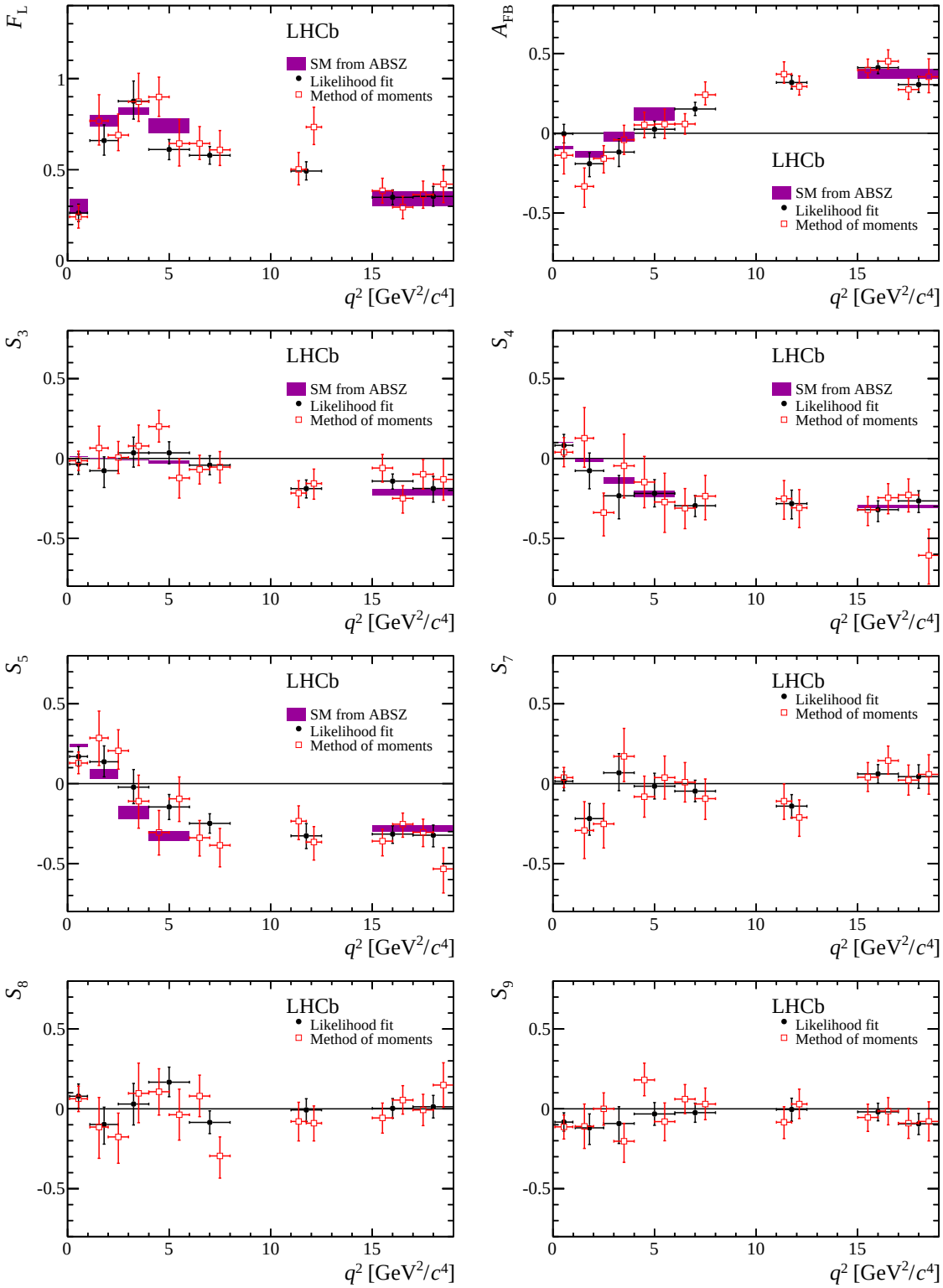

Figure 76: The *CP*-averaged observables in bins of q^2, determined in a maximum likelihood fit to the data and by the method of moments. The shaded boxes show the SM predictions based on the prescription of Ref. [3].

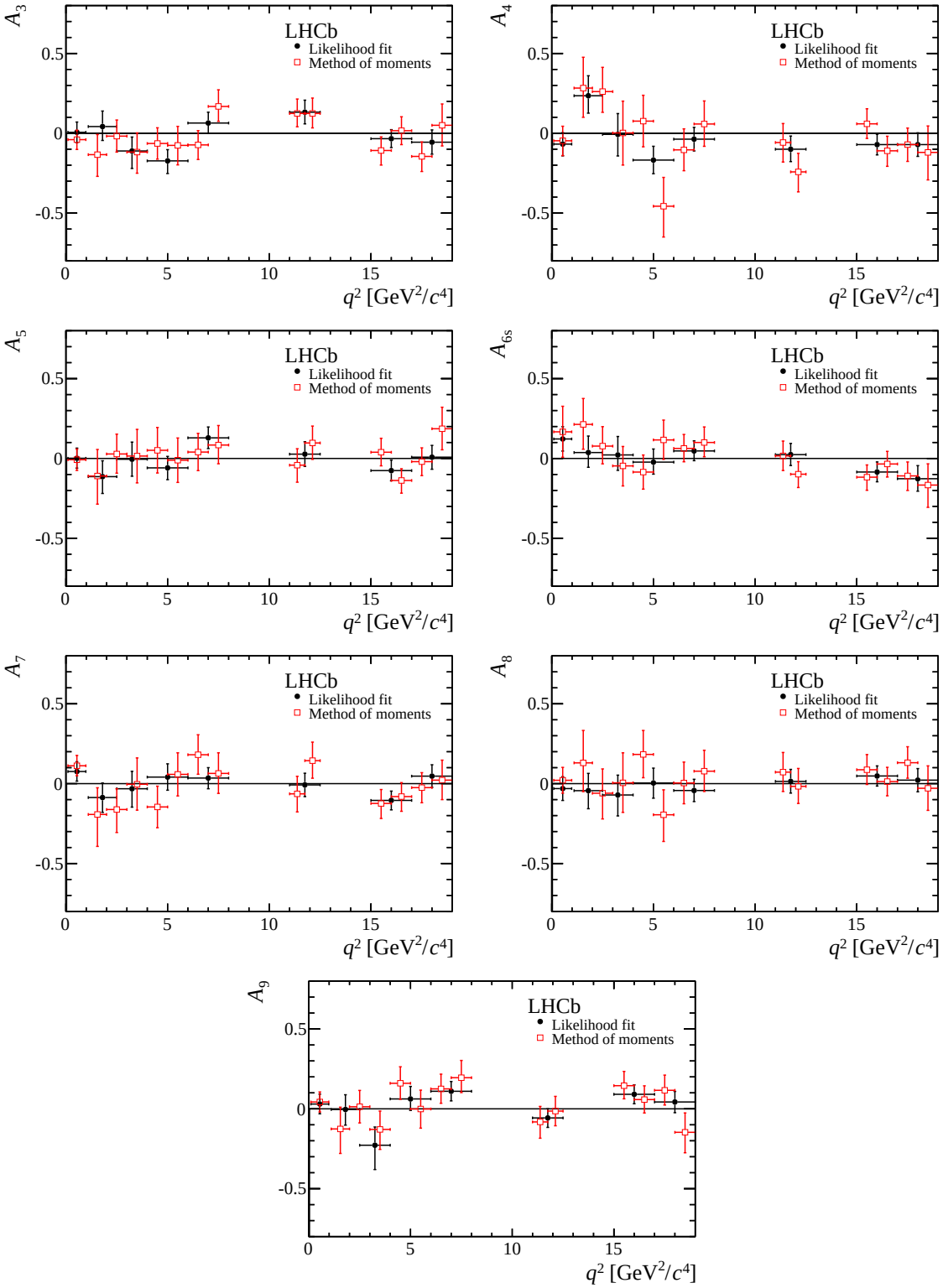

Figure 77: The *CP*-asymmetric observables in bins of q^2, determined in a maximum likelihood fit to the data and by the method of moments.

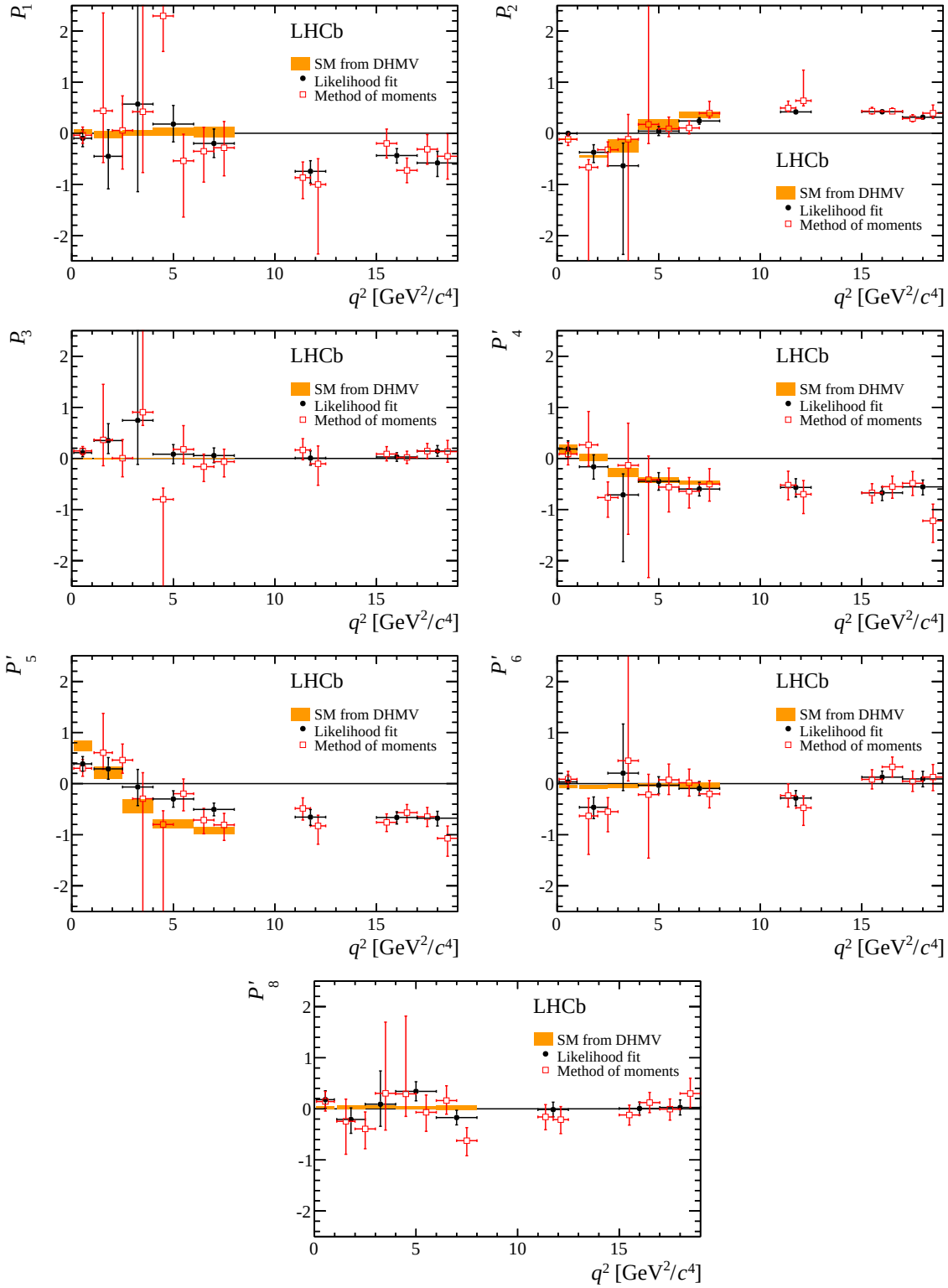

Figure 78: The optimised observables in bins of q^2, determined in a maximum likelihood fit to the data and by the method of moments.

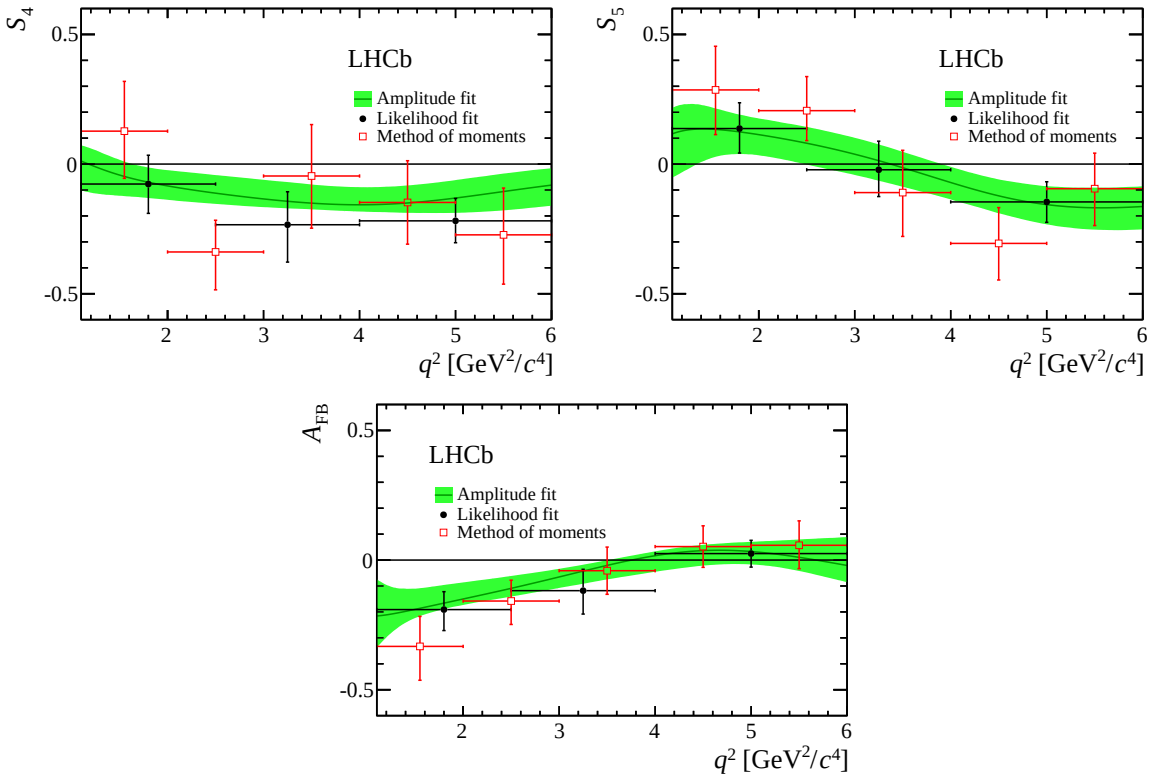

Figure 79: Observables S_4, S_5 and $A_{\rm FB}$ determined by fitting for the q^2 dependent decay amplitudes. The line indicates the best-fit to the dataset. The band indicates the 68% interval on the bootstraps at each point in q^2. The data points indicate the result of the likelihood fit and the values of the observables determined by the method of moments in bins of q^2.

Supplementary Information

1 Comparison between 1 fb^{-1} and 3 fb^{-1} results

A comparison between the result obtained for P_5' in this paper and the result from the 1 fb^{-1} LHCb analysis from Ref. [6] is shown in Fig. 80.

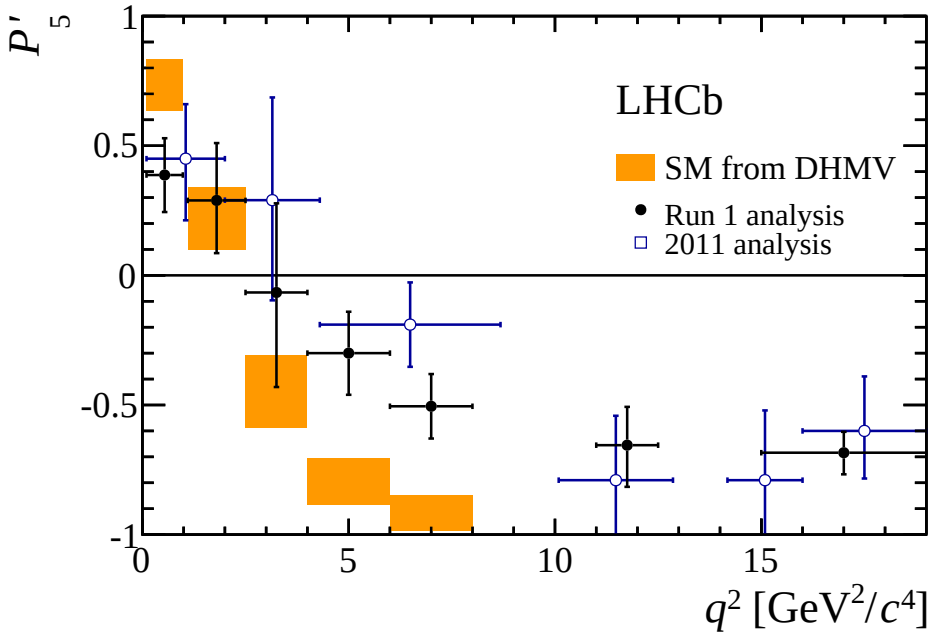

Figure 80: The observable P_5' in bins of q^2. The shaded boxes show the SM prediction taken from Ref. [4]. The blue open markers show the result of the 1 fb^{-1} analysis from Ref. [6].

2 1D projections for the moment analysis

Figure 81 shows the distribution of the signal candidates in $\cos\theta_l$, $\cos\theta_K$ and ϕ in the q^2 bins $0.1 < q^2 < 0.98\,\mathrm{GeV}^2/c^4$ and $15.0 < q^2 < 17.0\,\mathrm{GeV}^2/c^4$. The data has been both background subtracted (using the sPlot technique) and weighted to account for the angular acceptance. The signal distribution derived from the angular moments is overlaid.

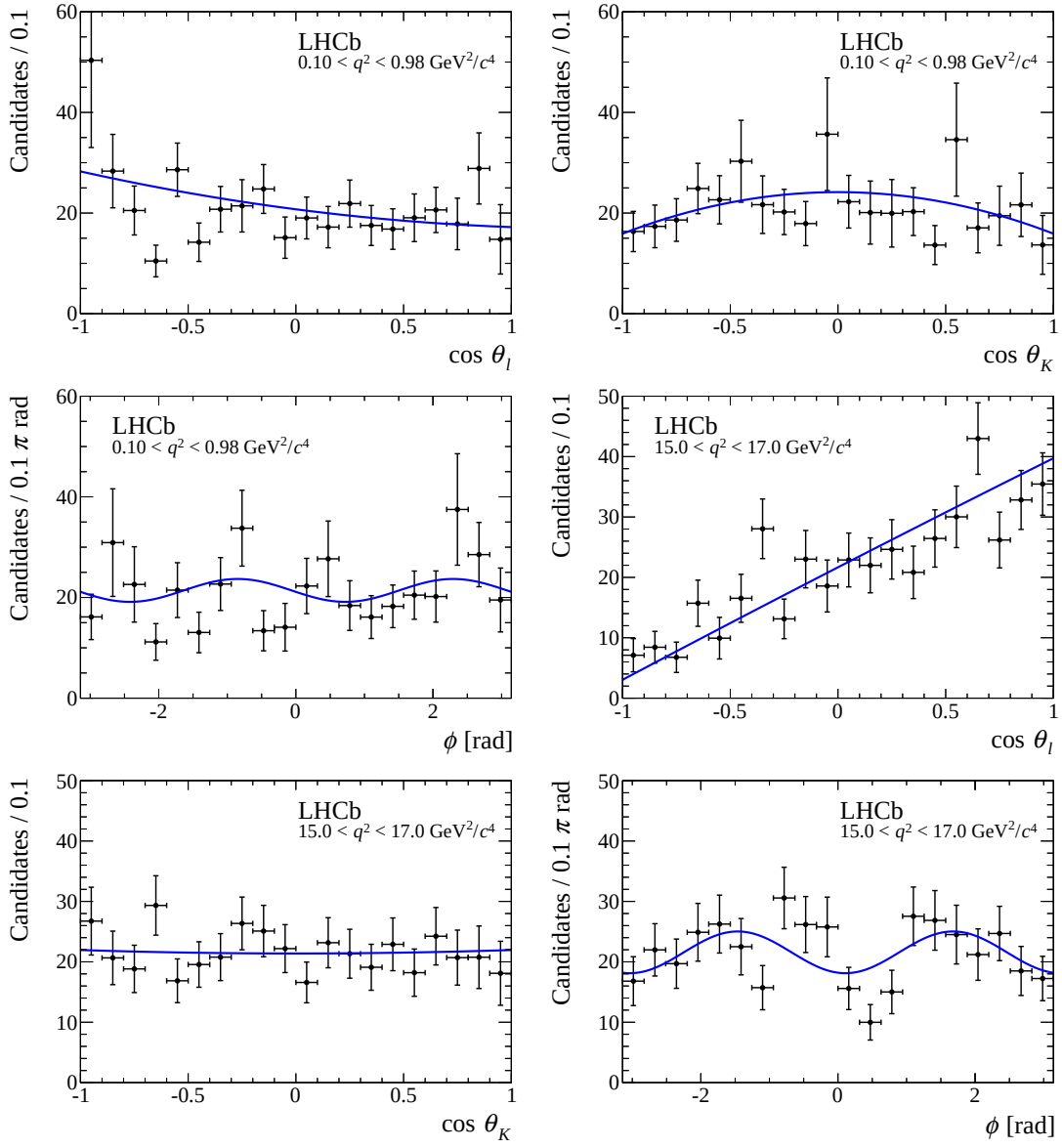

Figure 81: Background-subtracted data, weighted to account for the angular acceptance. The line is the expected angular distribution derived from the angular moments.

3 Visualisation of P_5'

The integral of $f_5(\vec{\Omega})$ over ϕ or $\cos\theta_K$ is zero. It is therefore not possible to determine S_5 (or P_5') from a single angle distribution. The discrepancy between the data and the SM prediction can, however, be visualised by partial integration with

$$\begin{aligned}\int_{-1}^{+1}\int_{0}^{\pi/2} \frac{\mathrm{d}^3\Gamma}{\mathrm{d}\cos\theta_l,\mathrm{d}\cos\theta_K\,\mathrm{d}|\phi|}\mathrm{d}\cos\theta_l\,\mathrm{d}|\phi| \\ -\int_{-1}^{+1}\int_{\pi/2}^{\pi} \frac{\mathrm{d}^3\Gamma}{\mathrm{d}\cos\theta_l,\mathrm{d}\cos\theta_K\,\mathrm{d}|\phi|}\mathrm{d}\cos\theta_l\,\mathrm{d}|\phi| \\ = \frac{9}{16}S_5\sin 2\theta_K\end{aligned} \tag{1}$$

or

$$\begin{aligned}\int_{-1}^{+1}\int_{0}^{+1} \frac{\mathrm{d}^3\Gamma}{\mathrm{d}\cos\theta_l,\mathrm{d}\cos\theta_K\,\mathrm{d}|\phi|}\mathrm{d}\cos\theta_l\,\mathrm{d}\cos\theta_K \\ -\int_{-1}^{+1}\int_{-1}^{0} \frac{\mathrm{d}^3\Gamma}{\mathrm{d}\cos\theta_l,\mathrm{d}\cos\theta_K\,\mathrm{d}|\phi|}\mathrm{d}\cos\theta_l\,\mathrm{d}\cos\theta_K \\ = \frac{3}{8}S_5\cos\phi\ .\end{aligned} \tag{2}$$

The data, the best fit to S_5 and the SM expectation for this pair of quantities is shown in Fig. 82.

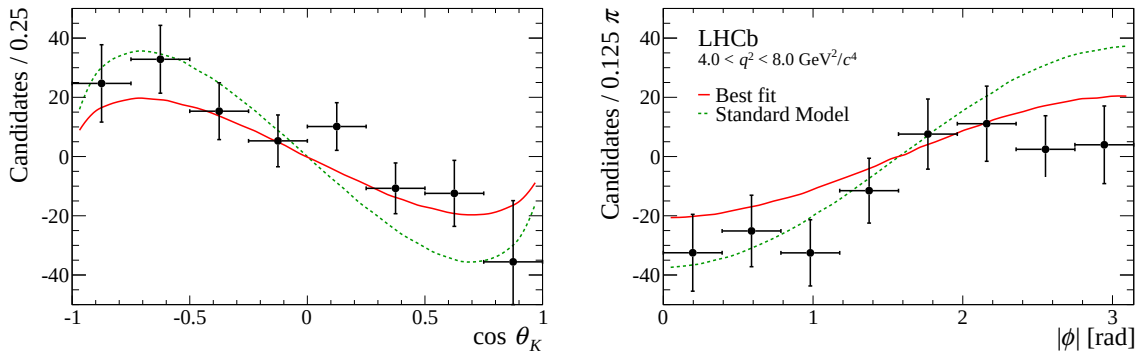

Figure 82: Visualisation of the discrepancy between the data (data points), best fit (red line) and the SM expectation (green dashed line) for S_5.

The observable S_5 also corresponds to the asymmetry between the regions labelled *up* and *down* in Fig. 83. The distribution of candidates in $m(K^+\pi^-\mu^+\mu^-)$ in the range

$4.0 < q^2 < 8.0\,\mathrm{GeV}^2/c^4$ in these two regions is also shown in Fig. 83. The asymmetry due to S_5 is clearly visible. The best-fit asymmetry from the likelihood fit to the data and the predicted SM asymmetry are also shown.

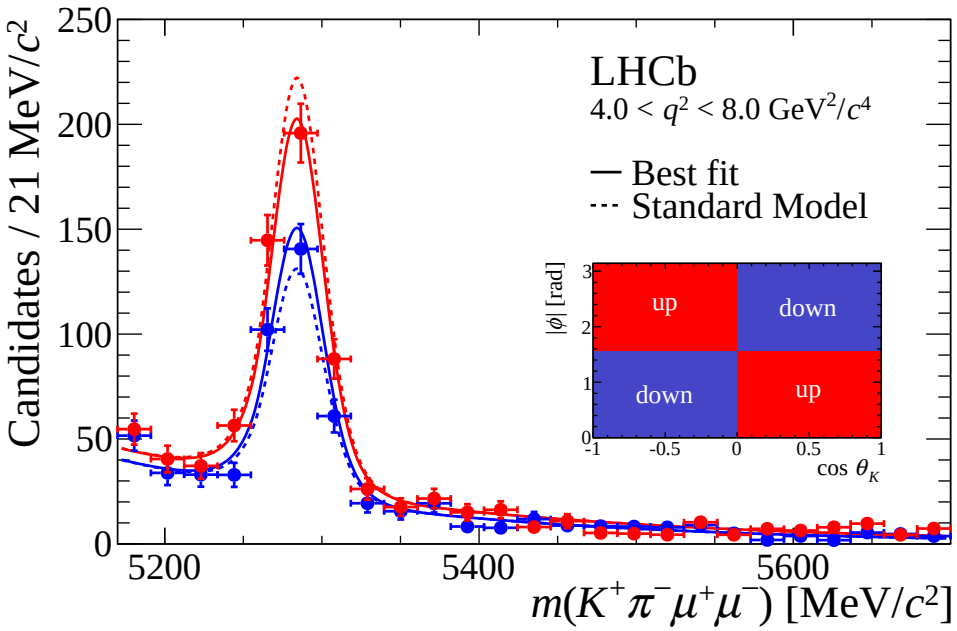

Figure 83: Visualisation of the asymmetry of the data due to S_5. The inset illustrates the two regions in $\cos\theta_K$ and ϕ that can be used to compute S_5. The two histograms show the distribution of candidates in $m(K^+\pi^-\mu^+\mu^-)$ in the dataset for the *up* and *down* regions. The data are overlaid with predictions for the signal yield given the best-fit (solid line) and SM (dashed line) values of S_5.

4 P_5' displayed in the range $[-1, +1]$

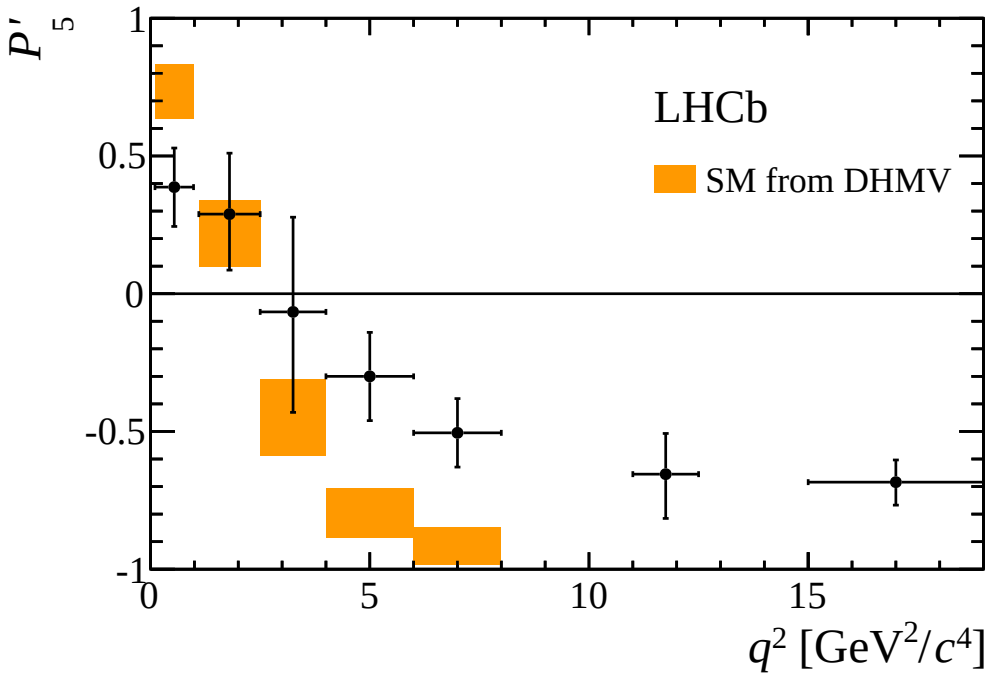

Figure 84: The angular observable P_5' from the likelihood fit displayed in the range $[-1, +1]$.

References

[1] G. J. Feldman and R. D. Cousins, *Unified approach to the classical statistical analysis of small signals*, Phys. Rev. D **57** (1998) 3873, arXiv:physics/9711021.

[2] B. Sen, M. Walker, and M. Woodroofe, *On the unified method with nuisance parameters*, Statistica Sinica **19** (2009) 301.

[3] W. Altmannshofer and D. M. Straub, *New physics in $b \to s$ transitions after LHC Run 1*, Eur. Phys. J. **C75** (2015) 382, arXiv:1411.3161.

[4] S. Descotes-Genon, L. Hofer, J. Matias, and J. Virto, *On the impact of power corrections in the prediction of $B \to K^* \mu^+ \mu^-$ observables*, JHEP **12** (2014) 125, arXiv:1407.8526.

[5] A. Khodjamirian, T. Mannel, A. A. Pivovarov, and Y.-M. Wang, *Charm-loop effect in $B \to K^{(*)} \ell^+ \ell^-$ and $B \to K^* \gamma$*, JHEP **09** (2010) 089, arXiv:1006.4945.

[6] LHCb collaboration, R. Aaij *et al.*, *Measurement of form-factor-independent observables in the decay $B^0 \to K^{*0} \mu^+ \mu^-$*, Phys. Rev. Lett. **111** (2013) 191801, arXiv:1308.1707.